Development And Validation Of A Near Infrared Specular Reflectance Flow Cell For Online Monitoring Of Microalgal Cultures

by

Cloribel Alejandra Santiago Flores

A thesis submitted in partial fulfillment of the requirements for the degree of

Master of Science

In

Chemical Engineering

Department of Chemical and Materials Engineering

University of Alberta

Abstract

Humankind is living in a world of rapid changes. Facts and situations that today seem to be permanent may be history tomorrow. Accordingly, in the future, energy sources may be different, new, and more sustainable. Oil derived from microalgae is one of those promising options. Microalgae have been getting increasing attention during the past decade and especially in the most recent years as a result of their numerous advantages.

Industrialization of microalgae is still in its early stages since microalgal processes possess diverse challenges that require further improvement. As a result, microalgal culture optimization is one area where plenty of work can be done. With this in mind, indisputably, a feasible, quick, and reliable monitoring system of the cultivation process is essential.

Spectroscopy is a widely employed technique for online monitoring of a variety of chemical processes due to its capability to quickly gather information. This work explores the feasibility of monitoring the course of microalgal cultures using near infrared (NIR) spectroscopy. It is important to realize that in order to achieve this objective, several limitations intrinsic to microalgal processes need to be overcome.

NIR spectroscopy reflectance was evaluated as a potential technique to monitor microalgal cultures. A NIR Specular Reflectance Flow Cell was successfully developed to allow for continuous monitoring, taking on account the technical requirements of the procedure and the distinctive characteristics of microalgal cultures. The capability of the flow cell to monitor microalgal cultures was investigated by determining glucose concentrations (10 – 100 g/L) in aqueous solutions and culture media (non-sterile and

sterile) and quantifying biomass density (5 - 50 g/L, dry weight). Linear relationships between NIR absorbance and the concentrations of both biomass (dry weight) and glucose were observed. Oil estimation using whole algal cells was also explored but unfortunately, the response to the range of the evaluated oil concentration (0.4 – 0.9 g/L) was very small. To finalize the evaluation of the flow cell, the monitoring of 60 independent microalgal cultures was conducted to determine biomass density and possibly glucose. Simultaneous determination of biomass and glucose was not successful due to the large influence that biomass has on the NIR spectra.

“Everything should be made as simple as possible but not simpler”

- Albert Einstein

I dedicate this thesis to my children, Saúl and Sofía.

I'll hold you in my heart forever.

Acknowledgements

I appreciate the opportunity to express my gratitude to all the people that have accompanied me during my studies at the university and in my life.

I am grateful to my supervisor Dr. William McCaffrey for giving me the opportunity to join his research group as well as for all his support and encouragement to develop and complete my research.

I recognize the invaluable help of Elliot Cameron, Vinay Bavdekar, Kassandra McLean, and Andrew Volk. Elliot you are always willing to lend a helping hand. Thank you for all your assistance.

I value the friendship that I found and shared with some of my peers during these years. You always put a smile on my face. I treasure as well all the support and encouragement from the friends that Canada has gifted to me. Thank you.

Gonzalo thank you for your help and believing in me. I give special thanks to my family for being with me despite the distance. My deep appreciation also goes to all my friends that are away from me.

Contents

List of tables

List of figures

Nomenclature

Greek symbols

ν	Kinematic viscosity
α	Inclination angle of the flow
ρ	Density
Υ	Surface tension
τ_o	Boundary shear stress
γ	Specific weight
σ	Interfacial tension
θ	Contact angle
λ	Wavelength
π	Pi

Roman symbols

NIR	Near infrared
CCU	Carbon capture and utilization
EPA	Environmental Protection Energy
GHG	Greenhouse gas
GM	Genetically modified
DNA	Deoxyribonucleic acid
EDTA	Ethylenediaminetetraacetic acid
WSSE	Weighted sum of squared errors
AIC	Akaike information criteria
BIC	Bayesian information criteria
HPLC	High performance liquid chromatography
EPS	Extracellular polymeric substance
DO	Dissolved oxygen
TSS	Total suspended solids

PCV	Packed cell volume
FAME	Fatty acid methyl esters
TLC	Thin layer chromatography
MS	Mass spectrometry
HPAEC	High performance anion exchange chromatography
VOCs	Volatile organic compounds
GC	Gas chromatography
IR	Infrared
EN	Electric noses
pO_2	Partial pressure of oxygen
RTD	Resistance temperature detectors
OD	Optical density
PAM	Pulse amplitude modulated
MIR	Mid infrared
IRS	Infrared reflectance spectroscopy
A	Absorbance
I_0	Intensity of incident optical radiation
I	Intensity remaining after interaction with the sample
T	Transmittance
R	Reflectance
As	Relative absorbance of the sample
$As*$	Absolute absorbance of the sample
$Ar*$	Absolute absorbance of the reference
e	Molar extinction coefficient
d	Path length
C	Molar concentration
Re	Reynolds number
V	Mean flow velocity
L	Characteristic length
R_H	Hydraulic radius
A	Flow area

WP	Wetted perimeter
W	Width
D	Depth
Fr	Froude number
y	Hydraulic depth
g	Standard acceleration due to gravity
We	Weber number
Q	Volumetric flow
G	Gibbs free energy
s	solid
l	liquid
v	vapor
k	wavenumber
l_c	Capillary length
P	Pressure
P_a	Air atmospheric pressure
P_l	Liquid phase pressure
R	Radius
PLS	Partial least squares
RMSE	Root mean square error

1

Introduction

In this chapter the problem statement and the purpose of this work are presented. In addition, a general overview of the breadth of the thesis is described.

1.1 Problem statement

Microalgae are a potential source of renewable fuels. They can be easily cultivated under a broad range of conditions, and many species are able to accumulate an abundant amount of oil. These are only a couple of the many advantages of microalgae. However, microalgal cultures typically have low densities. Thus, it is necessary to optimize their culture conditions in order to realize their full potential. An extensive understanding of their non-linear growth dynamics is essential to achieve feasible processes. Unfortunately, the data needed for optimization is very difficult to obtain. Microalgal cultures are hard to monitor due to the complex and time-consuming nature of the required analytical techniques.

Real-time measurements enable efficient and economical monitoring of biochemical processes but they are dependent on the use of online analyzers. The development of better analytical technologies is the foundation of an effective process analysis system, where the analytical information may be used in a closed loop control within the process control system *(1)* . Spectroscopy is a valuable monitoring process tool with the potential to replace slow and cumbersome off-line analytical techniques, because it makes possible to gather data in a fraction of seconds rather than hours or days.

1.2 Statement of purpose

The general aim of this research work was the use of NIR Spectroscopy for online monitoring of microalgal cultures. The specific parameters to be determined were biomass, glucose, and lipid concentration.

1.3 Thesis overview

During this thesis a NIR Specular Reflectance Flow Cell for online monitoring of microalgal cultures was developed.

Chapter 2 provides a general description of microalgae, microalgal processes, and how they are currently monitored. Infrared and Raman spectroscopy are also introduced, with reference to the work previously realized in my research group with Raman spectroscopy. The specific spectroscopy technique used in the flow cell (specular reflectance) is described as well. An overview of optical sensors and chemometrics is presented. To finish, an introduction to the regimens and characteristics of capillary open channels is provided.

Chapter 3 describes the instrumentation and the reference analytical methods used throughout this work. It also contains the methodology followed to cultivate the microalgae used during the flow cell assessment.

Chapter 4 describes how the flow cell was developed. It details how the different operating parameters were established, adjusted, and refined in order to obtain a functioning flow cell. All the methods used to improve its performance are described as well.

Chapter 5 contains all the research trials used to evaluate the functionality of the flow cell. It also includes the final validation of the performance of the flow cell during the monitoring of microalgal cultures.

Chapter 6 includes the conclusions of the thesis and a series of recommendations for future work.

2
Background

This chapter offers a brief description and highlights different benefits and peculiarities of microalgal cultures. Knowledge of the growth and dynamics of microalgal cultures is essential to develop suitable and reliable online sensors that report on key cultivation parameters. These sensors are crucial for real-time optimization and control of microalgal cultures to successfully produce biofuels or other specialty chemicals.

2.1 Microalgal cultivation

Microalgae are the original source of crude oil. Millions of years ago, microalgae bloomed, died, and settled in the sea floors. After a series of physicochemical processes, these microalgal deposits became oil *(2)* . Today microalgal cultivation is considered one of the carbon capture and utilization (CCU) technologies by transforming carbon dioxide emissions into valuable products, while reducing greenhouse gases, and providing economic benefits *(3)* .

Indeed, microalgal cultures are important not only from an environmental and economic point of view but also for national energy security reasons. Only those countries, which find and develop new energy sources, will no longer depend on the resources of other countries *(4)* . It is crucial to acknowledge that during the current decade the United States, Europe Union, and big emerging economies, like China or Brazil, will demand more energy *(5)* . In addition, according to the United Nations by 2050 agricultural production should double in order to feed more than 9 billion people around the world *(6)* . This increasing demand for food and energy will open the opportunity for microalgal producers to play a key role in the economy.

Many strains of microalgae produce and accumulate oil, which is easily refined into gasoline, diesel, and jet fuel. Additionally, they have the potential to be a high-yield source of biomass and high-value co-products, such as antioxidants, proteins, and carbohydrates, along with other benefits like bio-remediation without compromising food supplies, rainforest or arable land. As a result, they are attracting increasing interest and investment from biofuels, petroleum, pharmaceutical, and agribusiness industries *(2, 7-10)* . In 2010, just in San Diego California, four important microalgal laboratories were working with $1 billion in funding from private and public sectors *(8)* . To illustrate the potential value of microalgal metabolites, astaxanthin, one antioxidant with numerous benefits on human health, was been sold up to $12,000/kg in 2013 *(11)* . Furthermore, microalgae-based molecules can be of higher quality compared to the corresponding synthetic alternatives, when these are only available in specific isomers *(12)* .

There are 80,000 to 100,000 different microalgal species. Currently, several companies are cultivating around 200 species worldwide. Algenol, which is producing ethanol, diesel, jet fuel, and gasoline for around $1.3/gallon, got a certification from the Environmental Protection Energy (EPA) in January 2015, given that, its fuels meet the requirements of the Renewable Fuel Standard. Therefore, fuel blenders and refiners can now use these microalgal fuels to meet the requirements of the Clean Air Act, since they are able to achieve up to 69% reduction in greenhouse gas (GHG) emissions compared with gasoline *(12-14)* . Additionally, Sapphire Energy is producing Green Crude Oil in desert climates from microalgae, using sunlight, CO_2, and salt water. This crude oil is compatible with existing refinery infrastructure *(15)* . Another example of successful microalgae production and commercialization is shown by Solazyme, a San Francisco based company. Solazyme has a broad range of functional products for industrial, fuel, food, and personal care applications *(16)* .

Some of the main benefits of microalgal cultures are: *(2, 6, 17-19)*

a) Their versatility, *e.g.*, certain species of microalgae are salt-tolerant and can grow in saltwater, while others have the ability to grow in sewage or hot spring water.
b) Their great metabolic adaptability depending on their physiological state, *i.e.*, externally stressed or non-stressed.

c) Since they can use waste streams, such as carbon dioxide emissions or sewage to grow, they have the potential of being environmentally sustainable.
d) They are a steady source of biomass, because it is not a seasonal crop.
e) They can be grown in different climates.
f) No need of fertilizers or pesticides

When planning to grow microalgae for biofuels production, the first task microalgal producers have, is the identification of strains with high lipid yields and fast growth rates. For the selected strains, producers also need to determine the best cultivation and harvesting systems along with strategies to reduce water and energy consumption *(10, 19, 20)* . Use of strains from culture collections is advantageous because much of the growth requirements characterization has been done. In contrast, use of indigenous strains, which have an inherent adaptability to changes in environment and climate, require isolation as well as determination of optimal culture conditions and feasibility of their production. This time consuming, labor intensive, and costly process may be worthwhile, if adaptability of indigenous strains give favorable results in the long term *(21)* .

There are three pathways to obtain microalgal products: i) processing the whole biomass; ii) processing of extracts and residual biomass; and iii) direct recovery of metabolites from the culture *(19)* . Indeed, microalgal technology has evolved to a great extent. Nowadays, through the use of synthetic biology, it is possible to use microalgal cells as mini-refineries by making them able to consume carbon dioxide and excrete hydrocarbons like kerosene and ethanol directly *(10, 22)* .

Finally, it is important to mention that microalgae products may be enhanced through genetic modification. A major concern with this approach is the production of genetically modified (GM) microalgae with the potential of being stable in nature, representing a risk to the environment and ultimately human health *(23)* . Fortunately, the probability of environmental release of these modified microalgae decreases depending on the cultivation system used. Enclosed bioreactors represent low risk and could be regulated under existing laws. However, release of GM microalgae may be inevitable if microalgae

are cultivated in open pond reactors. In that case, a stepwise sequence from small scale to larger scale with adequate risk assessments and more stringent regulations are required *(24, 25)* . Sapphire Energy received approval for the first experimental outdoor use of GM microalgae in 2013 by EPA *(25)* . At the present time no harmful release of GM microalgae is known.

2.1.1 Microalgal cell

Microalgae are photosynthetic microorganisms (*i.e.*, prokaryotic cyanobacteria and eukaryotic protists), found either in marine or fresh water environments *(19, 23)* . Although cyanobacteria, also known as blue-green algae, belong to the bacterial domain, they have the ability to perform photosynthesis and assimilate inorganic nutrients *(26)* . Since cyanobacteria lacks of nucleoid, its DNA is not organized in chromosomes and lies free in the cytoplasm with the photosynthetic membranes. In contrast, eukaryotic microalgae possess nucleus, and their cytoplasm is divided into compartments and membrane bounded organelles (*e.g.*, Golgi body, mitochondria, endoplasmic reticulum, vacuoles, and plastids). The cell wall of eukaryotes is usually composed by a microfibrillar layer of cellulose and sometimes surrounded by an amorphous layer that is either silicified or calcified. There are a variety of ways that are used to characterize microalgae. A commonly used categorization of eukaryotic microalgae is: green algae (*Chlorophyta*), red algae (*Rhodophyta*), and diatoms (*Bacillariophyta*) *(7, 27)* .

Microalgae usually reproduce by cell division, but other types of asexual reproduction occur, such as fragmentation, and production of spores. Microalgae also have different types of cell organization: unicellular, colonial, and filamentous *(7)* .

Microalgae are characterized by having a fast uptake of nutrients from the medium. Indeed, nutrient uptake rate may be faster than growth rate. In addition, microalgae may accumulate large amounts of specific metabolites under unfavorable growth conditions. These characteristics make impractical to consider microalgal biomass as a pseudo-chemical component with a relatively defined empirical chemical formula *(28)* .

2.1.2 Microalgal kinetics

Microalgal metabolisms

Microalgae are well adapted to grow in a variety of environments, including photoautotrophic, heterotrophic, photoheterotrophic, and mixotrophic *(29)* .

Photoautotrophic cultivation occurs when microalgae use light as energy source, and CO_2 as a carbon source *(29)* . When a culture reaches elevated cell density, self-shading is one of the main factors that can ultimately limit its growth rate. Nevertheless, most microalgae species are photoautotrophs *(28)* .

Heterotrophic cultivation takes place when microalgae are able to grow using organic compounds as source for both energy and carbon, *i.e.*, microalgae have the ability to grow under dark conditions *(29)* . Growth in these cultures is limited by nutrient availability or accumulation of inhibitory compounds in media *(28)* . In addition, not all microalgae or metabolites of interest can be produced under dark conditions *(30)* .

Photoheterotrophic cultivation is when microalgae use light as an energy source and organic compounds as a source of carbon in order to propagate *(29, 31)* .

Finally, mixotrophic cultivation happens when microalgae grow through a combination of photoautotrophic, heterotrophic, and photoheterotrophic growth modes *(29, 32)* .

Cultivation systems

Microalgae are cultivated using either open or closed growth systems, briefly described in the following section *(7, 12, 18, 27, 28, 30, 33-36)* :

Open growth systems include un-stirred ponds, lakes, and lagoons as well as stirred ponds (circular or raceway). Raceways ponds, which are widely used for production of *Spirulina* and *Dunaliella*, usually are between 0.2 and 0.5 m deep. They are operated in a continuous production cycle with simple regular maintenance and cleaning. Open systems are relatively inexpensive but processing conditions are not optimal, and their consumption of water is elevated. Indeed, microalgae able to grow in these systems are

generally extremophiles. In other words, they require highly selective conditions (*e.g.*, extreme pH, temperature or brackish to saline water), which prevent contamination. Regardless, a variety of open microalgal growth systems are being used at commercial scale worldwide.

Closed ponds are an alternative to open ponds. Although closed ponds have an increasing cost, they are still substantially cheaper than closed growth systems, with the advantage of countering several drawbacks present in open systems, such as restriction to specific strains, evaporation, and temperature fluctuation in the growth media.

On the other hand, closed systems include a variety of photo-bioreactors and bioreactors configurations, like tubular (vertical, horizontal, and helical), flat panels, stirred tanks as well as airlift or bubble columns. Closed systems not only reduce the risk of contamination and evaporation; they also have better operating control conditions (*i.e.*, temperature, pH, aeration, mixing, CO_2 concentration along with light intensity and regime), which make them more efficient in terms of productivity and quality of the final product. However, closed systems present higher costs and some drawbacks like biofouling. So far the easiest reactors to scale up, by increasing the number of modules, are the horizontal or helical tubular designs, along with vertical flat panels and bubble columns *(12, 18)* . Unquestionably, more room for innovation in bioreactor design still exists.

It is crucial for large-scale microalgal production to develop cheaper and more efficient cultivation systems.

Reactor operation mode

Batch culture is the simplest microalgal culture mode, since it is cheap, easy to manipulate, and requires relatively low volumes of media. At the beginning of a batch, all of the necessary nutrients are added to the vessel. No further nutrients are added during the cultivation. This means that food supply is limited, since nothing is added or removed. Once the desired cell concentration or the final product concentration is reached, the culture is harvested *(28, 31, 37)* .

In fed-batch cultures, nutrients are continuously added until the reactor reaches its maximum operating volume, at which point cells are harvested *(28)* .

In semi-continuous cultures, the culture is diluted regularly by removing a fraction of the reactor volume and adding fresh medium at a given time. This procedure is followed in order to maintain cells in nutrient replete exponential growth phase and to restrict biomass density *(28, 37)* .

In continuous cultures, cells are harvested while fresh medium is constantly added at balanced rate, in order to achieve a constant dilution rate. If total reactor volume is kept steady and optimum concentrations maintained, an indefinite exponential growth phase is reached *(28, 31, 37, 38)* .

In perfusion cultures, spent medium is removed while fresh medium is added. Therefore, microalgal cells are retained in the reactor to overcome the low density present in continuous systems *(28)* .

Mixing

In photoautotrophic cultures, agitation rate, within specific limits, enhances biomass productivity by reducing the length of the dark period at which cells are exposed, thus improving light regimen (see Figure 2-1) *(39)* .

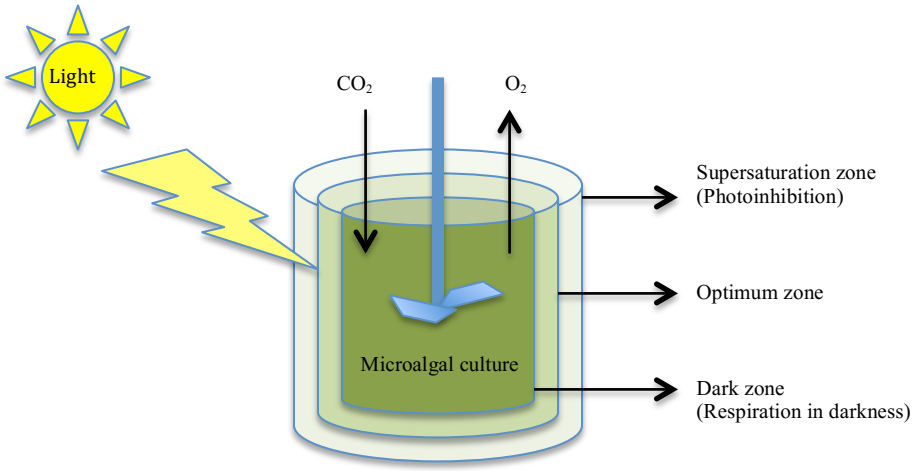

Figure 2-1 Self-shading effect is overcome through adequate mixing in phototrophic cultures

Adequate mixing guarantees satisfactory mass transfer, prevents cell sedimentation, and biofilm formation as well as clumping. In addition, mixing reduces gradients of nutrients, light, and temperature during microalgal culture, which is essential to produce consistently high yields of biomass. However, excessive bubbling, micro eddies close in size to microalgal cells, and particularly shear stress can produce cell damage, affecting the culture performance. The extent of damage will depend on the species of microalgae (*i.e.*, size, morphology as well as composition and thickness of the cell wall) and the growth environment. Use of carboxymethyl cellulose, for example, has a protective effect on microalgal cultures due to a reduction in the friction factor and therefore in the shear rate *(30, 31, 40)* .

In many photoautotrophic reactor configurations, mixing is achieved by the injection of CO_2 into the system. Since CO_2 is a major nutrient, mixing and gas transfer are particularly interconnected in those cases, given that the main resistance to CO_2 transport lies in the liquid film *(30)* .

When pumping is used in microalgal cultures, different pumps, such as centrifugal, positive displacement, peristaltic or diaphragm, are often used. Each type of pump can impact the maximum observable specific growth rate for a given culture system. One of the main factors influencing the performance of microalgal cultures is the number of passes through the pumps *(30)* .

Microalgal growth phases

Microalgae undergo the following growth phases during a simple homogeneous batch culture: lag, log, deceleration, stationary, and death phases (see Figure 2-2). These phases represent the response of microalgae to changes in culture conditions and depend on the inoculum. Inoculum size should be between 5 and 10% by volume. A biomass density vs. time graph follows an S shaped curve *(31, 38)* .

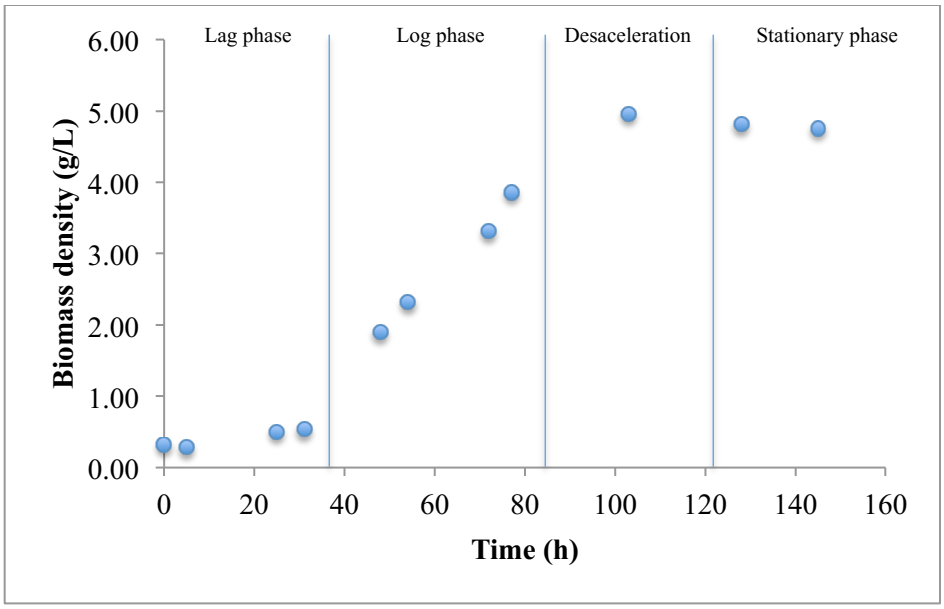

Figure 2-2 Mixotrophic batch microalgal culture (July 2013)

In the lag or adaption phase, minimal growth is observed. The duration of this phase could be reduced, if young cells adapt to new growth medium and environmental conditions before inoculation, and also if those young cells are taken from a culture that is currently growing in the log phase *(31, 38)* .

Log phase or exponential growth occurs when cell density increases exponentially with time while cells are dividing at a constant rate *(31, 38)* . This phase usually only occurs in a non-nutrient limited culture. Deceleration or linear growth happens when a decrease in logarithmic growth starts, as a consequence of the beginning of nutrient limited conditions or self-shading in systems using light as an energy source *(31)* .

When equilibrium between the maximum concentration of microalgal biomass and loss by degradation processes is reached, stationary phase takes place. The maximum viable concentration in a closed system is achieved at the start of this phase *(31)* . The stationary phase ends when the microalgal cell death rate becomes dominant, usually as consequence of limited nutrient conditions or accumulation of toxic metabolites. Eventually death rate becomes exponential *(7, 31)* .

Nutrient requirements

The main elements required for microalgae are carbon, nitrogen, phosphorous, sulfur, potassium, and magnesium. Iron is important but required in small amounts. In addition, basic minerals, such as manganese, nickel, vanadium, cobalt, zinc, boron, copper, and molybdenum are essential trace elements *(31)* .

Carbon constitutes about 50% of microalgal biomass. Its supply will depend on the type of microalgal metabolism. When algae require an inorganic carbon source, usually CO_2 enriched air or waste emissions are supplied, unless microalgae is able to utilize carbonate or bicarbonate supplied as salts. Sugars, molasses, acetic acid or even some hydrocarbons may be supplied in case microalgae is able to assimilate organic carbon sources *(31)* .

Ammonia, urea, amino acids, nitrate, and sometimes nitrite are some of the nitrogen sources used by algae. Urea has been reported to be the optimum nitrogen source for mass cultivation of *Chlorella*. Nitrogen assimilation and respiration, are interacting processes, thus they share common metabolites and enzymes *(28, 31)* .

Phosphorous is used for most cellular microalgal processes and is usually acquired as inorganic phosphate ($H_2PO_4^-$ or HPO_4^{2-}). Sulfur is part of some essential amino acids. It is generally provided as inorganic sulfate, which is usually reduced before being incorporated into cellular material. Potassium is necessary for the activity of several enzymes, protein synthesis, and osmotic regulation. Magnesium occupies a strategic position in photosynthesis, being the central atom of the chlorophyll molecule *(31)* .

Iron helps microalgae to assimilate nitrates and nitrites, deoxidize sulfate, fix nitrogen, and synthetize chlorophyll. Chelating agents, like EDTA, are used to enhance its solubility. Since trace elements play an important role during nutrient uptake and subsequently on microalgal growth by competitive mechanisms as well as by synergistic or antagonist reactions, the effect of one metal ion should consider the influence of the others *(18, 31)* .

Nutrient uptake and toxin production is influenced, for example, by the effect of detrimental shear forces on dinoflagellates. García Camacho *et al.* observed an increase

in nitrate and phosphate uptake as well as enhancing of toxin production with increased cell damage and suppressed growth in view of changes in cell metabolic activity *(41, 42)* . However, Leupold *et al*. found that morphologically robust species benefit from increasing tip speed and friction velocity, up to an optimum value, by having a positive effect on metabolic activities *(43)* . Clearly, cultivation conditions affect nutrient uptake of microalgae *(26)* .

Growth dynamics

Biochemical composition of microalgal biomass is greatly dependent on the cultivation conditions. Thus, understanding the dynamic behavior of microalgal growth is the first step to improve process design, scale-up, optimization, and control *(44, 45)* .

Microalgal systems have two important characteristics: first, the uncoupling between nutrient uptake and growth, and second, their exceptional capacity to produce specific metabolites during stress conditions. The latter may be a metabolic strategy of microalgae to survive during unfavorable conditions *(28, 46)* . In other words, during the stationary phase of growth, microalgal cultures can exhibit secondary metabolism, *i.e.*, specific metabolites can be produced after the growth phase is complete. Stationary phase may be induced, by limiting one or more variables that control growth rate. For instance, *H. pluvialis* is first cultivated continuously under nutrient replete conditions in photo-bioreactors. Later a portion of the culture is transferred to open ponds under nutrient limited conditions to induce astaxanthin production *(19, 21)* .

Microalgal cultures have different metabolic responses depending upon which nutrient is limiting. Nitrogen limiting conditions, for example, have been used to increase lipid content, since microalgae have the ability to produce and store large amounts of oil in lipid bodies under those conditions. Thus, most of the carbon available is bound into lipids. In eukaryotic algae, the most common store lipids are triglycerides (nonpolar or neutral lipids), accounting for almost 80% of the total lipid fraction. The oil stored can be used to support microalgal growth, either as an energy supply under light limited

conditions or to build membranes for the next generation. Nitrogen deficient cultures, however, will grow slower than cultures that are replete with nitrogen. It has been demonstrated that growth can be maximized when there is an intermediate availability of nitrogen. In contrast, high nitrogen concentrations inhibit microalgal growth. Therefore, kinetics of nitrogen uptake and its effect on microalgal growth is very important to optimize microalgal culture growth *(7, 28, 29, 31)* .

Specifically, De la Hoz Siegler *et al.* observed that during a single nitrogen limited batch growth of *Auxenochlorella protothecoides*, there are significant variations of oil content in microalgal cells, as a result of the balance between growth and oil production. Moreover, it was demonstrated that oil production or consumption is independent of growth despite that both processes occur simultaneously. In other words, for nitrogen-limited cultures, the initial concentration of the carbon source did not have a significant effect on the final biomass and oil concentrations; nor was the final oil concentration dependent on the initial availability of the nitrogen source. On the other hand, the lowest oil content was obtained from carbon-limited cultures. This result is expected, since lipids are composed solely of carbon, hydrogen, and oxygen. However, initial nitrogen availability affected growth and also the carbon source consumption. An intermediate level of nitrogen availability was optimal to maximize growth rate, while high nitrogen content inhibited it. Furthermore, low nitrogen concentration resulted in limited growth. This reduction in growth was the result of a nonlinear dependence of the growth rate on the initial nitrogen concentration. A simple model able to describe this effect was a pure quadratic model. Moreover, while carbon consumption occurred with an increase in biomass, depletion of nitrogen in media was observed within the first quarter of the experiment (40 h) without an immediate variation in biomass. Therefore, an uncoupling between growth and nitrogen uptake was observed. This luxury uptake prevented the use of classical unstructured models to describe the growth dynamics. As a consequence of this uncoupling, about a fivefold temporary intracellular accumulation of nitrogen compounds was registered despite a residual nitrogen concentration in media. This residue increased at the last stage of the culture, displaying how microalgal cells export amino-compounds, such as proteins and oligopeptides to the media. With the information

described above and using a structured compartmentalized cell approach that divided the cell into three main compartments (*i.e.*, metabolically active biomass, lipid body, and nitrogen pool) a model was developed to describe the effect of nitrogen and carbon substrate concentrations on biomass growth and oil production rates. The kinetic expressions that best represented the experimental observations were chosen, by considering the minimized weighted sum of squared errors (WSSE) and the Akaike and Bayesian information criteria (AIC and BIC). To build the model, it was first demonstrated that growth rate follows a hyperbolic profile with respect to the actual and the past content of intracellular nitrogen. In addition, there is a time delay between events that trigger the metabolic variation and the change itself. Therefore, the best fitting of the experimental data was obtained when an equation considering inhibition by the historical average of nitrogen content in cells was used to model the growth rate kinetics. Secondly, a Haldane inhibition model was chosen to describe the effect of glucose concentration on growth rate kinetics. Thirdly, a Michaelis-Menten kinetic expression was selected to model the nitrogen uptake rate kinetics. Finally, the best kinetic expression to illustrate oil production rate kinetics was determined to be a Michaelis-Menten type kinetic expression involving saturation by lipid content (*i.e.,* oil production rate decreases as intracellular oil content increases due to a finite storage capacity of the cell). At the end, the best fitting model was obtained when the specific growth rate was considered to follow a sigmoidal function of the external glucose concentration and the internal nitrogen concentration. This model was initially determined from batch reactor experimental data and then validated by obtaining good agreement between model predictions and experimental observations from a fed-batch culture, even when glucose and biomass concentrations were above the range used for the model calibration *(44)* .

It is relevant to emphasize that all the experimental data (*i.e.*, biomass density, glucose content in media, oil content in cells as well as total nitrogen in media and dry cells) used to calibrate and validate the model, was obtained offline. Traditional analytical methods were used, such as total suspended solids, high performance liquid chromatography (HPLC), elemental analysis, and fluorospectrometry.

2.1.3 Microalgal cultures optimization

Low yields and high production costs are two of the major drawbacks of microalgal cultures, particularly, when talking about production of bulk chemicals and biofuels *(7, 28, 44)* . By 2010, microalgal companies had to demonstrate that they have the technology to produce more than 1 000 tonnes of algal biomass or at least 440 liters of algal oil per year to their investors, in order to attract capital and grow into a commercial enterprise *(5)* . To achieve these targets economically, microalgal companies need to improve their processes (reactor design, process control, harvesting, and extraction). In 2014, large-scale commercial production of microalgae was still considered an infant industry *(12)* .

Understanding of the immediate and delayed reactions of microalgal culture dynamics to changes in environmental conditions is essential for appropriate optimization *(47)* . For example, it is important to optimize the overall microalgal process performance, taking into account the uncoupling of nutrient uptake and growth *(18, 28)* . Unfortunately, microalgal productivity and their biochemical configurations are highly affected not only by medium composition and nutrient profile, but also by the cultivation mode and its operating conditions. In addition, microalgae cultivation kinetics has an inherent nonlinear and time varying nature. Consequently, optimization of strain specific microalgal cultures depends on the informed and accurate manipulation of many interconnected factors, *i.e.*, an optimal control strategy for various nutrient streams, etc. This process requires the development of reliable dynamic models that satisfactorily describe and if necessary, simulate microalgal systems. Indeed, possessing the capability to continuously monitor microalgal systems is essential to develop a robust production system *(18, 19, 28, 44)* .

To illustrate, the model developed by De la Hoz Siegler *et al.* was used to optimize productivity of *A. protothecoides* in fed-batch cultures. It was demonstrated that high oil content for heterotrophic cultures is viable while maximizing growth rate. Regardless the

findings in autotrophic cultures that led to the conclusion that maximization of growth rates is more important than oil accumulation in microalgae *(28)* .

The objective of the optimization was to find the optimal feeding strategy for maximizing productivity of microalgal cultures. Assuming the model provided a satisfactory representation of the system, the problem was formulated as a model-based optimization. Two different approaches were used: open-loop model predictive control and adaptive model predictive control. The former implies that once the batch is finished, process data is analyzed to calculate the optimal feeding profile, which is later implemented for the duration of the next batch. The latter means that the optimal feeding profile is updated by re-estimating the model parameters as soon as new data is available, using as initial conditions the current ones *(28)* .

Adaptive model predictive control is especially suitable to reduce the possibility of mismatch when working with models whose parameters represent the sum of various interacting phenomenon. Unfortunately, this approach is absolutely dependent on the fast and accurate acquisition of the current estimated values of the process output, which ideally should be acquired through online monitoring of the process *(28)* .

Although sampling and estimation of the current values were done offline, the optimized heterotrophic microalgal culture reached a biomass production of 144 g/L and lipid productivity of 20.2 g/L×d compared to 20 g/L and 0.94 g/L×d for the non-optimal fed-batch culture. This significant increase in biomass production and lipid productivity was achieved by adjusting both the nitrogen availability, to intermediate deficient conditions, and the carbon to nitrogen ratio as well as by manipulating the feeding profiles into the bioreactor using an adaptive model predictive control strategy *(28)* .

When optimal growth is achieved, the culture has the benefit of minimum growth stress, which usually results in changes in the intracellular composition. During the work of De la Hoz Siegler *et al.* described above, it was demonstrated that high biomass productivity promotes accumulation of unsaturated fatty acids, which are more suitable for biodiesel production *(28)* . Indeed, fatty acid composition varies not only quantitatively but also qualitatively, according to the physiological status and culture conditions of microalgae *(19)* . In another example, Angelis *et al., (46)* optimized biomass and exopolysaccharides

(*i.e.* extracellular polymeric substances, EPS) production in co-cultures of microalgae and macromycetes. EPS production was enhanced during co-cultures in comparison with monocultures, and a different type of EPS was even produced. Furthermore, when glucose concentration, agitation speed, and initial pH, were further optimized, an increase of 61% in biomass and 33% in EPS production was registered. EPS are important for medical applications because they are able to stimulate the immune system. In a final example, oxidative stress, triggered either by the addition of specific chemicals or prolonged exposure to intense illumination, was deliberately induced to increase antioxidant content of microalgal cultures *(18)* .

2.1.4 Monitoring of microalgal cultures

Model based predictive control of microalgal cultures is dependent on the quality of the limited available measurable factors that influence culture composition, growth rate, and the physiological state of microalgae. Measurable parameters include temperature, pressure, pH, dissolved oxygen (DO), flow and agitation rates, liquid level, nutrient availability as well as biomass and metabolites produced *(31, 37, 48, 49)* .

Until 2012, only few technological advances to monitor algal composition were available. Indeed, biomass characterization was still in its infancy. Most algal samples were analyzed by conventional wet chemical methods with the help of gas and liquid chromatography and far from being standardized *(50, 51)* . On the other hand, by 2014, the analytical methods used to accurately determine chemical composition of microalgae-based feedstocks for biofuels production were critical for commercialization of microalgae. Efficient production of biodiesel, for example, requires suitable analysis of all microalgal products, including carbohydrates, lipids, and proteins *(52, 53)* .

Process monitoring has been classified according to the following categories *(54)* :

a) Offline monitoring, which happens when sampling is manual, and the sample is analyzed in a remote location.
b) At-line monitoring occurs when sampling is also manual but the sample is analyzed using an analyzer within the manufacturing area.

c) Online monitoring takes place when the sensor is connected to a process, and sampling is automatic. Therefore, the sensor continuously monitors a portion of the process stream.
d) In inline monitoring the whole process stream is continuously monitored, as the sample interface is located in the process.

Offline monitoring procedures

The standard process monitoring approach in bioprocess industries has been the use of traditional offline measurements. Unfortunately, they are time consuming and expensive. In addition they generate chemical waste and usually require qualified staff *(28, 50, 55)* .

The standard measure of any culture is usually the biomass concentration. Dry-weight is estimated using the common total suspended solids (TSS) method. It does not differentiate between microalgal biomass and suspended non-biological solids. On the contrary, it includes all particles collected by filtration or centrifugation. To minimize errors, it is important to wash microalgal cells with buffer in order to remove salts and contaminants, ensure that the culture is homogeneous when sampling, and execute the analysis by duplicate. Microalgae cells should be dried avoiding excess heat, usually between 80 and 110 °C. Finally, to avoid absorption of moisture, always weigh samples immediately after drying and cooling *(31)* .

Packed cell volume (PCV) is a variant of the TSS method. Here solids settle in a graduated capillary tube at the bottom of special centrifuge tubes. It is expressed as percentage of the total sample volume *(31)* .

Turbidity is a fast and nondestructive procedure for characterizing culture density. It is carried out by visual observation using a Secchi disk when water is not colored by itself. Otherwise, it is conducted by measuring absorption with a colorimeter or spectrophotometer at a given wavelength (*e.g.*, 550 nm). When a colorimeter or spectrophotometer is used, measurement is based on the scattering coefficient, which is a complex function of cell size and shape, along with the presence of any other scattering substances. Unfortunately, these circumstances can lead to erroneous results *(31)* .

Microscopic examination is used to quantify microalgae. The main disadvantages of this procedure include incorrect sampling, dilution estimation, filling of the chamber, and an extremely small sample analyzed (1 ml). It is unsuitable for microalgae that grow in colonies or with a complex morphology *(31)* .

Chlorophyll content is a complex but more selective method to estimate phototrophic microalgal biomass. After pigments are extracted from cells using a solvent (*e.g.*, 80% acetone, ethanol or diethyl ether) an absorption measurement is taken using a pure solvent as blank. The wavelength utilized depends on the solvent used. Care should be exercised to protect pigments from light in order to avoid bleaching. Cyanobacteria contain water-soluble pigments not present in other microalgal species. Therefore, determination of these pigments is an excellent qualitative and quantitative method for detecting cyanobacteria. Pigments are extracted with 0.15 M NaCl by sonication and separated by centrifugation. Absorbance is measured at 565, 620, and 650 nm *(31)* .

Microalgal cultures produce different kinds of lipids, such as triglycerides, diglycerides, phospholipids, glycolipids, and hydrocarbons. The most common approach to quantify lipid content is the macro-gravimetric method. Here lipids are extracted with the help of a suitable solvent, which is later evaporated, allowing the quantification of lipid content as the retained material. Unfortunately, this method requires a relatively large sample. It is time consuming and labor-intensive, especially when many analyses are needed *(56)* . Accuracy is dependent on the choice of the extracting solvent because algal lipids are a complex mixture of polar and nonpolar molecules. Thus, the polarity of the solvent will affect the yield of extracted lipids *(51)* .

Staining methods in combination with fluorospectrophotometry are also common methods for in vivo quantification of neutral lipids. They are also the most suitable for oil estimation of different microalgal strains *(56)* .

Determination of lipids as total fatty acid methyl esters (FAME) is one option to quantify the potential of algal biomass for biofuels production. An *in situ* trans esterification of the microalgal biomass with an acid catalyst (hydrochloric acid in methanol) is the first step in this procedure. Later the calibration of a gas chromatograph with most of the fatty

acids usually found in microalgae is required for the analysis by external standard of the sample *(57)* .
HPLC, thin layer chromatography (TLC), and mass spectrometry (MS) are techniques also used for lipid analysis but definitely not suitable for large-scale sampling *(56)* .

Total carbohydrates in algal biomass are determined as monosaccharides, after inorganic acid hydrolysis of the complete biomass. The monosaccharide concentration is quantified by HPLC, high performance anion exchange chromatography (HPAEC) or a suitable spectrophotometric method *(57)* .
On the other hand, storage carbohydrates are determined as starch. After enzymatic degradation, the released glucose is measure using either two spectrophotometric assays or one HPLC-based method *(57)* .

The recommendation to obtain the most reliable results is the simultaneous use of several methods to avoid the compromise of specificity, precision or detection limit *(31)* .

Online and inline monitoring procedures

Process analysis is used to determine physical and chemical properties during a process to enable dynamic process changes, process monitoring, and quality control. Indeed, adequate monitoring of microalgal cultures enables the efficient control of variables influencing the process performance. Moreover, utilization of analytical data for control strategies makes online and inline monitoring an integral part of process engineering and control systems *(1, 58)* .

Due to the complexity of bioprocesses, monitoring of the gas and liquid phases are necessary. With current technologies, physicochemical variables can be monitored online in both phases. Only some biological variables like biomass, chlorophyll, and other pigments concentrations can be monitored as well *(58)* . Usually monitoring of the liquid phase is the most challenging.

Process state of the bioreactor can be determined by the online analysis of gases in the headspace of the bioreactor, for example, CO_2, O_2, H_2, and volatile organic compounds (VOCs). Pressure control is crucial for correct measurements. Techniques used for this kind of analysis include: mass spectroscopy (MS), gas chromatography (GC), infrared (IR) spectroscopy, dielectric constant measurement, semiconductor gas sensors, and electronic noses (EN) *(59)* .

Autoclavable inline sensors for temperature, pH, and partial pressure of oxygen (pO_2) are routinely used in laboratory and industrial bioreactors *(49)* .

In microalgal cultivation, pH is very important. It influences directly and indirectly the microalgal metabolism (*e.g.*, it determines solubility of carbon dioxide and minerals in media). Different species of microalgae have a specific pH value or range for optimum growth. In contrast, it is influenced by composition and buffering capacity of media, amount of CO_2 dissolved as well as temperature and metabolic activity of microalgal cells *(31)* . Supply of CO_2 to microalgal cultures, is usually controlled by pH monitoring, *i.e.*, a nonspecific control procedure. Measurements are performed with a standard potentiometric ion selective glass electrode. Undoubtedly, there is a risk of error because different dissolved ions may influence pH values *(30, 49, 60)* .
Platinum resistance temperature detectors (RTD) are used as temperature sensors, which are based on measurements of the electrical resistance of a Pt wire proportional to temperature *(49)* .
Dissolved oxygen measurements are made using Clark amperometric electrodes *(49)* .

Biomass concentration is estimated online using optical density (OD), which is calibrated by offline dry weight or microscopic cell counts. However, pigments and organelles of microalgae affect light absorbance significantly. OD can be combined with fluorescence measurements. Software sensors and *in situ* microscopy have also been used *(58)* .

Chlorophyll fluorescence measurements are performed *in situ* using pulse amplitude modulated (PAM) fluorometry *(58)* .

Appropriate integrated systems for online and inline monitoring of microalgal reactors are essential to understand complex and particular biological processes like microalgal metabolism. Allowing not only the creation of mathematical models to describe the influence of several operating parameters on the non-linear behavior of microalgal cultures, but also permitting the generation of suitable control strategies. These strategies will enable online optimization of the mentioned operating parameters (*e.g.*, mixing, gassing, diluting) while improving process efficiency and productivity as well as reducing cost and environmental pollution *(28, 48, 49, 61)* . However, these advance control strategies, which represent an engineering challenge, are still not very common in process plants *(62, 63)* .

In some microalgal cultures, for example, knowing oil content as well as cell and nutrient concentration at any given moment, may allow an appropriate process control *(55)*

NIR spectroscopy has the potential of providing a quick monitoring of microalgal cultures because it collects data easily. Therefore, it will compliment traditional methods, which will greatly contribute to bioprocess monitoring and control in both the research laboratory and the industrial production of microalgae *(56)* .

Enhanced process monitoring will lead to efficient bioconversions (*i.e.*, decreased costs of production, separation, and purification). These improvements are needed to achieve a competitive large-scale microalgal production with conventional processes *(7, 18, 64)* .

2.2 Infrared and Raman spectroscopy

Spectroscopic methods offer a noninvasive and nondestructive method to monitor continuous biological processes, where multivariate chemical information is obtained *(28)* . As described in the previous section, many of the traditional methods for characterizing the chemical composition of biomass are laborious, expensive, and destructive. More modern analytical techniques often involve the measurement of optical phenomena, since optical measurements obtained from the interaction between radiation and matter enable a rapid acquisition of a variety of analytical information. Optical properties of liquids, for example, depend on their composition *(65)* .

2.2.1 Basic principles

Infrared and Raman spectroscopy are complementary techniques. Their simultaneous application can be highly advantageous when characterizing a molecular structure because for a complete description of the vibrational motion of a molecule both techniques are needed *(60, 66)* .

In IR spectroscopy, the infrared light absorbed by the sample is measured as a function of the frequency of IR-active vibrational transitions. On the other hand, in Raman spectroscopy, an intense laser beam irradiates the sample, and the light scattered by a Raman-active vibration is observed. In both cases the associated energy depends on the structure of the molecule. IR-active vibrational transitions are those which dipole moment changes (*i.e.*, sensitive to polar functionalities, C=O) while Raman-active vibrational transitions are those in which polarizability changes (*i.e.*, sensitive to vibrations of homonuclear bonds, C=C). Indeed, symmetric vibrations are Raman-active, and anti-symmetric vibrations are IR-active. This effect is known as the mutual exclusion principle, and it is applicable to any symmetric molecule. Therefore, vibrations of covalent bonds are strong in Raman spectra. In contrast, ionic bonds are strong in IR spectra. Indeed, Raman spectroscopy is suitable for analysis of biological compounds in aqueous solutions because water is a weak Raman scatterer. However, water has strong absorption when using IR spectroscopy, interfering with the absorption signal from other compounds *(67)* .

IR spectroscopy comprehends far infrared (25 – 100 mm), mid infrared (MIR 2.5 – 25 mm), and near infrared (0.8 – 2.5 mm) ranges of the electromagnetic spectrum. In the MIR range fundamental vibrations are excited, and characteristic features as well as peaks can be assigned to specific chemical groups. MIR spectroscopy is a powerful tool for qualitative analysis, compound identification, and structure analysis. It is usually referred to as the fingerprint region. On the other hand, in the NIR range detection of overtones and combinations of molecular vibrations result in complex spectra, characterized by broad and overlapping features *(68-70)* .

2.2.2 Raman spectroscopy

It is possible to identify specific compounds (*e.g.*, lipids) using Raman spectroscopy, as the spectrum created by inelastic scattering, it is determined by molecular bonds of the compounds in the sample, generating a fingerprint *(55, 71)* .

Inelastic scattering occurs when the molecule is excited to a virtual energy state by exposing it to a monochromatic laser light of specific frequency (from the visible to the near infrared region), resulting in two possibilities. First, the molecule may return to the first excited vibrational level, instead of its original ground state, emitting a Raman line (Stokes line) of lower frequency. Second, the molecule may return to the ground state after starting from the first excited vibrational level, emitting a Raman line (anti-Stokes line) of higher frequency (see Figure 2-3). In either case the frequency difference corresponds to the fundamental transition. Stokes lines are usually used for Raman spectroscopy *(67)* .

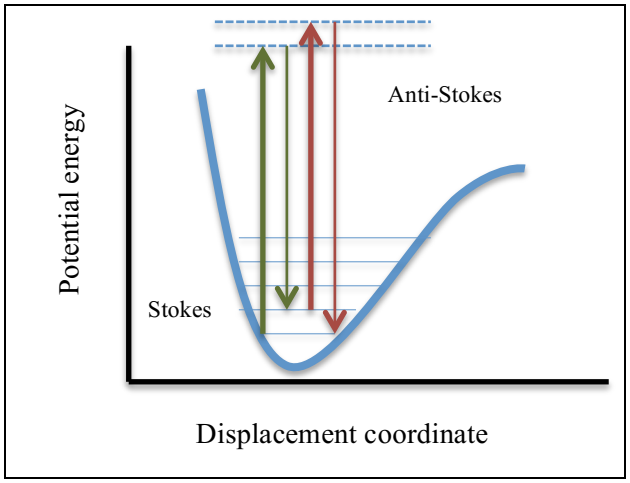

Figure 2-3 Stokes and Anti-Stokes lines produce by inelastic scattering

Raman scattering is very weak in comparison with the incident beam and is measured in the UV-visible region *(67)* .

Previous work

In a previous work within my research group, an online multivariate sensor, using Raman spectroscopy, was developed. This sensor was designed to monitor biomass, oil, and glucose concentrations in microalgal cultures. The Raman spectra generated were convoluted as a consequence of the high number of compounds present. An immersion probe with excitation wavelength of 785 nm was used to collect the data. Although, it was demonstrated that fluorescent background was present in the sample causing interference with glucose determination, the model built for glucose concentration was acceptable. Likewise, the sensor was robust for biomass determination but it was suggested to exercise caution for oil content estimation. This uncertainty was comparable to the one of the experimental procedures existing at that point, since all of them were prone to a considerable error. Given these points, the model built was validated, by comparing the model predictions for fed-batch cultures, using the set of parameters estimated from batch experiments, during online estimation in the bioreactor. It was found that there was a good match between Raman predictions and experimental measurements overall. Nevertheless, during the first 50 h of the culture, high variance was observed in glucose and oil determinations. Probably, as a result of the significant number of changes, both in the culture media and in the microalgal cell, during that lapse of time *(55)* .

Fluorescence is one disadvantage of using Raman spectroscopy in biological samples. It is generated when the incident beam wavelength is closer to the electrical excitation wavelength of compounds in the sample than to their vibrational excitation. The 785 nm red laser reduces fluorescent background and improves the signal in comparison with a 532 nm green laser *(71)* .

2.2.3 Near infrared spectroscopy

NIR spectroscopy is a fast, accurate, and nondestructive analytical technique, which often does not require sample preparation. If the analyte exceeds around 0.1 %, NIR

spectroscopy will usually offer acceptable results. In routine analysis, it is not a requirement to have specialized training; however, previous work may be needed for data interpretation, such as a chemometric method. Without a doubt, chemometric methods together with fiber optics, probes, and miniaturization are making NIR spectroscopy a valuable tool for industrial quality control and process monitoring, even when overlapped bands strongly decrease the specificity of NIR spectroscopy *(60, 67, 72)* . The petrochemical industry was a pioneer in recognizing the value of the NIR technique as an online tool and implementing it, which has led to improve process stability, pollution control, and more accurate blending procedures *(54)* .

Some of the main advantages of process analyzers based on NIR spectrometers are *(54)* :

- Frequent and touchless online analysis of multicomponent systems.
- Applicable for remote analysis.
- Operable in hostile environments.
- Appropriate for liquids and any morphology of solid samples.
- Pollution free, since no solvents are required.

In NIR spectroscopy, the sample absorbs specific frequencies from a polychromatic source, corresponding to overtone (*i.e.,* transition between energy levels) or combination vibrations *(67)* . Spectra of agricultural samples, for example, are composed of broad peaks as a consequence of the overlapping absorptions caused by overtones and combinations of vibrational modes involving C-H, O-H, and N-H molecular bonds *(54, 72)* . See Table 2-1 *(73)* . Overtone and combination vibrations generally have lower intensities (by a factor of 10 to 100 for each step) than their correspondent fundamental vibrations in the MIR range. This characteristic allows an adjustment on sample thickness (from millimeters up to centimeters) or volume when working with NIR spectroscopy. In addition, occurrence, frequency, and intensity of overtone and combination bands depend directly on the anharmonicity of the vibrating atoms. Polytetrafluoroethylene is used as NIR non-absorbing standard material (Spectralon®) as a result of the small anharmonicity constant despite the large dipole moment of the C-F bond *(60, 67)* .

Table 2-1 Frequencies of bond absorptions for generic functional groups

Wavelength (nm)	Bond vibration	Structure
1 143	C-H second overtone	Aromatic
1 160	C=O stretch fourth overtone	C=O
1 170	C-H second overtone	.HC=CH
1 195	C-H second overtone	$.CH_3$
1 215	C-H second overtone	$.CH_2$
1 225	C-H second overtone	.CH
1 360	C-H combination	$.CH_3$
1 395	C-H combination	$.CH_2$
1 410	O-H first overtone	ROH, Oil
1 415	C-H combination	$.CH_2$
1 417	C-H combination	Aromatic
1 420	O-H first overtone	ArOH
1 440	C-H combination	$.CH_2$
1 446	C-H combination	Aromatic
1 450	O-H stretch first overtone	Starch, H_2O
1 450	C=O stretch third overtone	C=O
1 460	Sym N-H stretch first overtone	Urea
1 463	N-H stretch first overtone	$.CONH_2$
1 471	N-H stretch first overtone	CONHR
1 483	N-H stretch first overtone	$.CONH_2$
1 490	N-H stretch first overtone	CONHR
1 490	O-H stretch first overtone	Cellulose
1 490	Sym N-H stretch first overtone	Urea
1 492	N-H stretch first overtone	$ArNH_2$
1 500	N-H stretch first overtone	.NH
1 510	N-H stretch first overtone	Protein
1 520	N-H stretch first overtone	Urea
1 530	N-H stretch first overtone	RNH_2
1 540	O-H stretch first overtone	Starch

Table 2-1 (cont'd) Frequencies of bond absorptions for generic functional groups

Wavelength (nm)	Bond vibration	Structure
1 570	N-H stretch first overtone	CONH
1 620	C-H stretch first overtone	$=CH_2$
1 685	C-H stretch first overtone	Aromatic
1 695	C-H stretch first overtone	$.CH_3$
1 705	C-H stretch first overtone	$.CH_3$
1 725	C-H stretch first overtone	$.CH_2$

In the near infrared range (780 to 2 500 nm), water absorbance peaks are less broad and strong than in MIR range, which reduces the risk of missing valuable spectral information related to low concentration analytes. However, in biological applications where high water concentrations are present (above 80%), NIR determinations are strongly influenced by the spectral signature of water with peak absorptions at 970, 1 190, and 1 450 nm *(72, 74)* . It is also important to remember that the hydrogen-bonding network of water molecules is not only sensitive to temperature changes but also to changes in concentration of dissolved salts and biopolymers, such as proteins or carbohydrates as well as to changes in pH. As a result, the overtone and combination bands show large variance when aqueous samples with wide variation in composition are analyzed *(54)* .

Reflectance

The return of radiation by a surface or specifically an interface, without a change in wavelength, is called reflection *(75)* . Reflectance spectroscopy has the potential to reveal compositional information, by detecting the wavelengths of light that are reflected. Depending upon the wavelength, light that is not reflected from the sample is absorbed, scattered, or transmitted according to the chemical composition of the sample *(76)* .

If a surface absorbs at specific wavelengths of light, the relative intensity of the light decreases. Generally, the intensity of the light reflected depends on the angle of incidence as well as the refractive index, surface roughness, and of course, absorbability of the sample *(77)* . Therefore, reflectance spectroscopy is a convenient tool for qualitative and quantitative analysis. It is widely used to determine optical properties of turbid materials

(*e.g.*, milk and fruit juices) and to characterize films as well as surfaces *(78-80)* . One of the main benefits of reflectance spectroscopy is the absence or minimal sample preparation. With adequate calibration, infrared reflectance spectroscopy (IRS) is able to provide accurate concentration estimates for multiple components *(50)* .

For a thin layer (0.5 – 20 mm) the reflectance spectrum is similar to a transmission spectrum, while for a monomolecular layer, the spectrum is predominantly a function of the refractive index. The refractive index is defined as the ratio of speed of light in vacuum to the speed of light in the material of interest and depends on the solution composition *(65, 81)* .

In general, there are two types of reflection: specular (where the angle of incidence is equal to the angle of reflection) and diffuse (where the angles of incidence and reflection are different). While most surfaces return both specular and diffuse reflections, some may return mostly specular reflections and others predominantly diffuse reflections *(75)* .

Specular reflectance spectroscopy is a nondestructive method where the mirror-like reflection, which is proportional to the amount of gloss on a shiny surface, is used for the characterization of surfaces as well as coatings or thin films deposited on or pressed against a solid reflective surface (substrate) *(75, 77)* . Testing of lubricated surfaces, degradation studies of protective coatings, and analysis of polymers on the surface of food containers are only some of the different uses of specular reflection. To illustrate, it was observed that specular reflection of plastic encoder wheel samples, a component in a motor that is used for monitoring rotation and speed, decreased significantly (up to 84%) when sandblasting was applied on them *(76)* . On the other hand, the specular reflection from a thin film of aluminum chrome alloy on cured powder-coated wheels was observed to increase proportionally to deposition time *(82)* . These experiments show how smooth surfaces have higher specular reflection because most of the incident light is reflected in the same direction while rough surfaces increase the amount of diffuse reflectance *(83)* .

When working with thin films on a reflective substrate, specular reflectance is similar to a "double-pass transmission". Any wavelength not absorbed or scattered by the surface of the film or molecules within the film will reach the substrate making possible to collect specular reflection from the interfaces at the surface and also at the substrate after the beam has passed twice through the film. Both reflections may add together constructively or destructively, depending on the difference in their optical path lengths, which are determined by the film thickness, optical constants, and the wavelength of light used. These kind of specular reflectance spectra are usually of high quality and similar to the ones obtained from transmission measurements *(72, 84, 85)* .

An example of reflectance spectroscopy is the analysis of blood. Quantitative determination of the absorption of blood volume fractions in turbid media was successfully achieved by noncontact reflectance spectroscopy using a QR400-7-UV-BX probe, fixed at 17 mm and 13 ° angle from the sample. Baseline for these experiments was recorded using media without absorbers. The effective photon path range determined for this experiment was from 0.5 mm, at the maximum absorption, to 4 mm for the minimum adsorption of the solution *(78)* .

2.3 Fiber optic chemical sensors

According to the Cambridge definition, "Chemical sensors are miniaturized devices that can deliver real-time and online information on the presence of specific compounds or ions in even complex samples" *(86)* .
Analytical results of chemical sensors should be validated according to the following expressions: accuracy and precision. While chemical sensor performance can be characterized using the following criteria: Sensitivity, detection limit, dynamic range, selectivity, linearity, resolution, response time, stability, and life cycle *(65)* .

Optical methods are non-invasive and non-destructive *(49)* . The ideal optical sensor should also be highly sensitive and selective. For complex systems, interference should be minimized, and the optical signal deconvoluted *(87)* . In addition, it should be

developed to achieve maximum mobility and minimal dimensions *(65)* . Finally, the appropriate sensor should be rapid, robust, automated, and inexpensive while delivering versatile intracellular information *(50, 63)* . Unfortunately, major problems concerning optical methods include sensitivity to fouling, and also to the presence of turbidity and gas bubbles. Measurement noise is also usually higher than in other methods *(49)* .

One of the major application fields of fiber optic based sensors is bioprocess control where the sensor should also have the ability to endure sterilization as well as long-term stability *(49, 86)* . The adequate bioprocess sensor has to be developed in agreement with the specific demands of the process *(49)* .

2.4 Chemometrics

Chemometrics is a discipline that combines math with statistics to extract the most important information within huge data sets from samples of varying complexity. It was first introduced in 1972. It represents an opportunity to upgrade analytical and control functions in industrial processes with real time chemical analysis and control. In other words, chemometrics has addressed the challenge of moving from data to information to knowledge of the process. It is applied in two different ways for bioprocess monitoring, either to predict key process variables or to picture the course of the culture by identifying the response patterns of the used sensor systems to specific characteristics. Accordingly, one important component of chemometrics is multivariate data analysis, which is the core of qualitative and quantitative determinations of multicomponent assays on NIR spectroscopy. Multivariate calibration converts several wavelengths into precise and relevant information *(54, 63, 88-91)* .

Even NIR spectra of chemically simple substances have numerous broad bands that usually overlap (see Table 2-1). Therefore, identification of these bands, and their assignment to specific chemical bonds can be very difficult. Furthermore, spectra may be perturbed by the interaction of radiation with the physical structure of the sample which results in diffuse reflection *(54, 92)* .

In NIR spectroscopy, quantitative analysis is based on Beer's Law. According to this law the amount of light transmitted through a material decreases exponentially. As a result, Beer's Law states that there is a linear relationship between molar concentration of a substance and its absorbance, at a given wavelength. Absorbance is equal to the difference between the logarithms of the intensity of the light entering the sample and the intensity of the remaining light *(54, 70, 92)* :

$$A = \log I_0 - \log I = -\log(I/I_0)$$

Where:

A = Absorbance

I_0= Intensity of incident optical radiation

I= Remaining intensity after interaction (transmission or reflection) with the sample

The ratio I/I_O is called transmittance (T) when radiation is transmitted through the sample or reflectance (R) when radiation is reflected by the sample. Therefore, absorbance can also be written as *(54)* :

$$A = \log(1/T) = \log(1/R)$$

It is important to note that relative absorbance is usually measured by using a reference material. In the first place, the intensity of light transmitted through the reference is measured, later the same type of measurement is performed using the sample. Relative absorbance is obtained from the following equation *(54)* :

$$As(l) = As^*(l) - Ar^*(l)$$

Where:

$As(l)$ = Relative absorbance of the sample at l nm

$As^*(l)$ = Absolute absorbance of the sample at l nm

$Ar^*(l)$= Absolute absorbance of the reference at l nm

Note: $Ar^*(l)$ should be constant during the length of the work.

Beer's Law then relates concentration to absorbance in the following equation *(54)* :

$$A = e(d)C$$

Where:

e = molar extinction coefficient $(mol/L)^{-1}cm^{-1}$

d = path length (cm)

C = molar concentration

If concentration is stated as a function of the absorbance (inverse model), a linear calibration model is obtained:

$$C = A(b_1) + b_0$$

Here parameters b_1 and b_0 are determined by calibration, where at least two samples with known concentrations and absorbances are required.

Very often NIR spectra contain variation from numerous sources that are not of a predictive nature. Therefore, the typical approach for the evaluation of NIR data is first to pre-process the spectra (smoothing or standardization) and then to calibrate a model. Thus, data is usually split in two subsets. One subset is used for calibration modeling while the second is used for prediction testing with independent data *(54, 68)* .

2.5 Capillary open channel flow

One method to develop a robust sensor is to employ a noninvasive approach that uses a fiber optic sensor imaging a free flowing liquid surface.

If liquids are transported from one location to another, using structures open at the top (*i.e.*, open channels), the flow is referred to as open channel flow. The free surface is usually exposed to atmospheric pressure. This kind of flow is, in general, more complicated than flow in pipes *(93, 94)* .

2.5.1 Classification

When describing a flow field, it is convenient to think of individual particles. Each particle is considered a small mass of fluid, which consists of a large number of molecules, occupying a small volume, and moving with the flow *(95)* .

Open channel flows are classified into various types *(93-98)* :

Steady flow: when the flow velocity and the liquid depth at a given point do not change with respect to time, thus local acceleration is zero.
Unsteady flow: if flow velocity and depth at a given point change with respect to time. Its analysis is usually more complex.

Uniform flow: if flow velocity at a given instant of time does not vary within a given length of the channel (either in magnitude or direction), *i.e.*, velocity profile and depth at all cross-sections along the length of the channel remains the same. In other words, the accelerating (component of the weight of the fluid in the downstream direction) and resistive (shear stress at the bottom and sides of the channel) forces are equal along the length of the channel.
Non-uniform flow: when the flow velocity at a given time varies with respect to distance, *i.e.*, depth of the liquid continuously varies from one section to another.

Laminar flow: when fluids flow with no significant mixing of neighboring fluid particles, showing a smooth and regular pattern of movement in definite paths so that the flow apparently moves as thin layers on top of each other. Viscous forces dominate.
Turbulent flow: if liquid particles move in irregular paths so that quantities such as velocity and pressure vary with respect to time and space. Inertial forces dominate.

Table 2-2 shows the classification for each regime depending on the geometry used for the flow.

Table 2-2 Classification of flows according to Reynolds number

	Pipe flow	Channel flow
Laminar flow	< 2,000	< 600
Turbulent flow	> 4,000	> 2,000

Reynolds number is the ratio of inertial and viscous forces:

$$Re = (VL)/\nu$$

Where:

V = mean flow velocity (m/s)

L = characteristic length (m)

ν = kinematic viscosity (m^2/s)

In free surface flows, either hydraulic depth (*i.e.*, the flow area divided by the top width) or hydraulic radius R_H (*i.e.*, the flow area divided by the wetted perimeter) may be used as the characteristic length. Flow area (A) is the cross-sectional area of flow normal to the direction of the flow. Top width is the width of the channel section at the free surface. The wetted perimeter (WP) is the length of the intersection line of the wetted channel surface with a cross-sectional plane normal to the flow direction (see Figure 2-4). In the case of Reynolds number, hydraulic radius was used as characteristic length.

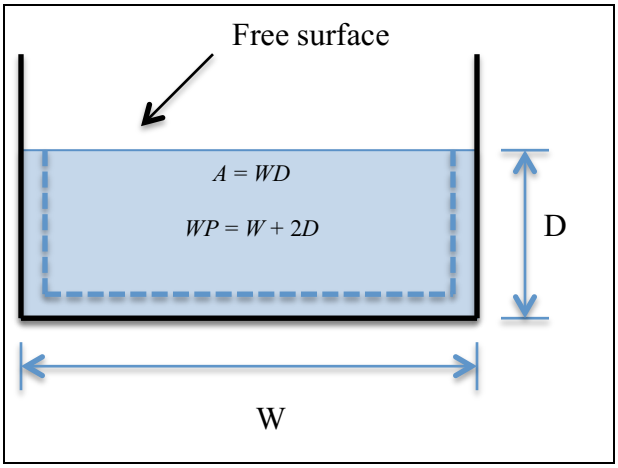

Figure 2-4 Cross-sectional diagram of a rectangular channel

Laminar open channel flows are very unusual in real life applications. Smooth and glassy flow surfaces may be the result of the surface velocity being less than that required to form capillary waves. Small depths may produce laminar flows in open channels.

The key dimensionless parameters responsible for the free surface regime are the Froude and Weber numbers.

Froude number (*Fr*) is the ratio of inertial and gravitational forces. It is used to classify open channel flows into subcritical, critical, and supercritical flows, depending on the value of the critical velocity. Critical velocity is the velocity of a gravity wave having small amplitude. In a subcritical flow ($Fr < 1$), flow velocity is less than the critical velocity (*i.e.* the velocity of the liquid is small, which allows a small disturbance in the flow to travel against the flow and affect the conditions upstream), and depth is greater than the critical depth. In a critical flow ($Fr = 1$), flow velocity is equal to the critical velocity. Finally in a supercritical flow ($Fr > 1$), flow velocity is greater than the critical velocity (*i.e.* a small disturbance cannot propagate upstream), and depth is less than the critical depth.

For a rectangular channel, Froude number is defined as:

$$Fr = V/(gy)^{1/2}$$

Where:

y = hydraulic depth (m)

g = standard acceleration due to gravity (9.8066 m/s^2)

The effective Froude number increases as the inclination angle of the flow (α) increases, since the component of gravity perpendicular to the free surface vary as $g_I = g \cos \alpha$.

The Weber number is important when the surface curvature is comparable in size to the liquid depth (*e.g.* droplets, capillary flows, ripple waves and small hydraulic models). It is the ratio between inertial forces and surface tension forces.

$$We = (\rho V^2 L)/\Upsilon$$

Where:

ρ = density (kg/m^3)

L = characteristic length (m)

Υ = surface tension (N/m)

In the case of Weber number, mean flow thickness was used as characteristic length. In the regime of weak turbulence, Fr and We are small (<<1), which means that there is little or no surface disturbances due to the stabilizing effect of the capillary and gravity forces. In strong turbulence (Fr >>1 and We>>1) neither surface tension nor gravity can restrain fluctuating eddies. In between there is a transitional region where the free surface is substantially disturbed but not broken. There are two more regions where surface is not disintegrated, for each one either gravity or surface tension is dominant.

2.5.2 Velocity distribution

Flow velocity in the channel varies from one point to another due to shear stress (at the bottom and at the sides of the channel) and to the presence of the free surface. Therefore, series of boundary layers are formed successively, which leads to a parabolic distribution of the velocity of motion. Velocity profiles are quite complex, with a maximum velocity in the mid-plane about 20 percent below the surface. Components of velocity in the vertical and transverse directions are usually neglected owing to its minimal contribution. Thus, only the flow velocity in the direction of the flow is considered. Since the flow velocity is parallel to the channel bottom, there is no acceleration in the vertical direction *(93, 99)* .

2.5.3 Resistance equation

Flow at the center of the channel is influenced by side-wall effects, if the flow aspect ratio (*W*/*D*) is lower than 40. The boundary shear stress is defined in the following equation for a steady uniform flow down an inclined plane.

$$\tau_o = \gamma \sin \alpha \, R_H$$

Where:

γ = specific weight of the liquid (ρg)

If the channel flow is not uniform, the previous equation holds only approximately; the error introduced depends on the degree of uniformity *(98, 100)* .

2.5.4 Continuity equation

When working with incompressible liquids (*i.e.*, mass density of the liquid is constant), the law of conservation of mass implies that volumetric flow rates at all sections are equal, provided that no inflow or outflow exists *(93)* .

$$V_1 A_1 = V_2 A_2$$
$$Q_1 = Q_2$$

2.5.5 Surface tension

The surface tension coefficient of a liquid is defined as the ratio of the surface free energy (Gibbs free energy, G) with respect to the surface area of the liquid. It represents the mechanical features of attractive interaction among the molecules on the surface of the liquid. Surface molecules are more attracted to molecules within the liquid (*i.e.*, cohesion) than to molecules of the gas at the surface, which causes the maximum number of surface molecules to enter the bulk of the liquid, minimizing the surface area.

Surfactants, some salts, and many organic molecules lower the surface tension of water because they sit in the surface attracting the surface water molecules. For all liquids, surface tension decreases as temperature rises *(94, 99)* .

Surface tension forces are important when capillary waves appear, and in the flow of a thin sheet of liquid over a solid surface *(94)* .

Surfactants

Surface tension of liquids can be modified by the addition of surfactants. A surfactant is a molecule with two parts. One part has an affinity to nonpolar media, and the other has an affinity to polar media. The hydrophobic part is usually formed, by one or more aliphatic chains. On the other hand, the hydrophilic part can be an ion (polar head), which has an affinity to liquids like water. Surfactants will remain at surfaces or interfaces forming oriented monolayers, so that each part can be in contact with the environment for which has the greatest affinity. When they accumulate at the liquid–vapor interface, surface tension decreases. The same behavior is observed with respect to contact angle, *i.e.* as the surfactant concentration increases, the contact angle decreases. Increase in concentration does not change the state of the surface, all additional surfactant molecules aggregate in micelles *(101-103)* .

2.5.6 Capillarity

Young's equation is the basic equation to describe capillary phenomena at surfaces. It relates the interfacial tensions (σ) between a solid (*s*), a liquid (*l*), and a vapor (*v*) phase using the contact angle that the liquid-vapor interface forms with the solid wall, following a mechanical equilibrium at the point where the three phases meet *(104)* .

$$\cos\theta = (\sigma_{sv} - \sigma_{sl})/\ \sigma_{lv}$$

Contact angle (θ) is used to determine the wettability of a solid material by a liquid. If it is less than 90°, the liquid wets the solid; if θ > 90°, the liquid is designated nonwetting (see Figure 2-5) *(105, 106)* .

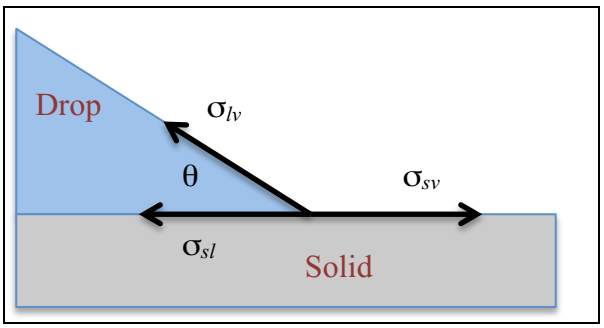

Figure 2-5 Three phase contact line of a liquid drop on a solid substrate

When a three-phase contact line (the line that separates wet regions from dry regions) is present, the speed at which a liquid can move over a solid surface is strongly affected (*i.e.* a macroscopic flow can be highly affected by physicochemical interactions with the substrate at molecular scales. If the liquid is forced to flow over a surface that it does not spontaneously wet in thermodynamic equilibrium, an interesting situation arises because it is energetically favorable for the liquid to leave most of the surface dry. In other words, if an external driving push the system away from the equilibrium, it undergoes a dynamical wetting transition *(107)* .

Fluctuations of the contact line around its average position are affected by roughness of the surface. Usually the contact line moves very slowly when it remains pinned on some defects *(108)* .

2.5.7 Unsteady flow

Unsteady conditions may be produce by waves. A wave is defined as a variation of the flow depth and the rate of discharged. It can be a temporal variation (when wave varies with respect to time) or a spatial variation (if the wave varies with respect to distance). In a shallow channel, the entire flow depth is disturbed as a wave passes a section. In this case, the ratio of the wavelength to the depth is greater than 20. When the scale is small,

velocity of propagation of any surface wave is greatly governed by surface tension forces. The velocity of waves with wavelength (λ) around 3 mm is affected by gravity by only 1.5%. Here the significant force ratio is inertia force/surface tension force. Surface tension force is tangential to the surface. Its presence drastically changes the dynamic boundary condition. The presence of pressure forces needs to be separately considered *(93, 94, 109)* .

If dissipation is neglected and flow is assumed two-dimensional, waves approach uniform wave trains, travelling at constant velocity. If a frame of reference moving with the wave is chosen, the flow can be considered steady. Waves with $\lambda < \lambda_{min}$ are dominated by surface tension and can be approximated by pure capillary waves for λ small *(109)* .

$$\lambda_{min} = 2\pi/k_{min}$$

$$k_{min} = (\rho g/ \Upsilon)^{1/2}$$

Where:

k_{min} = minimum wavenumber (m^{-1})

It is also useful to look at waves from a fixed point of view, where waves pass at constant velocity.

In open channels of small sizes (*e.g.*, 4 mm), a vapor liquid interface (meniscus) establishes through the free surface. The equilibrium shape of the meniscus results from the balance between surface tension and gravity. This balance is governed by the capillary length l_γ.

$$l_\gamma = (\Upsilon/ \rho g)^{1/2}$$

When the width of the channel is much larger than the water capillary length (~2.7 mm) the effect of gravity is predominant on the capillary force. The common criterion to differentiate between small and conventional size channels in engineering applications is 3 mm.

The interface is affected by surface tension and channel wall wettability, where the velocity profile is influenced by the surface-shape. The pressure generated by the surface tension, which tends to reduce the surface, is equilibrated by the capillary pressure (acting in direction of the coordinate z, see Figure 2-6), which tends to increase the surface.

The interplay of these forces explains the capillary rise or depression. Unless these forces are equivalent the boundary becomes curve with a resultant force towards the concave side. This resultant must be balance by a greater pressure at the concave side of the surface. The Young-Laplace formula links the pressure difference (ΔP) with the two main radii of curvature (R_{yz} and R_{xz}) and the surface tension of the air/liquid interface *(94, 107, 110-112)* .

$$\Delta P = P_a - P_l = \sigma\,(1/R_{yz} + 1/R_{xz})$$

Where:

P_a = Air atmospheric pressure

P_l = Liquid phase pressure

R_{yz} = Radius lying on the plane yz

R_{xz} = Radius lying on the plane xz

Figure 2-6 Diagram of an open channel flowing in direction of the coordinate x

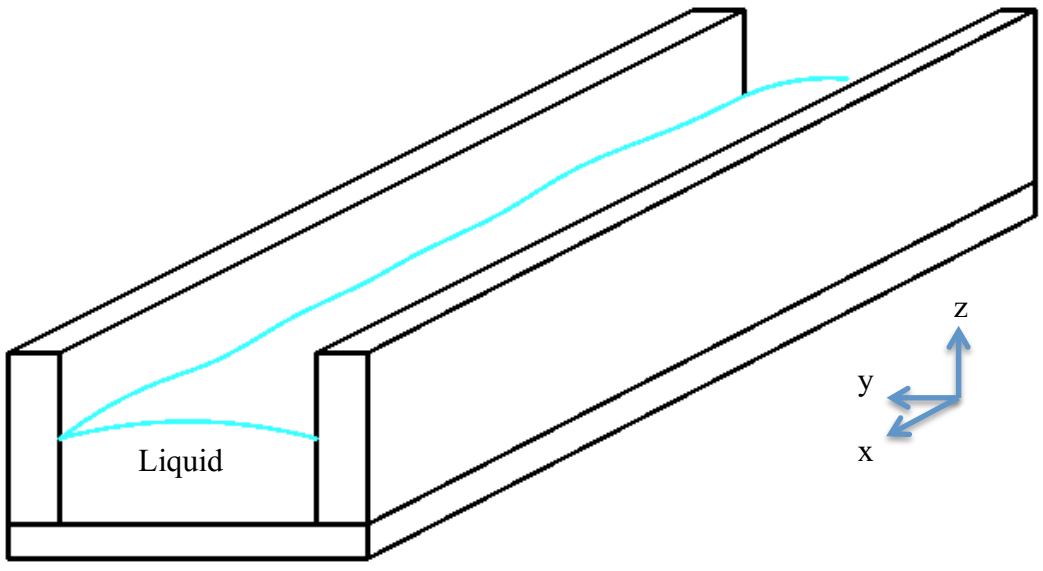

3

Materials and Methods

This chapter describes the materials required, and the analytical methods used to estimate process variables of interest.

3.1 Spectrometric setup

3.1.1 Spectrometer

The spectrometer used was a NIR-512 with a Hamamatsu detector G9204-512 InGaAs linear array and a wavelength range from 900 to 1 700 nm. The detector was operated at ambient conditions *(113)* .

3.1.2 Light source

The light source used was a LS-1 Series tungsten halogen white-light lamp with a VIS-Shortwave NIR range from 360 to 2 000 nm and equipped with a 10 000 hour, 2 800 K bulb. The lamp was allowed to warm up at least 30 minutes before it was used. In order to generate a dark spectrum, light was blocked, by inserting a metallic barrier in the 3 mm slot located between the lamp and the fiber coupler, as can be seen in Figure 3-1 *(114)* .

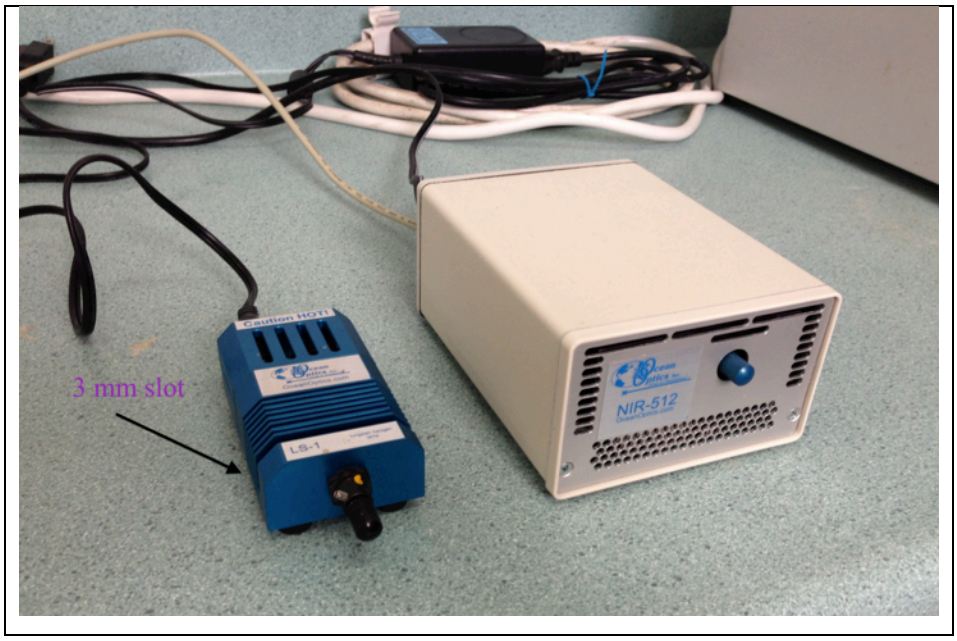

Figure 3-1 Spectrometer NIR-512 and lamp LS-1

3.1.3 Software

SpectraSuite® Spectrometer Operating Software by Ocean Optics was used for control of the spectrometer, real-time display, and collection of spectral data.

3.1.4 Reflectance probe

The probe used to collect data was a sterilizable premium reflection probe (QR400-7-VIS-BX from Ocean Optics). It is ideal for measuring diffuse or specular reflectance because it collects light from the same angle at which the sample is illuminated. This probe has seven optical fibers. Six of them are illumination fibers located around one read fiber, all placed in a stainless steal ferrule. Light travels through the illumination fibers to project six cones of light, which form a zone where the light overlaps in the center at the sample. This zone is exactly the place where the read fiber collects the reflected light to take it back to the spectrometer (see Figure 3-2). The reflection probe has precision SMA 905 connectors to attach it to the spectrometer *(115, 116)* .

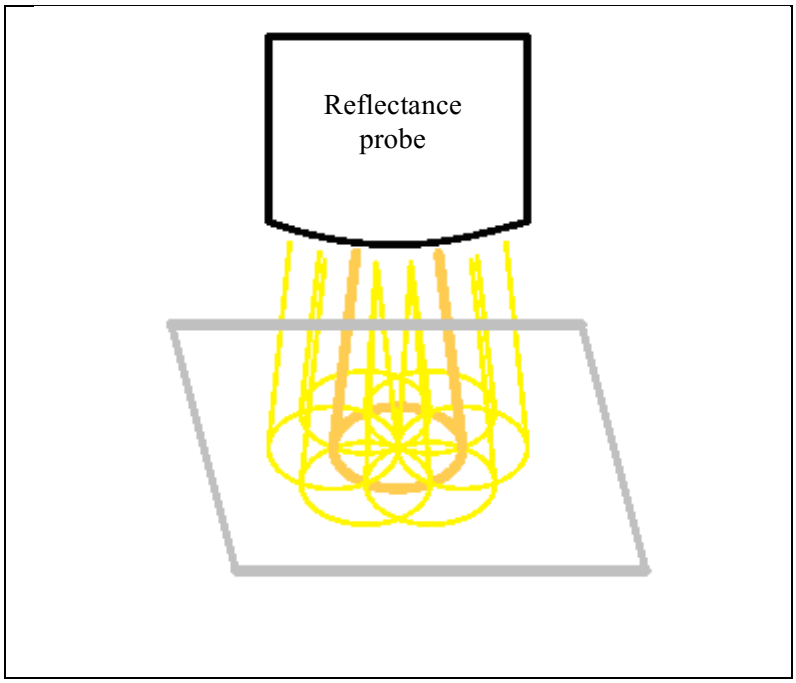

Figure 3-2 Six cones of light overlap and generate reflected light

3.2 Reference analytical methods

In the following section, the analytical methods used to determine biomass, glucose, and oil content are described.

3.2.1 Cell count and cell size distribution

Beckman Coulter Z2 Particle Count and Size Analyzer, was used to determine cell count and cell size distribution. The instrument was calibrated with a standard within the range of the typical cell size of *A. protothecoides* (3 to 6 μm). The standard used was Coulter CC Size Standard L5. The instrument configuration is shown in Table 3-1. Samples were diluted with Isoton® II solution using dust free Beckman Coulter Counter® Accuvette ST 25 mL vials and caps.

Table 3-1 Beckman Coulter Z2 particle counter and size configuration

Parameter	Value	Units
Select aperture	100	μm
Range	3 – 9	μm
Resolution	256	
Gain	128	
Current	1	mA

3.2.2 Cell dry weight

Total suspended solids method was used to determine biomass concentration. Graduated microcentrifuge tubes (1.5 mL) were brought to constant weight after 48 h drying at 75 °C, and their weight was recorded. All dried centrifuge tubes were weighed 20 min after they were removed from the drying oven. An aliquot of 1.4 mL from a thoroughly mixed sample was transferred to a microcentrifuge tube and centrifuged at 10 000 rpm during 10 min. The pellet was re-suspended, washed with 50x diluted saline phosphate buffer solution, and centrifuged again. After the final pellet in the microcentrifuge tube was dried at 75 °C for 48 h, the final weight was recorded. The average relative standard deviation was 3.2% for duplicate determinations of samples with biomass concentrations ranging from 3 to 13 g/L.

3.2.3 Glucose quantification

The supernatant obtained when samples from microalgal cultures were centrifuged at 10 000 rpm, was filtered using 0.2 mm syringe filters, and analyzed in an Agilent 1200 Series HPLC. The chromatograph was equipped with guard column and a SupelcoGel Pb carbohydrate column, at 70 °C. The eluent was Milli-Q® water. A refractive index detector operated at 35 °C was used. Specifications of the method are listed in Table 3-2. The method was calibrated by external standard method using a curve built with glucose solution standards from 0.1 to 60 g/L with a correlation coefficient of 1.000

Table 3-2 HPLC Glucose quantification method specifications

Parameter	Value	Units
Column internal diameter	7.8	mm
Column length	30	cm
Injection volume	10	mL
Flow rate	0.5	mL/min
Stop time	30	min
Post time	10	min

3.2.4 Neutral lipids quantification

Gravimetric method

Neutral lipids from microalgal cultures can be extracted using hexane. Since there are health concerns associated with hexane, all the steps involving this solvent were handled in a fume hood. Materials utilized were cleaned using a hexane rinse before the analysis. In a pre-weighed aluminum dish (42 mL), 50 mg of homogeneous, dried, and preferably pre-ground microalgae were weighed, and the mass was recorded. Microalgae was then transferred to a mortar together with 5 mL of hexane. This mixture was thoroughly ground for 5 minutes, starting with a gentle grinding and gradually increasing the strength and pace. Using a Pasteur pipette, the hexane and cell debris were transferred to a centrifuge tube with additional 10 mL of hexane that was used to carefully rinse the mortar and pestle. Extracted microalgae was centrifuged at 10 000 rpm and 4 °C for 10 min. The clear supernatant was recovered with a clean Pasteur pipette and taken back to the pre-weighed aluminum dish. The residue in the centrifuge tube was rinsed with extra 10 mL of hexane, and centrifuged again. This rinsing and centrifuging process was completed twice. Each time, the clear supernatant was recovered. The pre-weighed aluminum dish was then placed in a fume hood for the solvent to evaporate. Later, the aluminum dish was weighed to calculate the final neutral lipid content.

Fluorometric method

When numerous samples need to be analyzed, fluorospectrophotometry in combination with a staining method is a more practical option than the gravimetric method. Dry and ground microalgal samples and at least two microalgal standards within the lipid content range expected for the samples were prepared at a concentration of 5 g/L in water. In a multi-well plate, 10 mL of microalgal solution, 10 mL of 10 mg/mL Nile red solution, and 80 mL of 30 % v/v ethanol solution were added to each plate. Every sample was analyzed by triplicate. Using a fluorescence reader (Fluoroskan Ascent, Thermo Labsystems) each multi-well plate was incubated at 40 °C, and fluorescence was recorded. The excitation, and emission wavelengths were 530 and 604 nm respectively. The fluorescent measurements were converted to oil percentage using as external standard microalgal samples whose oil content was previously determined gravimetrically.

3.3 Microalgal cultures

Culture media composition is presented in Table 3-3. In addition glycine (used as nitrogen source) was added as required. If sugar is autoclaved together with other nutrient components, its degradation is enhanced *(117)* . In order to avoid precipitation and coloring during culture media preparation, three different working solutions were prepared, autoclaved at 121 °C for 30 minutes, and later mixed in a biological safety cabinet.

First, a Fe-EDTA complex stock solution was prepared by dissolving 12 g of $FeSO_4 \cdot 7H_2O$ and 16 g of EDTA (disodium salt dihydrate) in 800 mL of deionized boiling water. Once the solution was at room temperature, it was brought to 1 000 mL. A second stock solution was prepared with most of the trace elements (H_3BO_3, $MnCl_2 \cdot 4H_2O$, $ZnSO_4 \cdot 7H_2O$, $CuSO_4 \cdot 5H_2O$, and $Na_2MoO_4 \cdot 2H_2O$).

Glucose solution (working solution no.1) was placed from the beginning in Erlenmeyer-flasks, while working solution no. 2 (containing Glycine, $FeSO_4 \cdot 7H_2O$, KH_2PO_4 and K_2HPO_4) and working solution no. 3 (containing H_3BO_3, $MnCl_2 \cdot 4H_2O$, $ZnSO_4 \cdot 7H_2O$,

$CuSO_4 \cdot 5H_2O$, $Na_2MoO_4 \cdot 2H_2O$, $MgSO_4 \cdot 7H_2O$, $CaCl_2 \cdot 2H_2O$ and Thiamine hydrochloride) were in media storage bottles. Please note that components of working solution no. 2 were added in the same order as they are mentioned to avoid precipitation. The ratio to prepare culture media was two parts of glucose solution by one part of each working solutions no. 2 and 3.

Table 3-3 Culture media composition

Component	Concentration	Units
Glucose	30	g/L
KH_2PO_4	2.8	g/L
K_2HPO_4	1.2	g/L
$FeSO_4 \cdot 7H_2O$	12	mg/L
H_3BO_3	11.6	mg/L
$MnCl_2 \cdot 4H_2O$	7.2	mg/L
$ZnSO_4 \cdot 7H_2O$	0.88	mg/L
$CuSO_4 \cdot 5H_2O$	0.32	mg/L
$Na_2MoO_4 \cdot 2H_2O$	0.12	mg/L
$MgSO_4 \cdot 7H_2O$	1.2	g/L
$CaCl_2 \cdot 2H_2O$	100	mg/L
Thiamine hydrochloride	40	mg/L

A. protothecoides cultures used during the evaluation of the flow cell were cultivated mixotrophically in cotton stoppered, narrow-mouth Erlenmeyer flaks (1 L) with 400 mL culture media. Inoculum size was 2.5% by volume. All cultures were kept at 25 °C in a shaker incubator at 100 rpm.

4

Development of the Flow Cell

This chapter illustrates how the NIR Specular Reflectance Flow Cell was conceived, developed, and built. The principle behind the development of the NIR Specular Reflectance Flow Cell was to create a continuous film of culture media that could be monitored in real-time with a reflectance probe using NIR Spectroscopy. The flow cell was developed considering the angle of incidence, surface roughness, and absorbability of the sample, since they affect the reflectance measurement. Thickness of the film (path length) as well as distance between the probe and the film were identified as crucial elements during the flow cell development. It was also evaluated how the adsorption and reflectance characteristics of the substrate play a key role in the reflectance determination. In addition, two important decisions were made with respect to materials of construction and inclination of the flow cell in order to have the most favorable setup for the analysis. Finally, integration time and the number of scans to average, used to collect data, were tuned to the flow cell operating conditions.

The sample was actively transported through the flow cell (*i.e.* a peristaltic pump was used to recirculate the fluid back to the container of the sample).
In order to have a homogeneous and representative sample during the spectra acquisition, agitation of the sample was set to 220 rpm while the culture was being recirculated.
Figure 4-1 shows the final setup of the experiment.

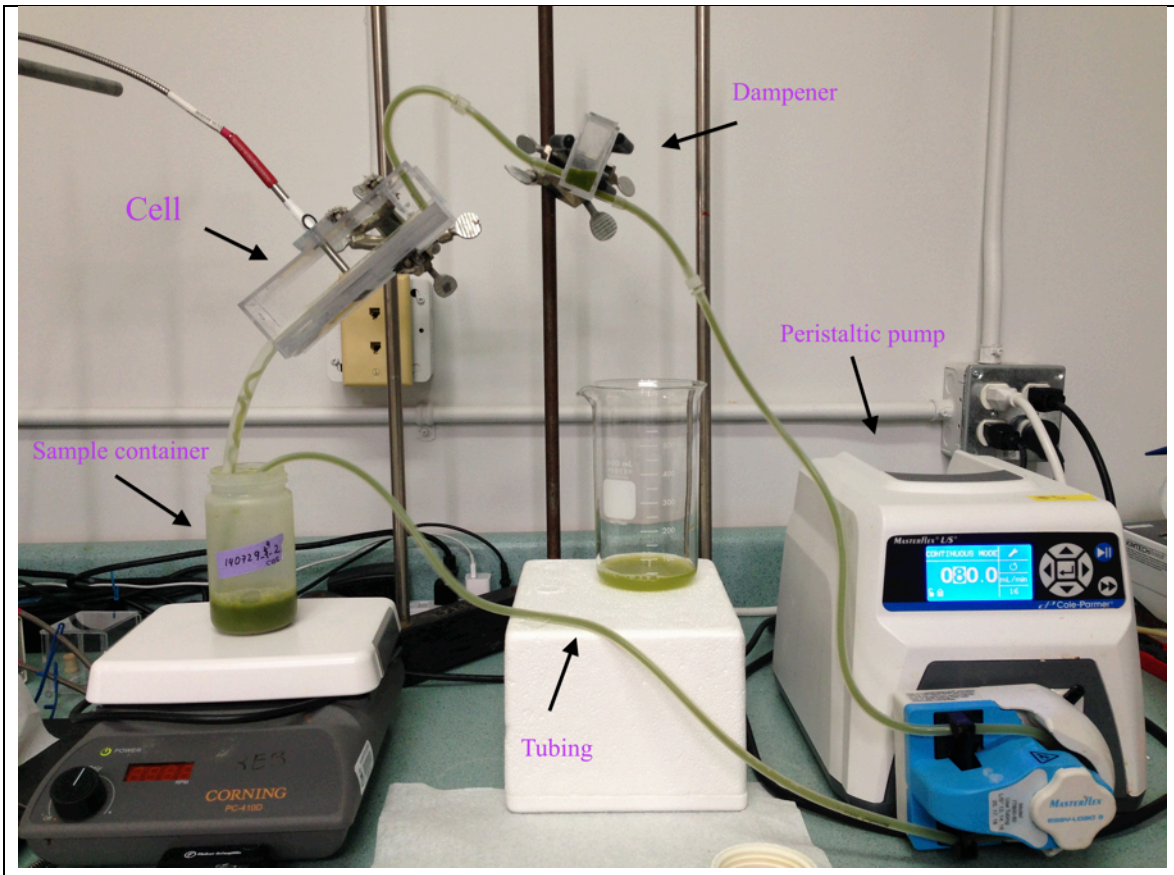

Figure 4-1 Final setup of the experiment

4.1 Flow cell material

Polycarbonate was chosen as the material used to construct the NIR Specular Reflectance Flow Cell in view of its thermal properties and ease of modification. Sterilization of the flow cell is possible because polycarbonate has a melting point of 155 °C. However, with a contact angle with water close to 90° *(118)* , polycarbonate has intermediate wettability. This characteristic brought additional challenges to our development, because together with the pulses caused by the peristaltic pump, they made difficult to create an even surface of the water film travelling on the polycarbonate surface. An even surface was required to obtain high quality specular reflectance that is needed to obtain good NIR data.

4.2 Substrate

A continuous thin film was formed on a reflective substrate in order to allow the collection of specular reflection from the interfaces at the surface of the film and at the substrate (see Figure 4-2). If light reflected from the substrate interface is high, a low maximum absorbance value is reached. To enable measurement of higher maximum absorbance levels, light reflected from the substrate should be minimized *(116)* . Therefore, a compatible substrate was carefully chosen during the flow cell development.

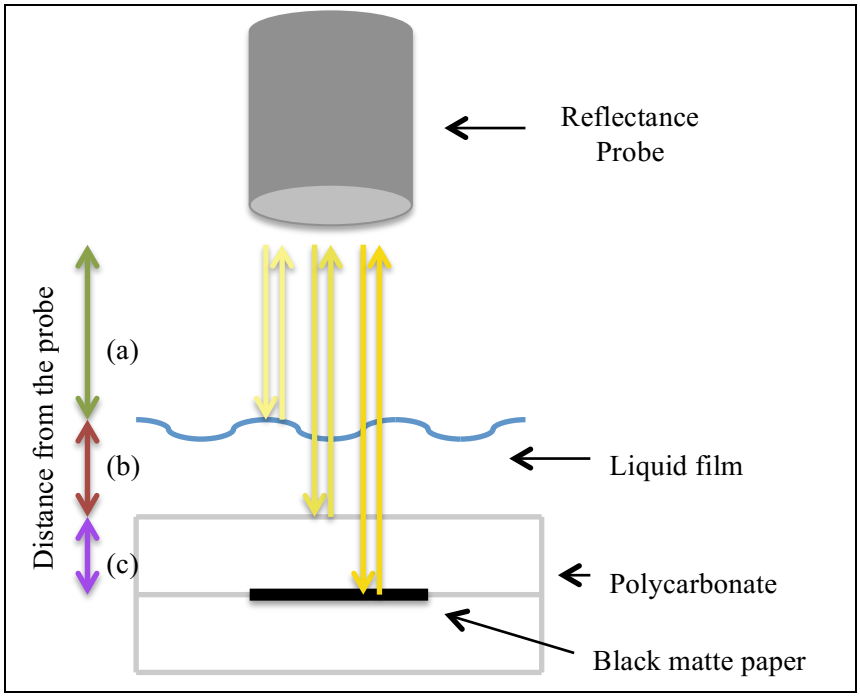

Figure 4-2 Specular reflection is obtained from three interfaces

Black surfaces are commonly used to minimize light reflected from the substrate. In theory, all wavelengths of light should be absorbed by a black surface; however, there are many shades of black with their own absorbance and reflectance properties. Sharp J. *(116)* , for example, used three different black paints to determine specular and diffuse reflectance. It was demonstrated that glossy black paint has the highest specular reflectance, while "chalkboard" black has higher diffuse reflectivity than flat and glossy

black paints. Curiously, flat and glossy black paints give similar diffuse reflectivity in the visible range, which means that they may look very similar in color to the eye, even when one reflects more light.

The first prototype of the flow cell in this study was constructed with a small piece of black matte paper under the plastic used to create the capillary open channel. With this configuration glucose was effectively determined (see Figures 4-3 and 4-4).

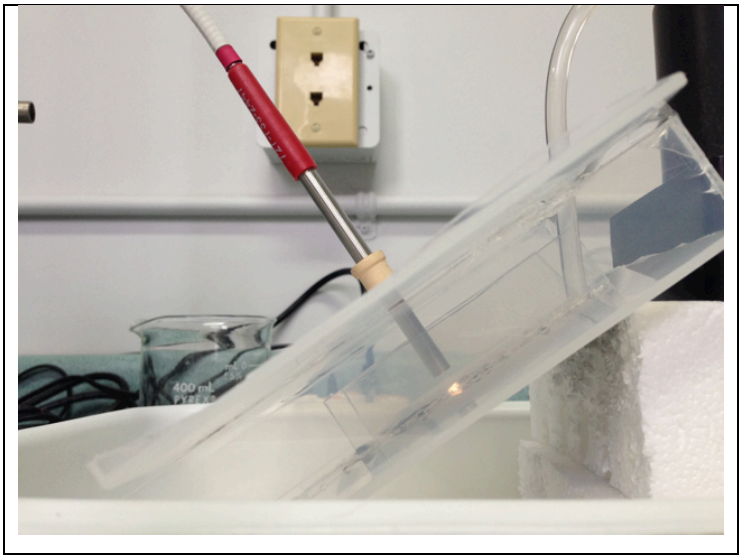

Figure 4-3 NIR Specular Reflectance Flow Cell Prototype I

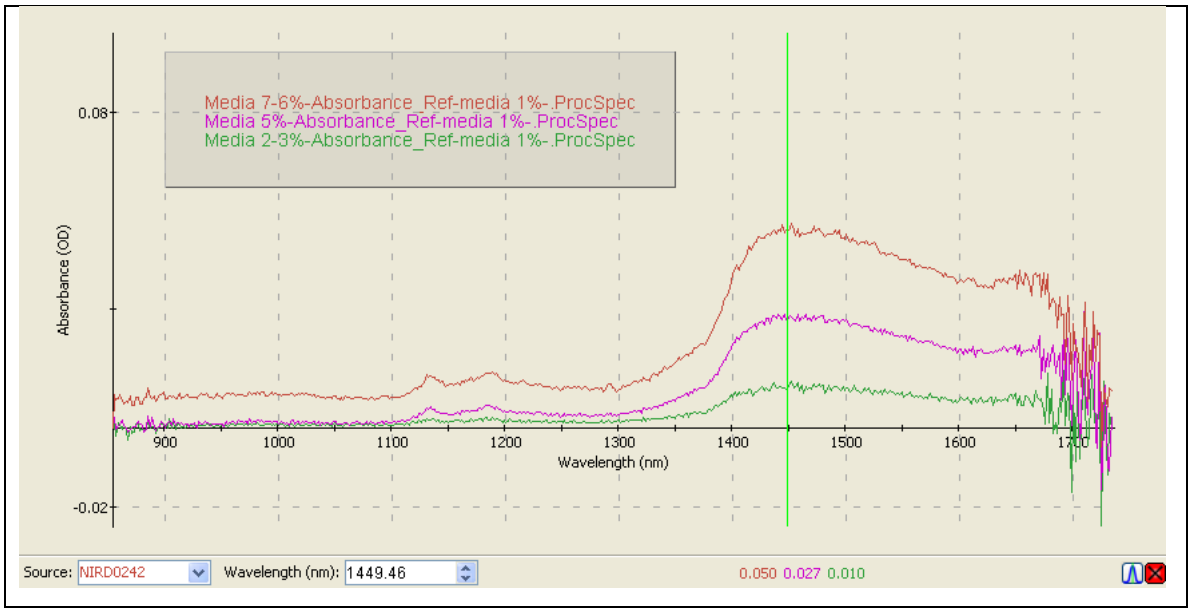

Figure 4-4 Spectra of glucose solutions in media (23, 50, and 76 g/L) Prototype I

Several substrates were tested with the flow cell prototype II (Figure 4-5), which had a base of stainless steel. Substrates tested were: black polycarbonate, clear polycarbonate by itself, and also using white paper, white plastic, black plastic, black matte paper, and ethylene-vinyl acetate between the clear polycarbonate sheet and the stainless steel base.

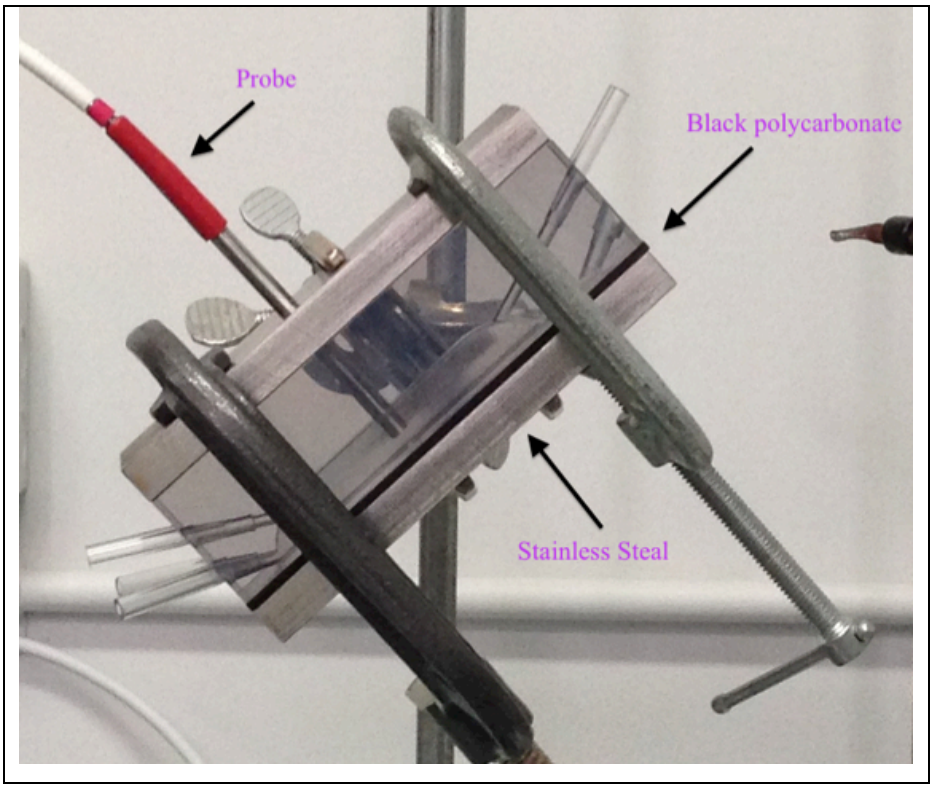

Figure 4-5 NIR Specular Reflectance Flow Cell Prototype II

Figure 4-6 shows how glucose could not be detected in the NIR Specular Reflectance Flow Cell, when the substrate was absorbing most of the light (black polycarbonate).

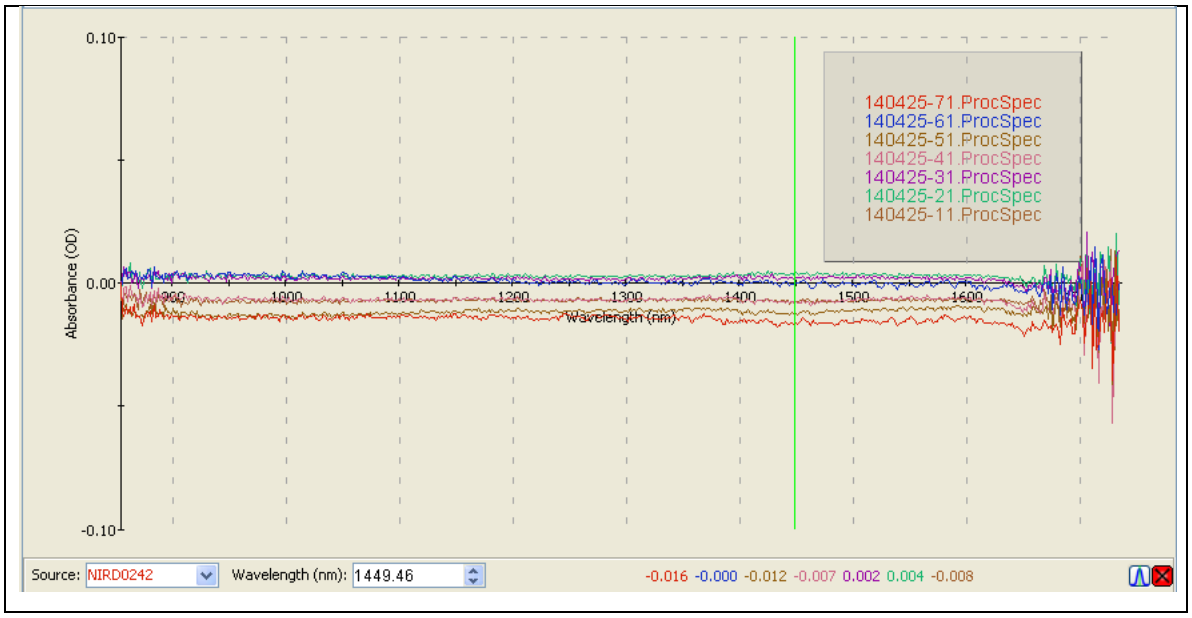

Figure 4-6 Glucose is not detected when light is absorbed by substrate (Prototype II)

In contrast, Figure 4-7 shows the interference obtained when the substrate was considerable shiny (black plastic) and giving high specular reflection as a consequence.

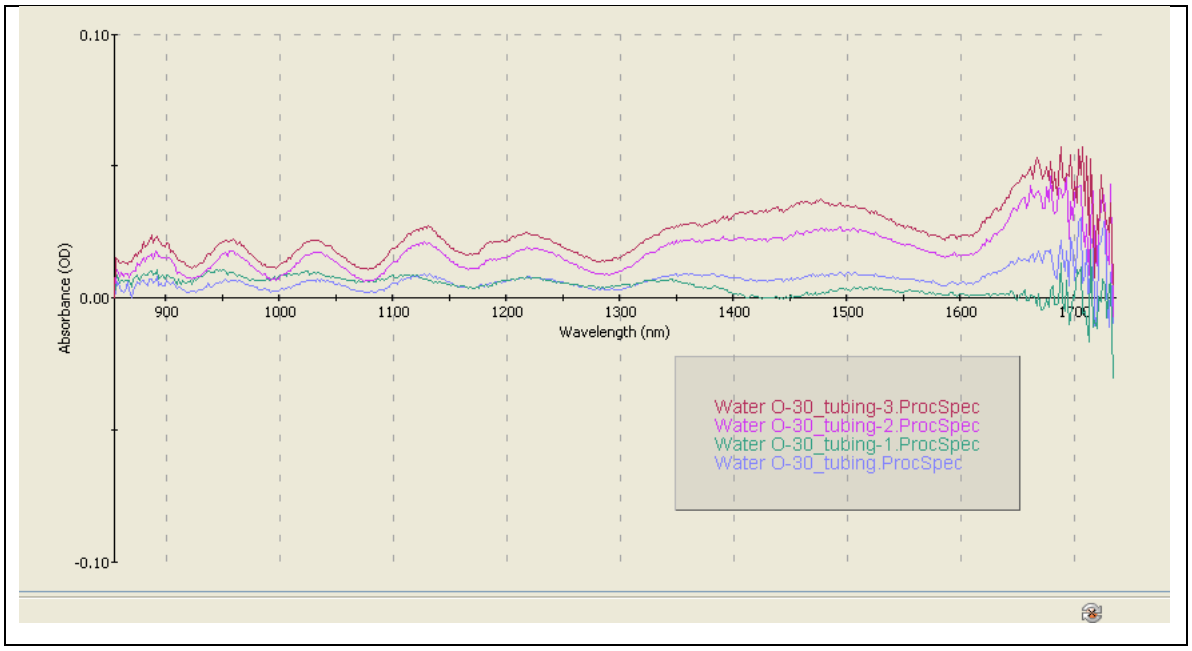

Figure 4-7 Interference due to high specular reflection (Prototype II)

In order to reduce the specular component of the light reflected from the substrate in the final model of the flow cell, a small piece of black matte paper was encapsulated between two 1/8” sheets of clear polycarbonate (see Figure 4-8).

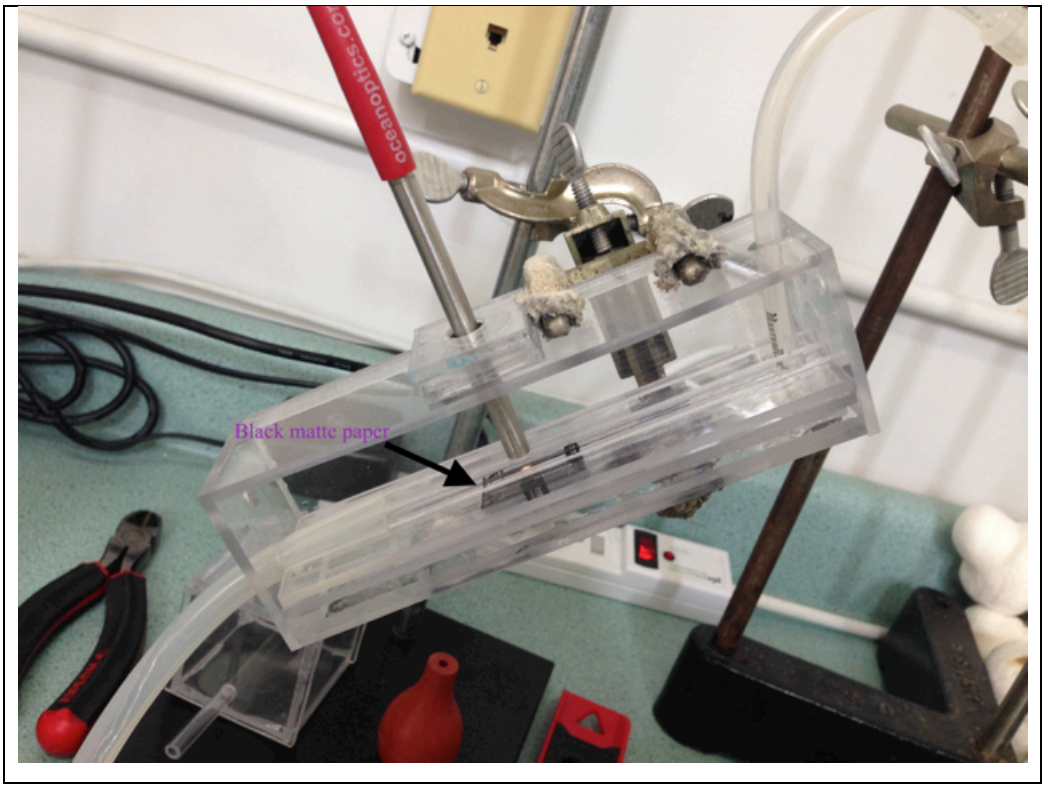

Figure 4-8 A black matte paper reduces the specular component of the light reflected from the substrate

4.3 Uniformity of the film (Surface roughness)

4.3.1 Flow rate

Flow rate was set at 80 mL/min (1.33×10^{-6} m^3/s) because this was the lowest flow rate at which an even film was formed in a 6 mm width channel with polycarbonate walls and floor. Table 4-1 shows the value of the mean flow velocity and dimensionless parameters in the tubing delivering the flow into the open channel and in the open channel as well.

Flow in the open channel was non-uniform (*i.e.* velocity and depth of the liquid continuously varies from one section to another), unsteady (*i.e.*, velocity and depth at a particular point varies with time), periodic, and isothermal. The periodicity was due to the peristaltic pump used to recirculate the flow.

Table 4-1 Mean flow velocity and dimensionless parameters of the flow in the cell

	Mean flow velocity	Re number (water)	Fr number	We number
Tubing	0.1767 m/s	613 Laminar flow		
Open channel	0.4444 m/s	213 Laminar flow	7.25 Supercritical flow	1.4

4.3.2 Slit and level guides

Figure 4-9 shows the arrangement of two important features of the flow cell: the slit through which the flow was delivered into the open channel, and the position of the lines that were inscribed in the walls of the channel to pin the contact line of the flow.

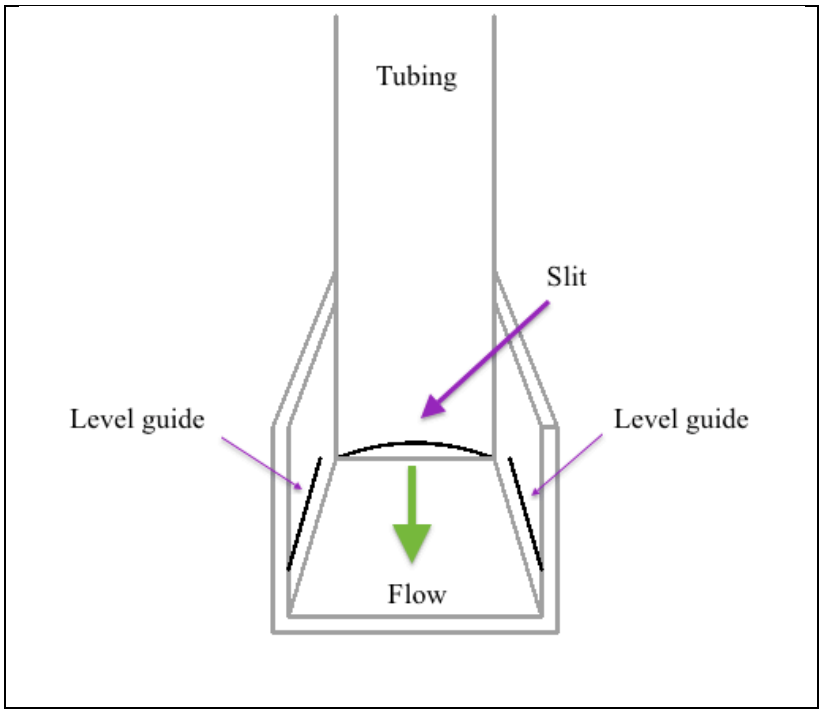

Figure 4-9 Diagram showing the arrangement of the slit and level guides in the capillary channel

Making the channel as wide as the external diameter of the tubing (Masterflex platinum-cured silicone HV-96410-16) delivering the flow into the channel was the first measure required to ensure a uniform spreading of the film within the walls of the channel.

The second measure taken was forcing the flow through a slit at the moment it was being delivered into the polycarbonate channel. The slit was formed between the edge of the tubing that was delivering the flow, and the bottom of the channel itself (see Figure 4-9).

When the flow passed through the slit, its velocity increased (see Figure 4-10), which resulted in a consistent dissemination of the liquid throughout the width and length of the channel by overcoming capillary forces that favored corner flow.

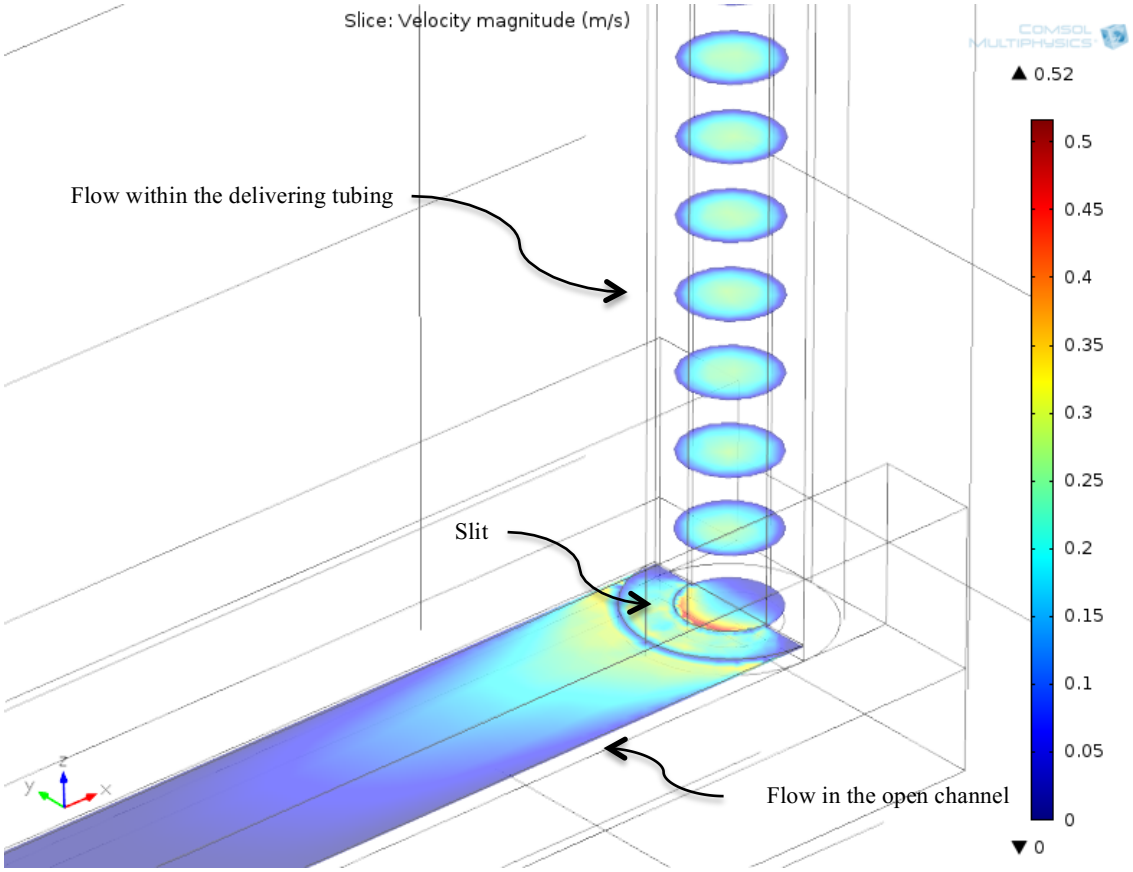

Figure 4-10 Velocity profile (m/s) of water (80 mL/min) while being delivered into the capillary channel

Since capillary forces were present between water and polycarbonate, the uniformity of the surface of the film was guaranteed by inscribing a line on each wall of the channel at about 0.5 mm from the bottom of the channel. This change in the geometry of the wall favored the consistent formation of an even surface of the film, under the assumption that the contact line of the flow was pinned along the lines inscribed.

The decision to inscribe a line to pin the contact line was taken after it was observed the effect of the addition of a surfactant (Antifoam O-30) to water on the variation of the baseline of the reference (water) during absorbance measurements.

Figure 4-11 shows the variation in absorbance obtained as a consequence of the different surfaces formed during the transient startup every time the flow was stopped and restarted. Flow was interrupted and continued either by pulling the tubing outside of the sample (water_tubing) and placing it back, as well as by turning the pump off (water_pump) and turning it on again.

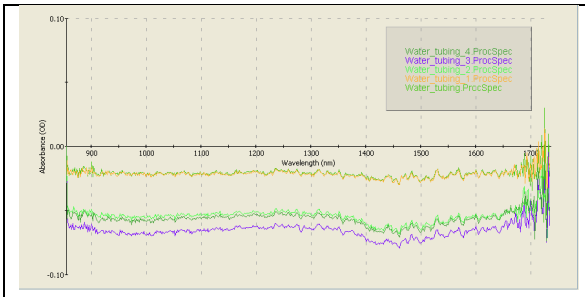

Water_tubing

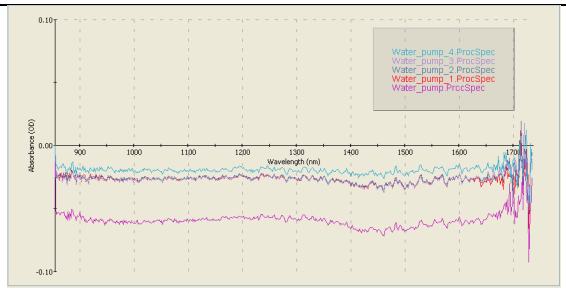

Water_pump

Figure 4-11 Absorbance variation as a result of variation in the surface of the film (Prototype II)

Figure 4-12 shows the improvement obtained when a surfactant (Antifoam O-30 at 5 ppm) was used.

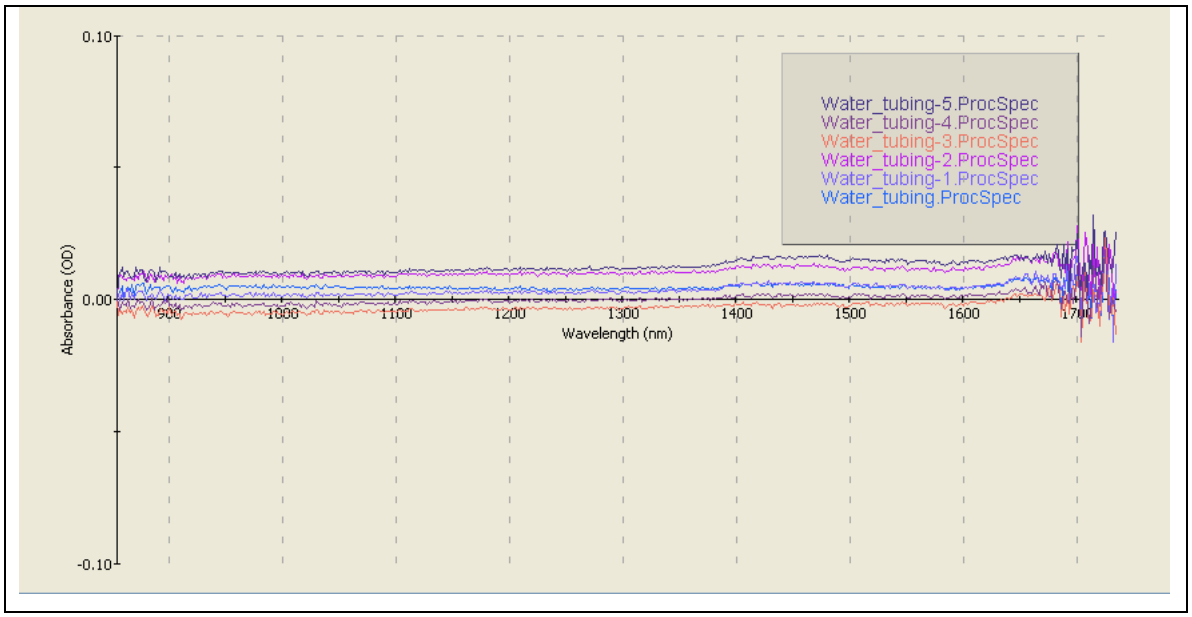

Figure 4-12 Improvement in absorbance variation with the help of a surfactant (Prototype II)

The NIR Specular Reflectance Flow Cell was developed to achieve a uniform and consistent surface of the film every time the flow was stopped and restarted. Figure 4-13 shows the stability of the baseline during our regular experiments.

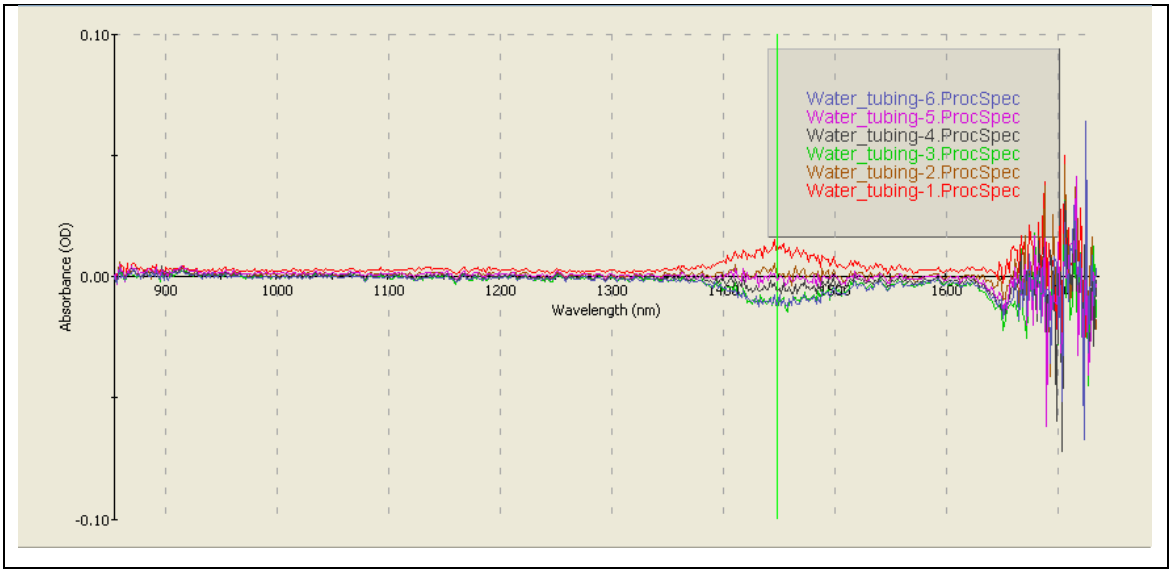

Figure 4-13 Baseline obtained in the final model of the flow cell every time the flow was stopped

4.3.3 Dampener

In order to minimize the effect of the pulses generated by the peristaltic pump, one small dampener (13.7 mL) was built (see Figure 4-14). Tubing connectors with an outside diameter similar to the inside diameter of the tubing were used to obtain the maximum unrestricted flow. The exit was slightly raised to create a small amount of back pressure, in order to partially fill the body of the dampener. The dead volume of the dampener was approximately 3.26 mL. The dampener was installed in an inclined position to avoid the accumulation of cells within it when working with microalgal cultures.

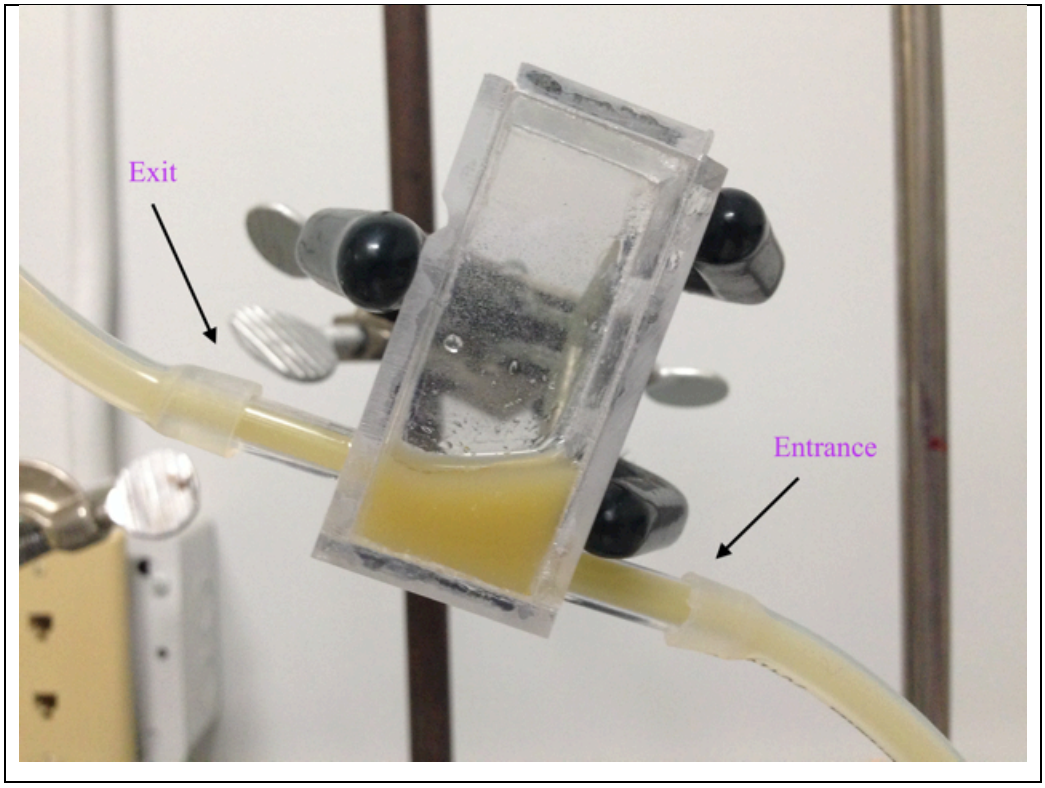

Figure 4-14 Final model of the dampener used during the experiments

When working with microalgal cultures, the volumetric flow was reduced from 80 mL/min to 20 mL/min, while the front of the culture flow entered, partially filled, and left the dampener to avoid the formation of bubbles inside. Once the front of the flow reached the capillary channel, the volumetric flow was gradually brought back to the working volumetric flow (80 mL/min) by increments of 10 mL/min.

Previously, water was used to evaluate three different setups, since it was necessary to reduce the presence of pulses in the flow but not to the point to considerably affect the transient startup of the flow in the open channel.

The three different setups were: in the absence of a dampener, with a 137 mL dampener, and with a 13.7 mL dampener. The transient startup and the stability of the fully developed flow were evaluated with all setups. Six spectra were collected for each case.

When no dampener is used the base line is fairly stable, however the effect of the pulses is present. With the help of the 137 mL dampener the pulses are significantly reduced but variation of the base line is increased as a result of the effect on the transient startup of the flow when capillary forces predominate. The use of the 13.7 mL dampener helps to reduce the effect of the pulses without a substantial effect on the transient startup of the flow. A consistent film is formed due to the right combination of inertia and capillary forces during the transient startup of the flow in the open channel. This effect and the effect on the fully developed flow can be observed in Figures 4-15, 4-16, and 4-17.

4.3.4 Thickness of the film

Thickness of the film was not actually adjusted, as it was mostly determined by the volumetric flow in the channel and lastly the level guides carved in the walls of the channel at about 0.5 mm from the bottom of the channel. Pulses from the peristaltic pump generated the formation of small waves in the flow. These waves were causing a non-uniform and unsteady flow in the capillary open channel of the flow cell. With the help of the dampener and the impact of the capillary and surface tension forces present, the effect of the peristaltic pump was reduced to the formation of ripples that seemed to travel under the surface of the film.

Since water was used as reference during our determinations, it was essential to attain the most uniform surface film of water in order to have a reproducible path length.

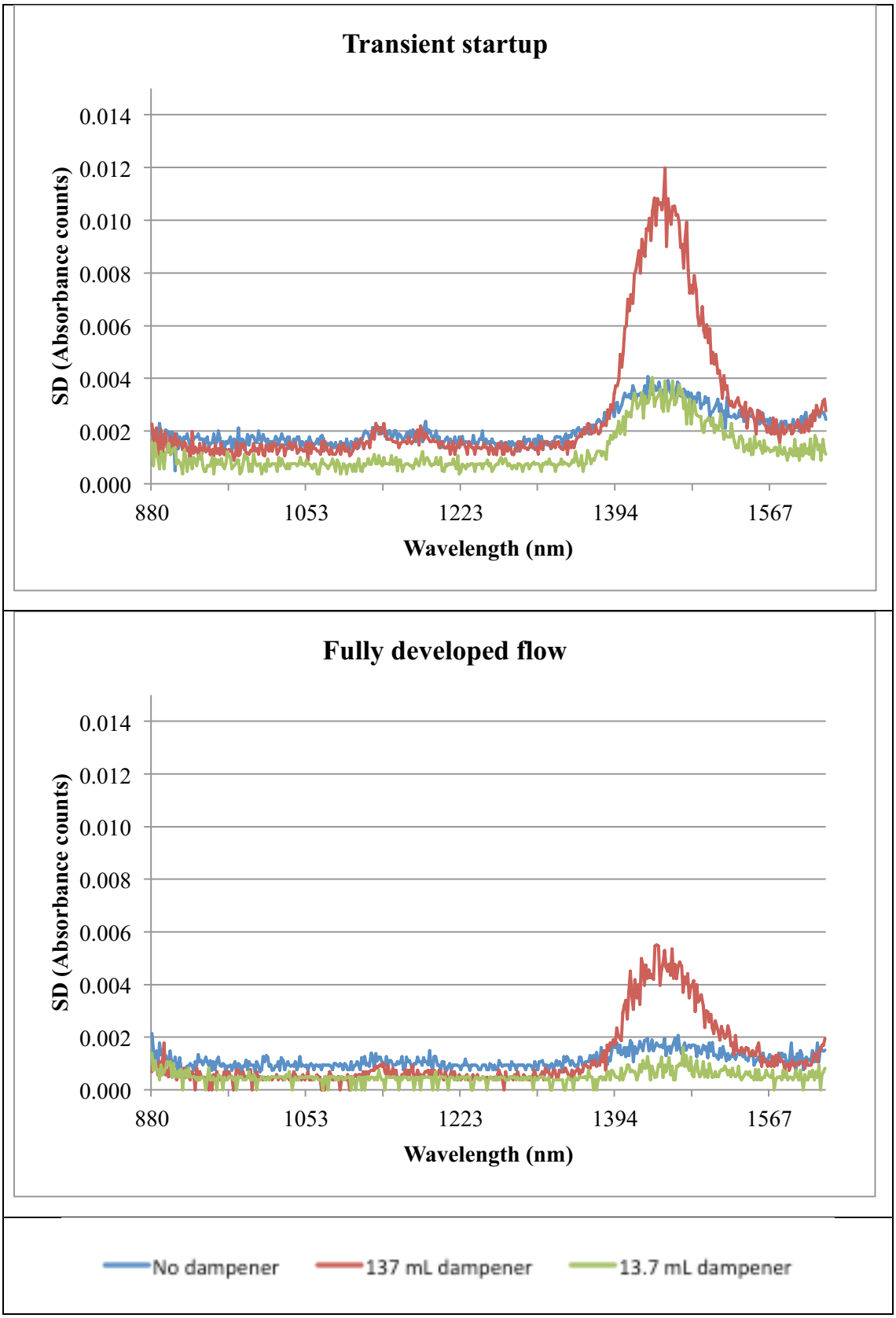

Figure 4-15 Effect of damped flow on the standard deviation of absorbance during the transient startup and in the fully developed flow

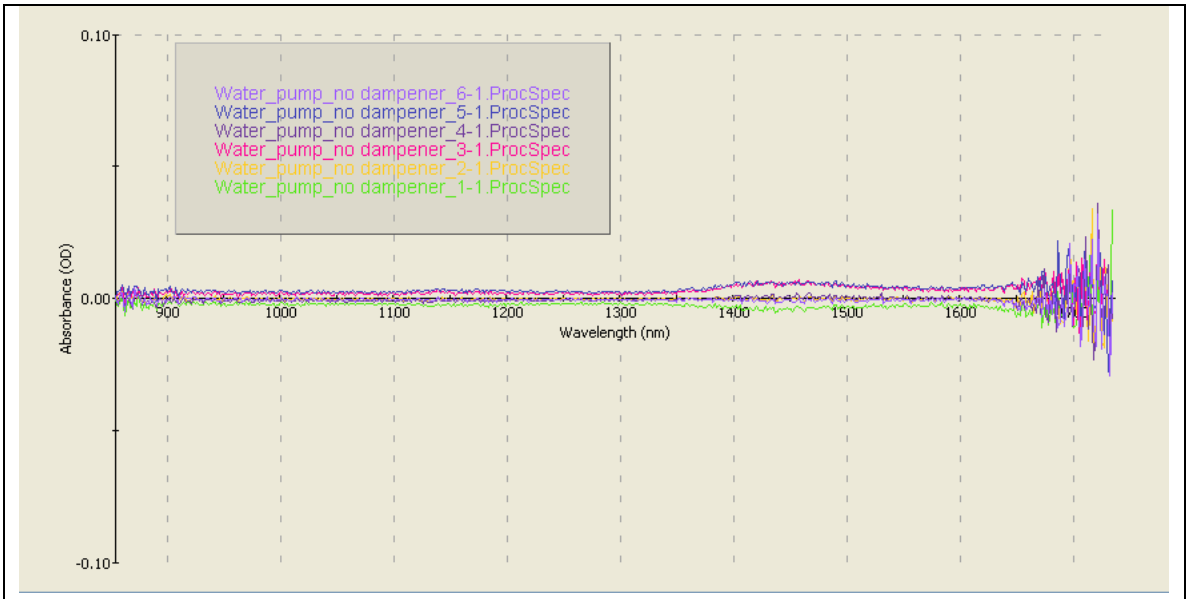

No dampener

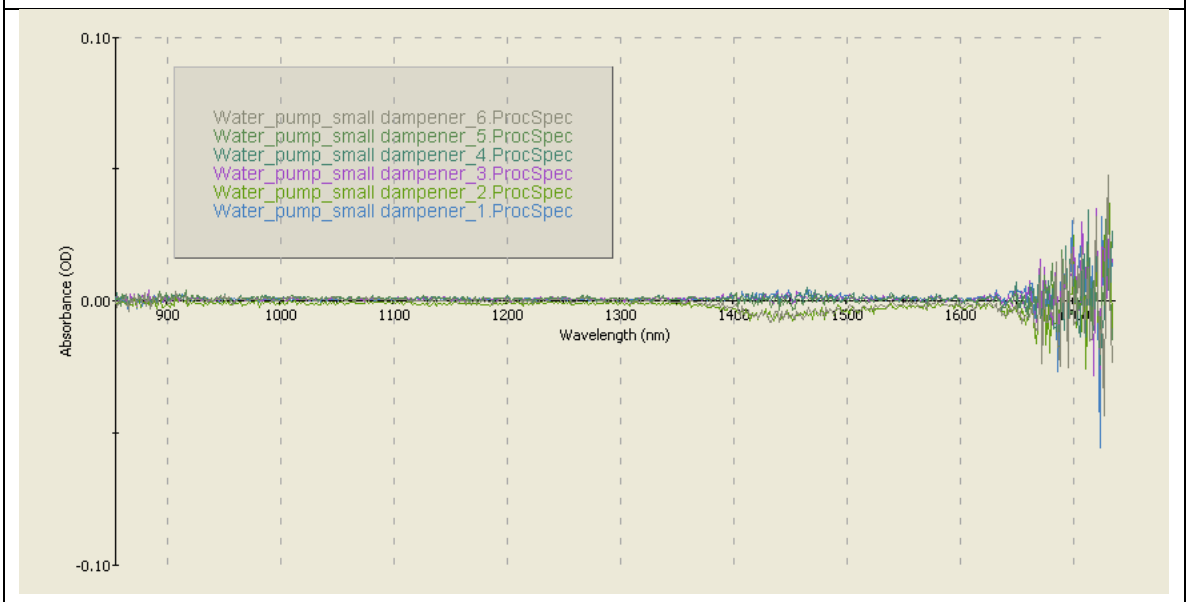

13.7 mL dampener

Figure 4-16 Improvement in the variation of the baseline during the transient startup

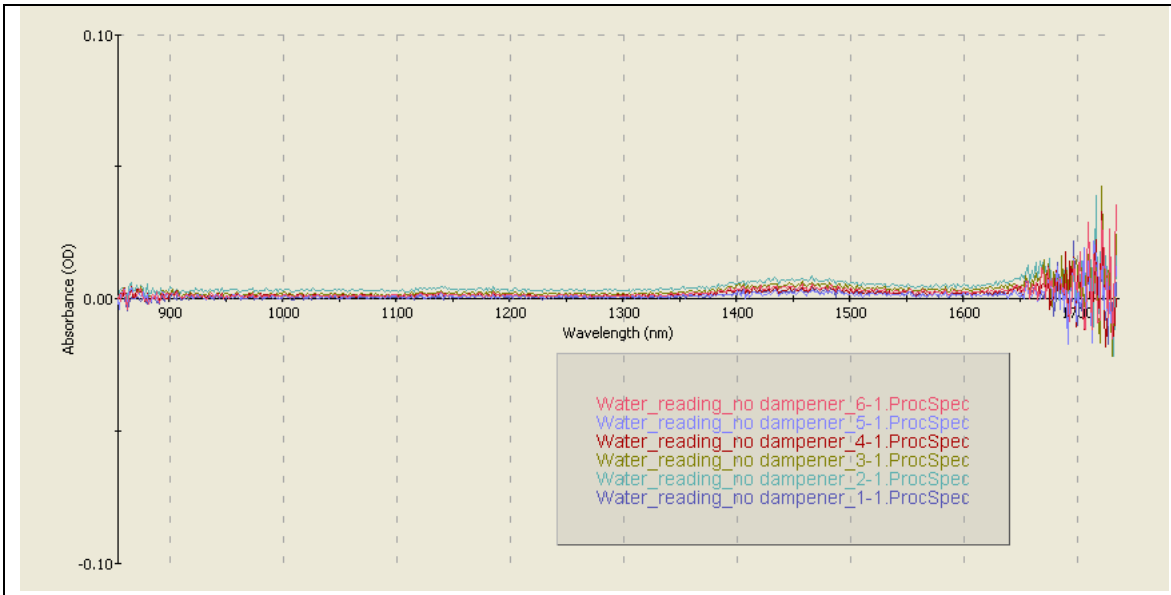

No dampener

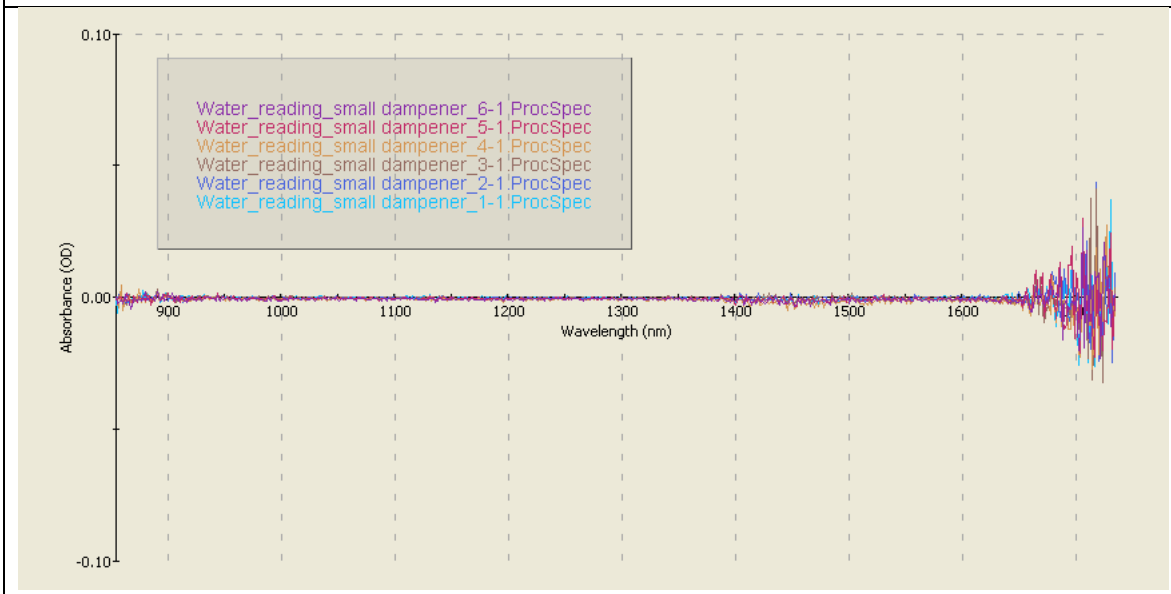

13.7 mL dampener

Figure 4-17 Improvement in the variation of the baseline of fully developed flow

4.4 Flow cell inclination

Precipitation of microalgal cells inside the flow cell should be avoided. The NIR Specular Reflectance Flow Cell was developed with an inclination of 40°, in order to increase the boundary shear stress according to the resistance equation. Since the flow aspect ratio is < 40, flow at the center of the channel is influenced by side-wall effects.

Flow aspect ratio: 12
Boundary shear stress: 2.7 Pa

The angle was arbitrary chosen, and no other angles were tested.

4.5 Barrier against bubbles

One of the difficulties encountered during the development of the NIR Specular Reflectance Flow Cell was the presence of bubbles in the capillary channel. If bubbles touch the probe, residual sample will cause interference. Two combined measures were put in practice in order to avoid the presence of bubbles. First, one spiky barrier was placed at the top of walls of the channel to disrupt relatively large bubbles, only one cm from the place where the liquid was been delivered (see Figure 4-18); and second, the reflectance probe was positioned slightly above of the walls of the channel. Therefore, "small'' bubbles that were not disrupted by the barrier, travelled downstream without contacting the probe. Bubbles are a particular problem with high cell density cultures.

4.6 Angle of incidence

In order to collect only specular reflectance, the probe was positioned at 90 degrees relative to the sample surface (see Figures 4-19 and 4-20) *(116)* . This parameter was not modified during experimentation.

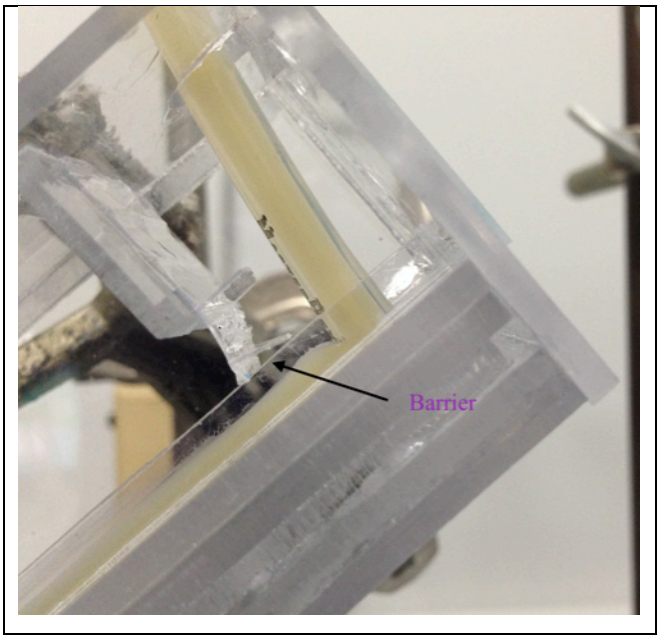

Figure 4-18 Barrier prevented bubbles from reaching the reflectance probe

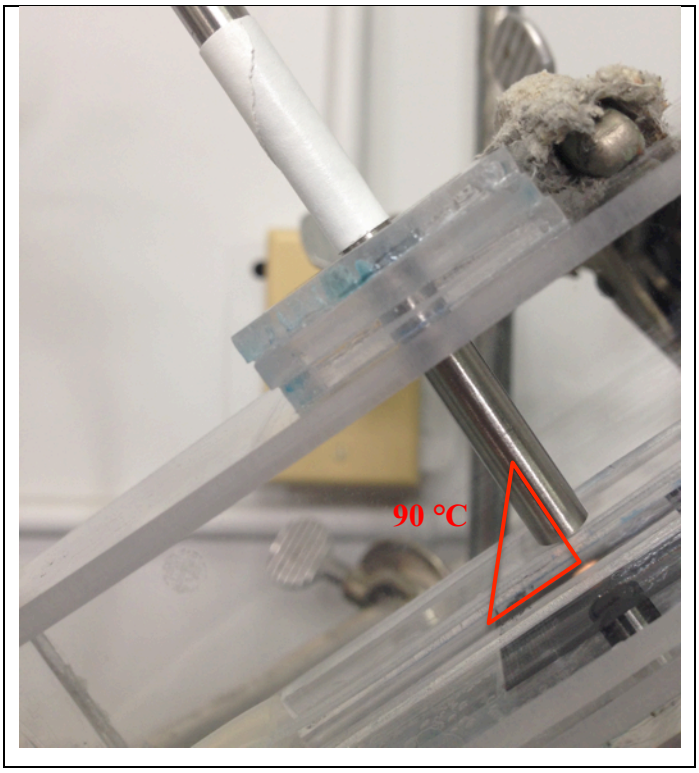

Figure 4-19 Angle of the probe with respect to the surface of the film

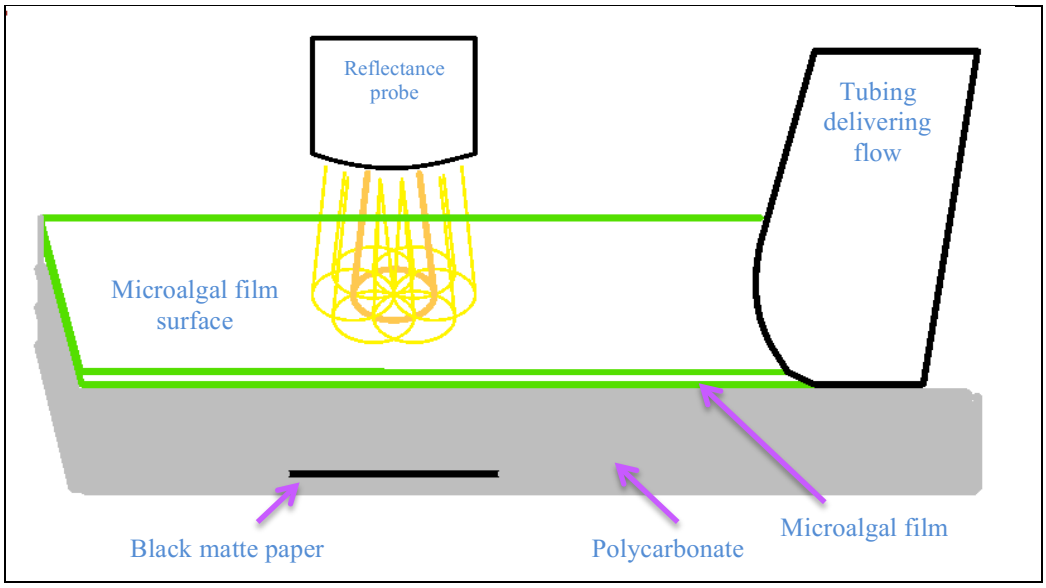

Figure 4-20 Diagram showing the arrangement to collect specular reflectance from the film

4.7 Spectrometer acquisition parameters

4.7.1 Integration time

Integration time is the time the detector monitors incoming photons. In the scope mode (the operating mode where raw data is displayed on the screen) of the SpectraSuite® Spectrometer Operating Software, integration time was adjusted to ensure the highest intensity obtained for the reference would be around 50,000 counts, which is approximately 85% of the detector saturation for the NIR512 spectrometer. These counts are impacted by a variety of factors including: the intensity of the light source, the reflectivity of the grating and mirror in the spectrometer, the transmission efficiency of the fibers, the response of the detector, and lastly the specific spectral characteristics of the reference. Integration time is particularly affected by distance between the probe and the film as well as the nature of the film and the substrate *(75)* . This value was set to 400 milliseconds.

Distance of the probe

All measurements were taken with the probe tip at the same distance from the sample during an experiment. This distance was adjustable, in order to allow for careful tuning to obtain a maximum intensity of 50,000 counts for the reference in the scope mode. This measured maximum intensity is very sensitive to the distance between the probe and the sample. It was found that the tip of the probe should be around 5 mm from the surface of the film in order to obtain the desired intensity (see Figure 4-21).

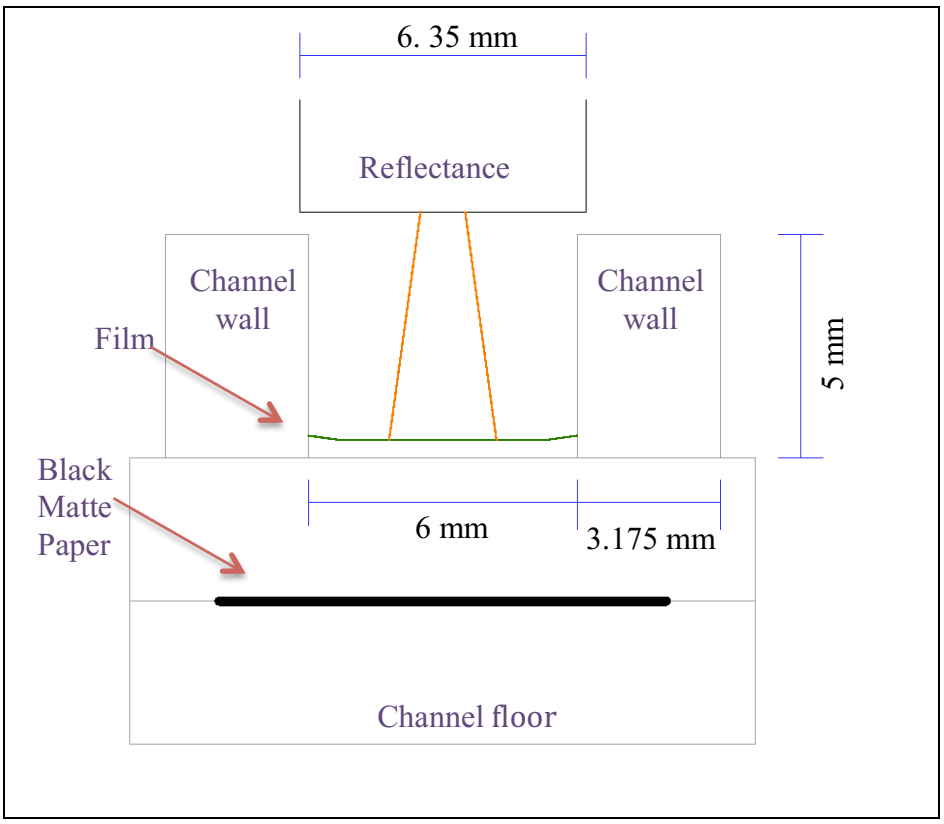

Figure 4-21 Front view diagram of the experiment set up

The diameter of the sample area, where the read fiber collects the reflected light, is around half of the distance between the probe tip and the sample *(116)* . Thus in the NIR Specular Reflectance Flow Cell, the diameter of the monitored sample area was approximately 2.5 mm (see Figure 4-22).

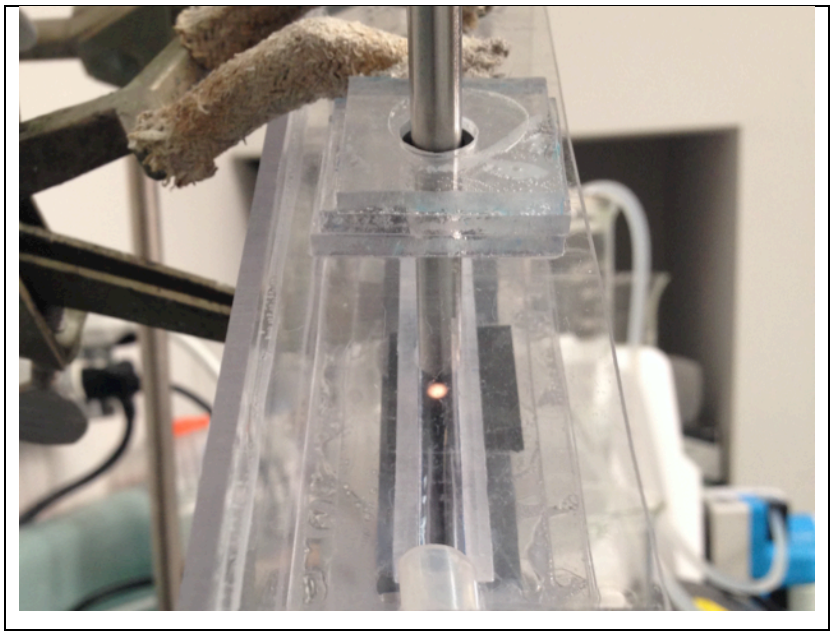

Figure 4-22 Illuminated surface area of the sample in the capillary open channel

4.7.2 Scans to average

The number of scans to average is the discrete spectral acquisitions accumulated by the device driver before the software receives a spectrum. The signal-to-noise ratio will improve with the number of scans to average *(75)* . The number of scans to average was set to 9.

4.7.3 Generation of a spectrum

An appropriate combination of integration time and the number of scans to average, made it possible to minimize the variation in the uniformity of the surface of the film given by the periodic pulses of the peristaltic pump. The chosen values (integration time of 400 milliseconds and 9 scans to average) were picked using a methodology of trial and error. With these values a spectrum was generated every 3 600 milliseconds (3.6 s) as can be seen in Figure 4-23.

The peristaltic pump gives 90.5 rpm for the working volumetric flow (80 mL/min). The pump has 3 rollers, which means that we had 4.53 pulses/s or 16.29 pulses/3.6 s. Ideally a spectrum should be generated capturing a cycle with a complete number of pulses. Capturing a cycle every 3 600 milliseconds gave an error of 1.8 %.

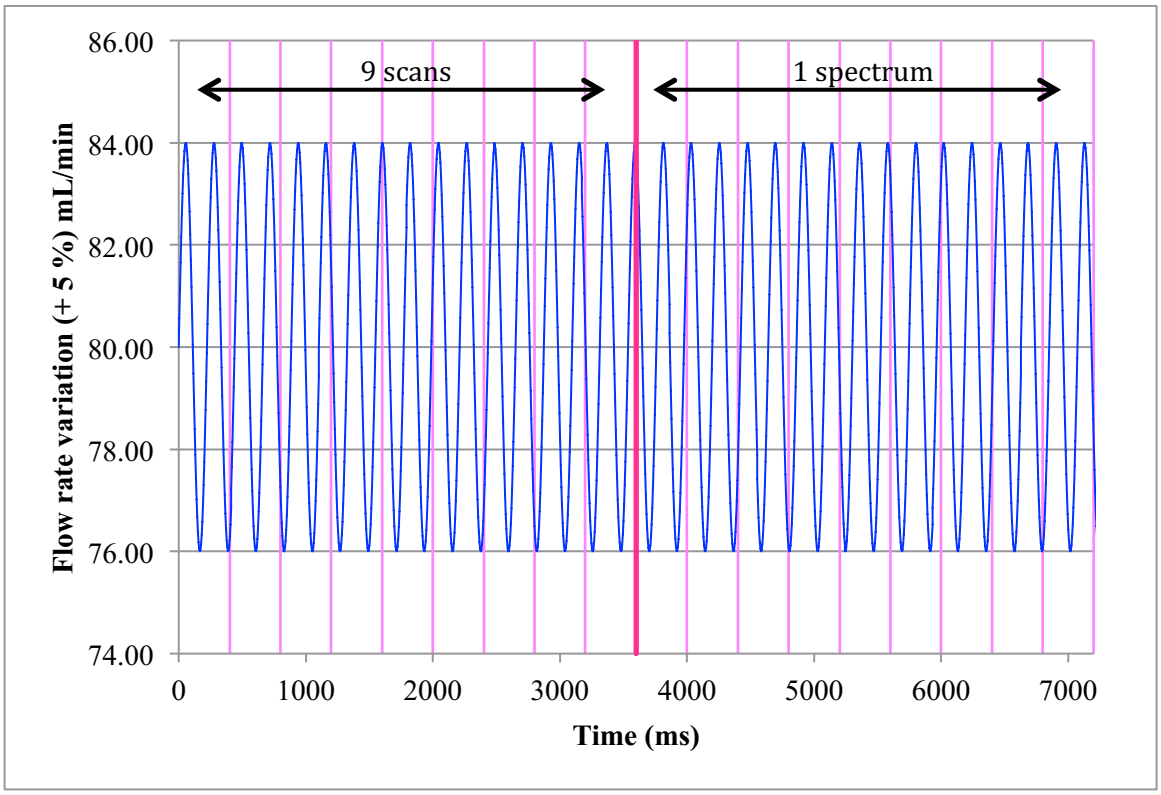

Figure 4-23 Variation of the flow rate (80 mL/min) & periodicity of the pulses given by the peristaltic pump used during acquisition of spectra

4.8 Temperature

NIR spectra are affected by sample temperature *(67)* . Regular experiments were conducted at ambient temperature, which was maintained at 24 °C with a maximum variation of ± 2 °C. Particular experiments were conducted using glucose solutions with temperatures varying from 14 to 34 °C in order to evaluate the impact of temperature changes during our regular determinations. Three samples were stabilized at 4 °C in a fridge, three more at 24 °C (room temperature), and three more at 40 °C in an oven. Their spectra were obtained at 14, 24, and 34 °C respectively (see Figure 4-24).

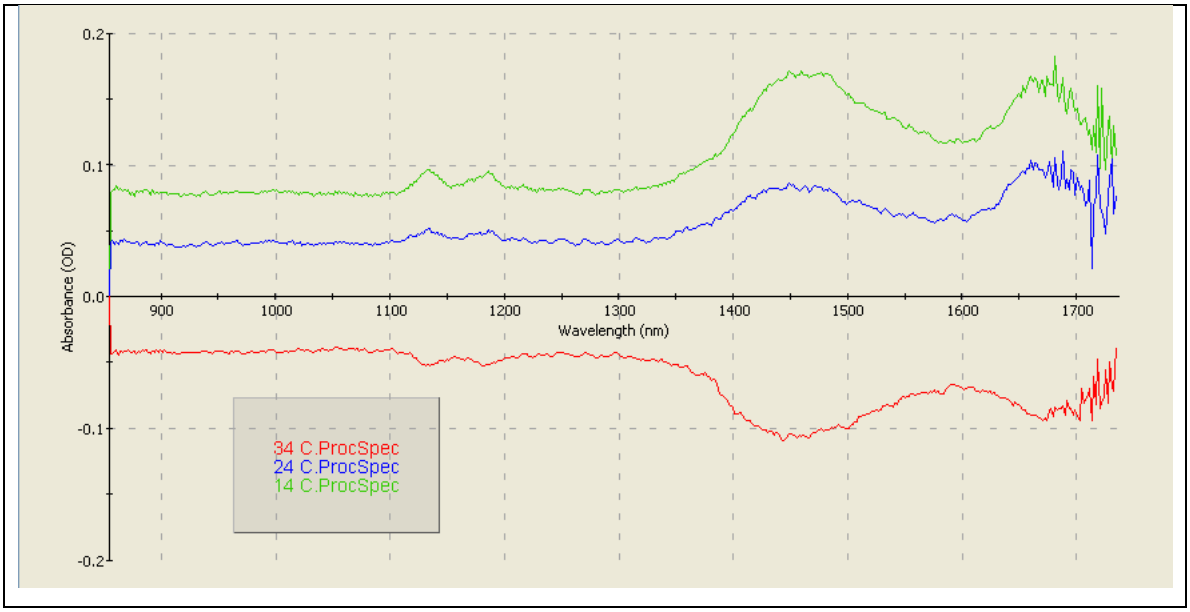

Figure 4-24 Glucose solutions (30 g/L) at 14, 24, and 34 °C spectra

The effect of the temperature in the spectra obtained is mainly observed as the effect caused by different heights of the surface of the film, being higher the surface of the film with lower temperature. This effect could be explained considering that surface tension decreases with increasing temperature. From these experiments, it was found that a temperature variation of 1 °C resulted in a coefficient of variation of 10 %.

Figure 4-27 shows the final set up of the NIR Specular Reflectance Flow Cell.

4.9 Sensor setup

For each experiment, the spectrometer was first set up according to the following procedure. First, a dark spectrum was stored in the scope mode window while light was blocked. Next, the corresponding reference sample was recirculated through the NIR Specular Reflectance Flow Cell at 80 mL/min. Considering that the integration time (400 milliseconds) and the number of scans to average (9) were fixed as well as the substrate, the distance between the probe and the surface of the film was adjusted in order to get a maximum signal of 50,000 counts in the scope mode (see Figure 4-25). This distance was (as mentioned before) usually around 5 mm. Then a reference spectrum, which equals to 100% reflection, was stored and saved.

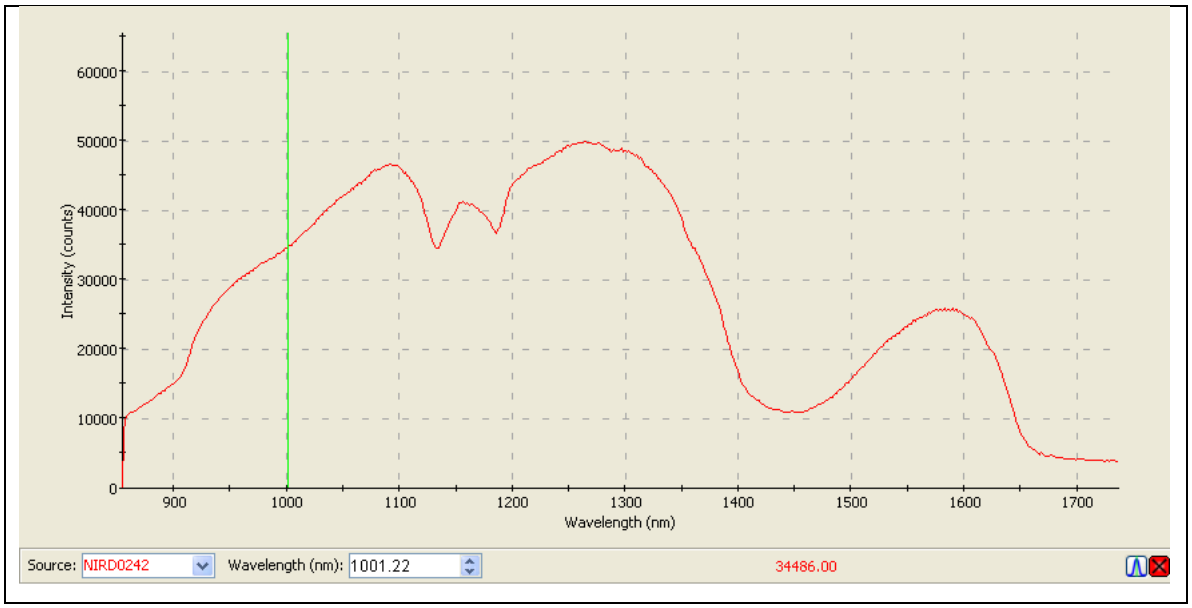

Figure 4-25 Maximum intensity set up at 50,000 counts for water

Finally the scope mode window was switched into absorbance mode. Here, it was verified that a stable surface of the film was being obtained in the capillary open channel as discussed before. Figure 4-26 shows the variation of the baseline of 6 consecutives spectra during our regular experiments.

Figure 4-26 Working baseline obtained from a stable surface of the film of the reference sample

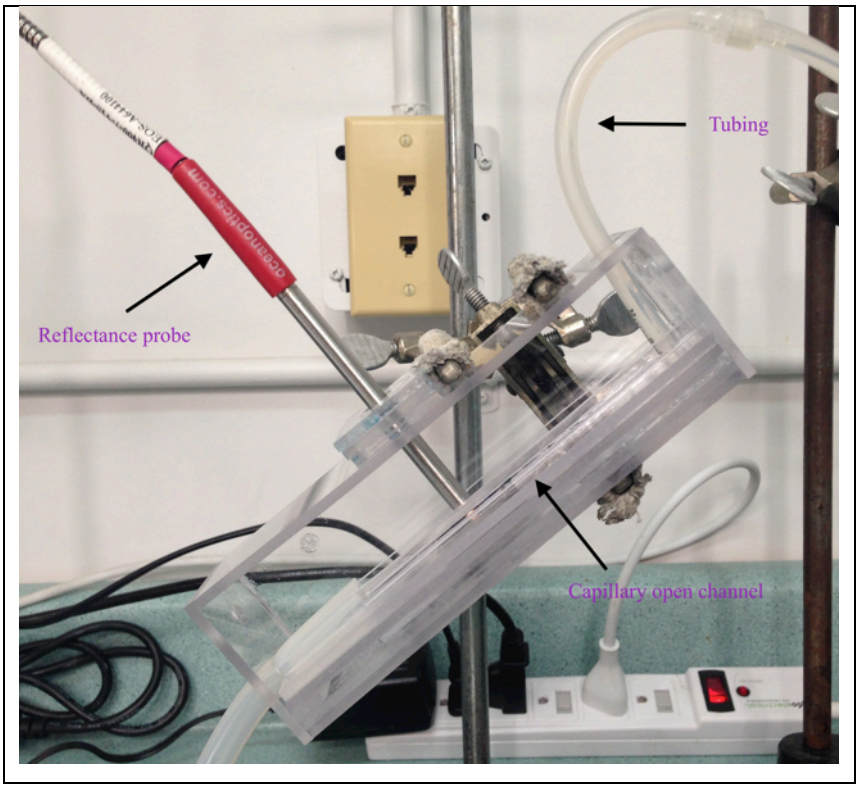

Figure 4-27 NIR Specular Reflectance Flow Cell final model

5

Assessment of the Flow Cell

This section presents and discusses all the results from the tests used to evaluate the flow cell biosensor. The evaluation of the individual sets presented was not realized with the objective to calibrate a model for future determinations. The objective of this work was to determine the functionality of the flow cell apparatus. Each trial was conducted with a slightly different configuration of the device. Caution should be used when comparing the results from different tests.

Results are also presented for the application of this sensor for the monitoring of *A. protothecoides* cultures.

Two wavelengths were chosen during the length of this research work due to their significant contributions to the spectra obtained. The suitable wavelengths chosen were the corresponding to the C-H second overtone (1 225 nm) and the corresponding to the O-H stretch first overtone (1 449 nm).

5.1 Evaluation of the NIR Specular Reflectance Flow Cell

Three different sets of measurements were performed to corroborate the functionality of the NIR Specular Reflectance Flow Cell. First, determination of glucose in water and culture media was explored. Later microalgal cultures were used to estimate glucose and biomass concentrations, independently and simultaneously. Lastly oil determination was assessed using nitrogen limited microalgal cultures.

5.1.1 Glucose Determination

Glucose in water

NIR specular reflectance of aqueous glucose solutions with five different concentrations (20, 40, 60, 80, and 100 g/L) was determined in the flow cell. Water was used as reference. Each sample was prepared in triplicate. Six spectra were obtained for each sample (see Figure 5-1).

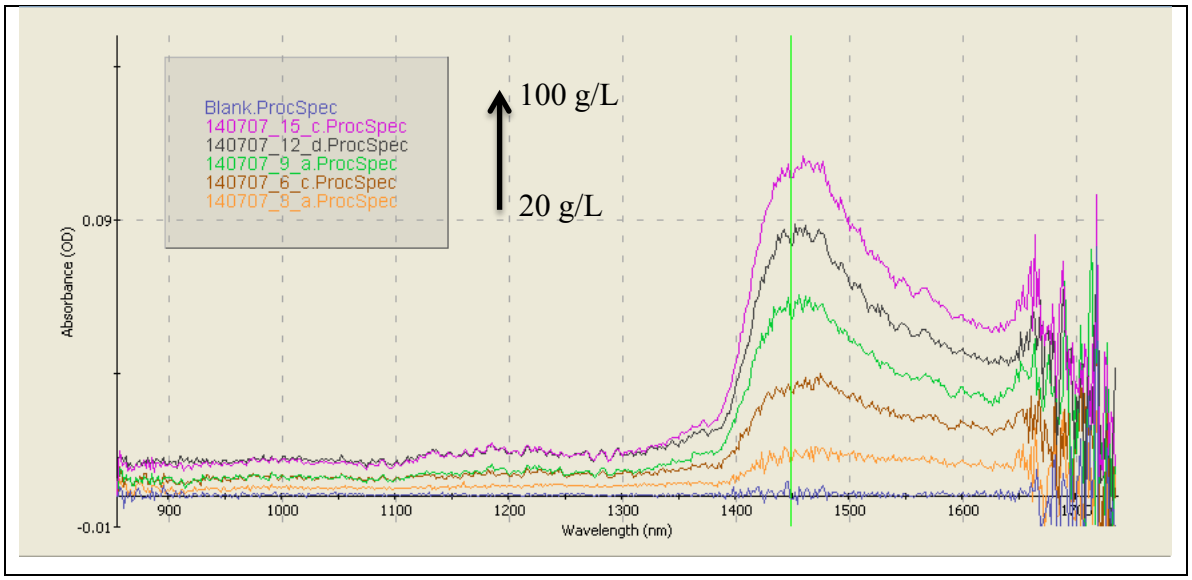

Figure 5-1 Aqueous glucose solutions (20 - 100 g/L) spectra

Wavelength of the maximum observed absorbance shifted from 1 478.79 to 1 458.08 nm with increasing glucose concentration. This region corresponds to the O-H stretch first overtone. Figure 5-2 shows the linear relation between glucose concentration determined by HPLC, and absorbance at 1 449 nm in aqueous glucose solutions.

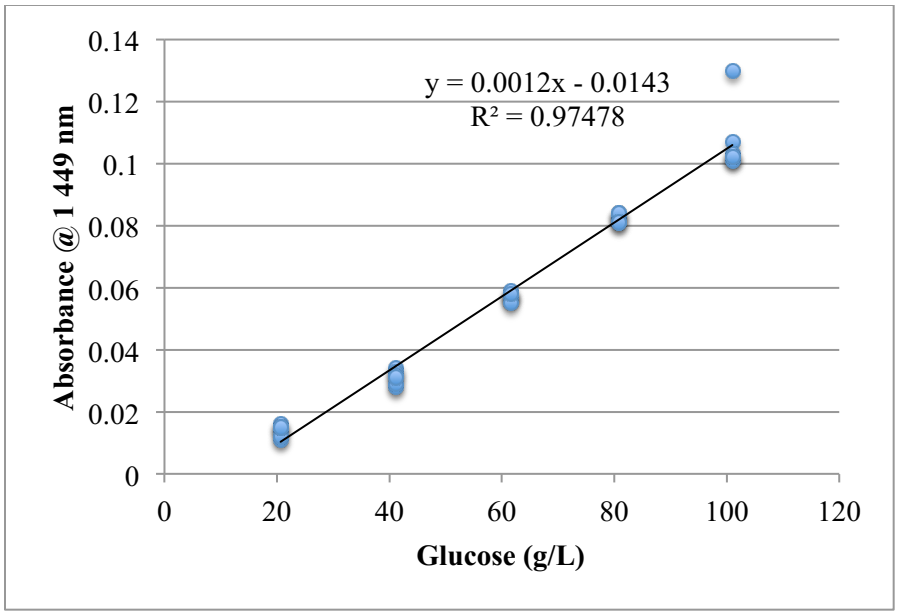

Figure 5-2 Glucose concentration in water as determined by HPLC & absorbance at 1 449 nm

Glucose in non-sterile media

NIR specular reflectance of glucose solutions in non-sterile media with six different concentrations (10, 20, 40, 60, 80, and 100 g/L) was determined in the flow cell. Media was used as reference (Figure 5-3 shows the spectrum of media using water as reference). Each sample was prepared in triplicate. Six spectra were obtained for each sample (see Figure 5-4).

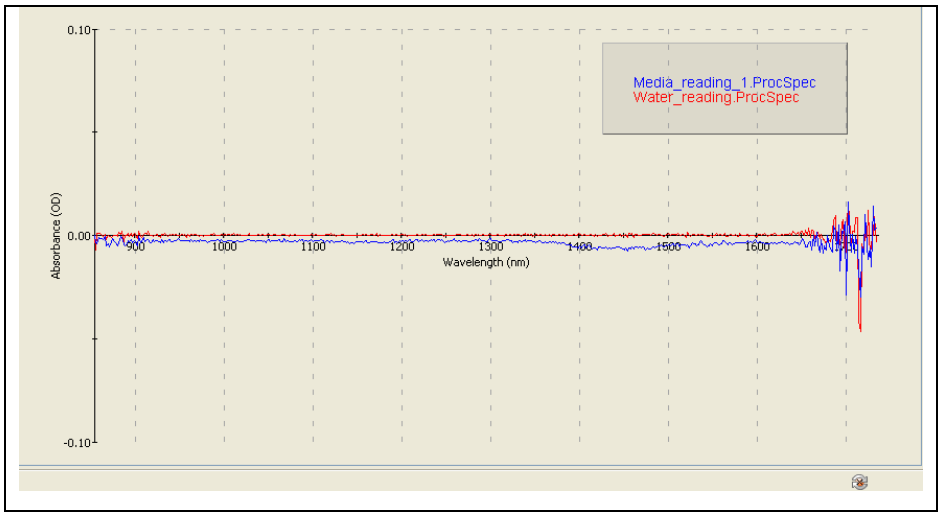

Figure 5-3 Media spectrum using water as reference

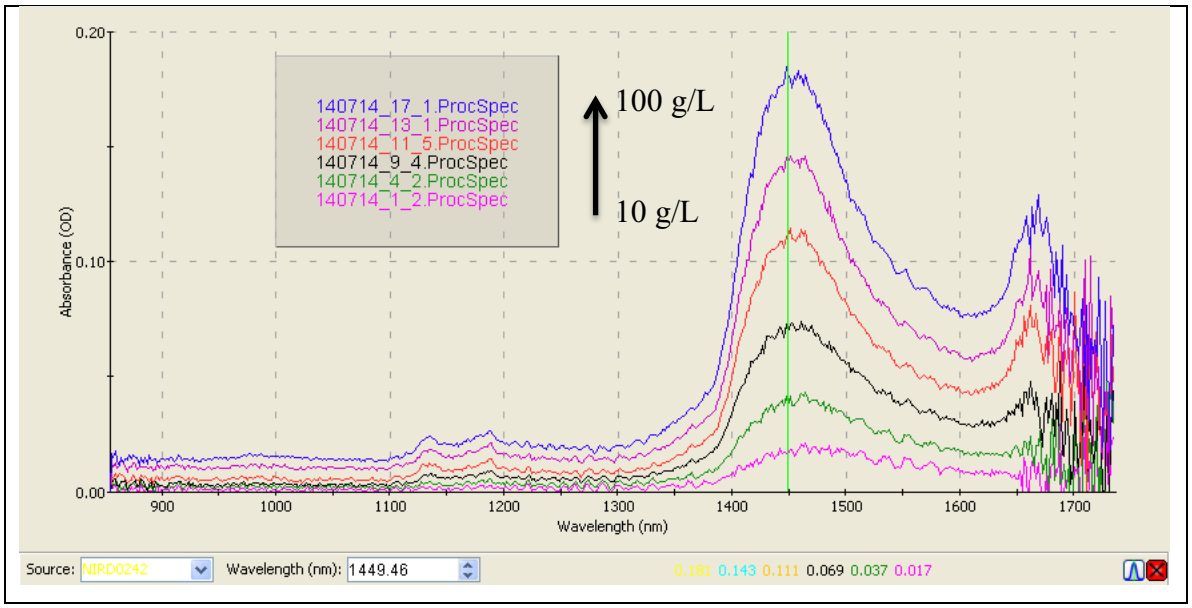

Figure 5-4 Glucose solutions in non-sterile media (10 - 100 g/L) spectra

Wavelength of the maximum observed absorbance shifted from 1 464.98.79 to 1 447.74 nm with increasing glucose concentration. This region corresponds to the O-H stretch first overtone. Figure 5-5 shows the linear relation between glucose concentration determined by HPLC, and absorbance at 1 449 nm in glucose solutions of non-sterile media.

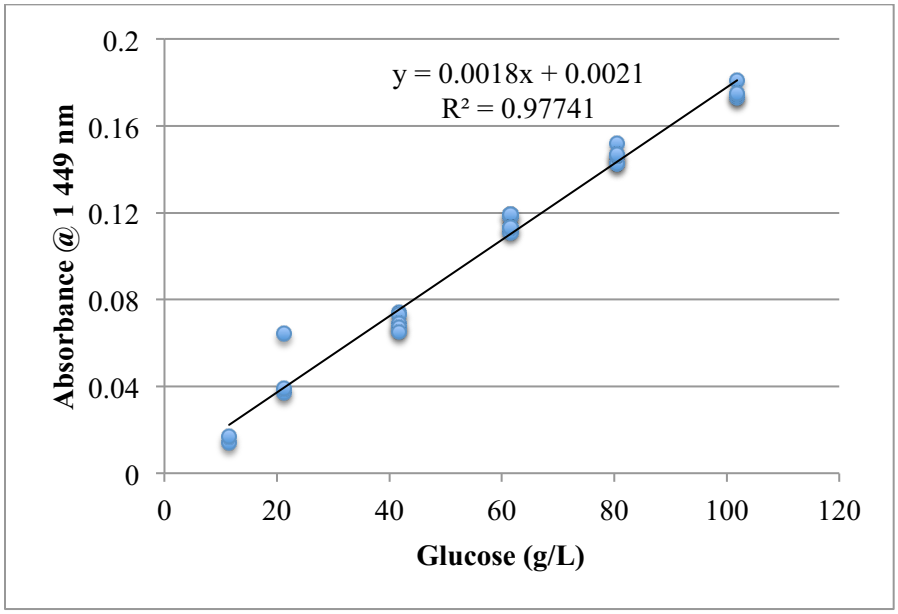

Figure 5-5 Glucose concentration in non- sterile media as determined by HPLC & absorbance at 1 449 nm

Glucose in sterile media

NIR specular reflectance of glucose solutions in sterile media with five different concentrations (20, 40, 60, 80, and 100 g/L) was determined in the flow cell. Water was used as reference. Each sample was prepared in triplicate. Six spectra were obtained for each sample (see Figure 5-6).

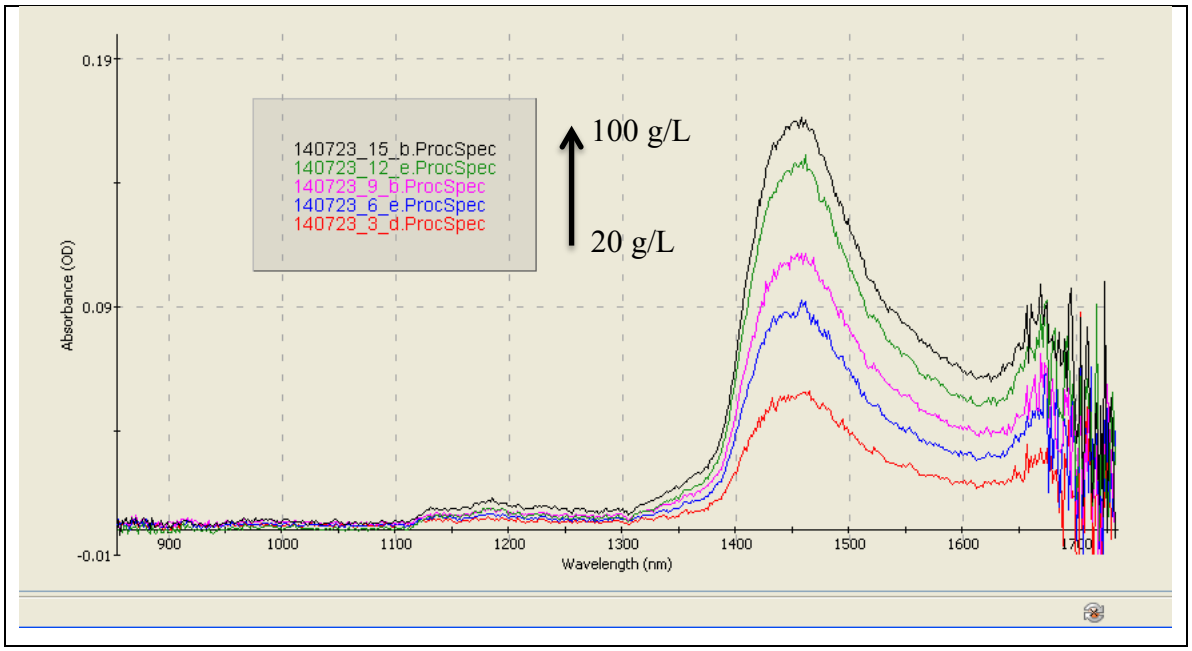

Figure 5-6 Glucose solutions in sterile media (20 - 100 g/L) spectra

Wavelength of the maximum observed absorbance (1 458.08 nm) did not shift with increasing glucose concentration. This region corresponds to the O-H stretch first overtone.

Figures 5-7 and 5-8 show the relation between glucose concentration determined by HPLC, and absorbance at 1 225 and 1 449 nm respectively, in glucose solutions of sterile media.

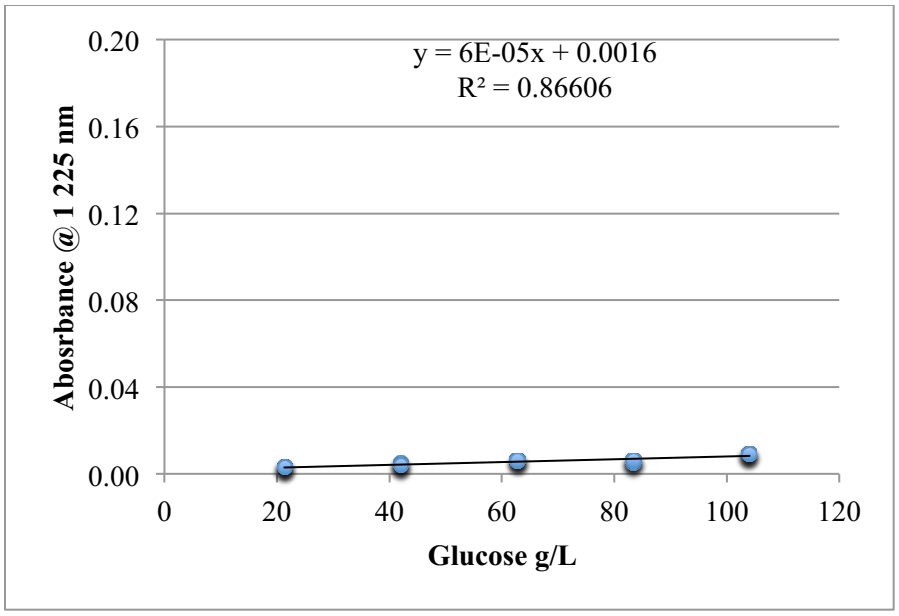

Figure 5-7 Glucose concentration in sterile media as determined by HPLC & absorbance at 1 225 nm

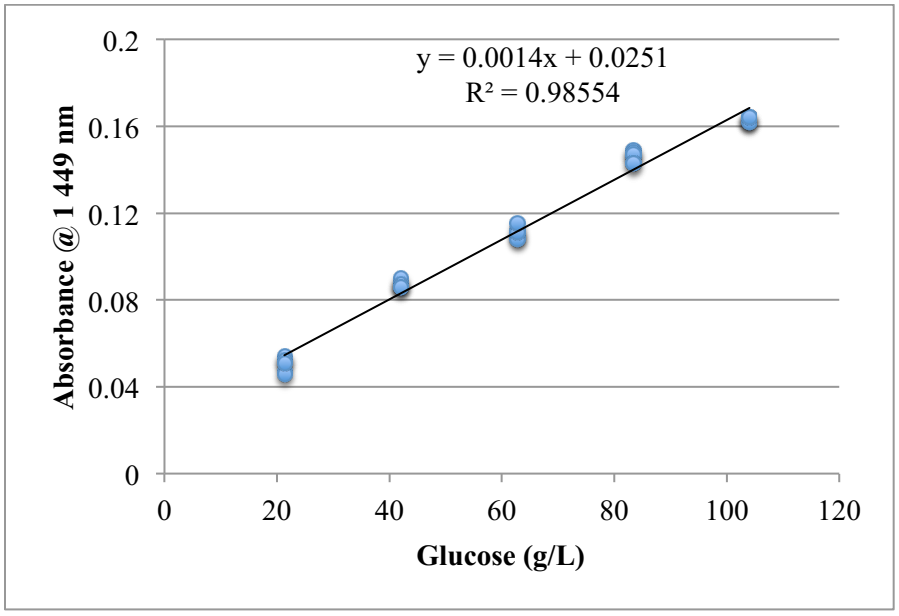

Figure 5-8 Glucose concentration in sterile media as determined by HPLC & absorbance at 1 449 nm

The shift of wavelength of the maximum observed absorbance, in the aqueous and non-sterile solutions, was noticed during the work of R. Giangiacomo *(119)* . However, in that study the shift was opposite, moving towards longer wavelengths with increasing sugar concentration at the water combination band (1 800 – 2 100 nm) as a result of the sugar –

water interactions. NIR spectra were collected in the transflectance mode from 1 100 to 2 500 nm, using a liquid sample cell with 0.25 mm thickness at 25 ± 1 °C.

The different behavior (non shifting of wavelength of the maximum observed absorbance) of the spectra obtained from glucose in sterile media may be caused by the presence of heat induced sugar breakdown, which is a well-known degradation effect of autoclaving (*e.g.*, the formation of 5-hydroxymethyl-2-furaldehyde (HMF), one of the major heat-induced decomposition products of hexoses) *(117, 120)* .

5.1.2 Biomass Determination

Fresh water green microalgae *A. protothecoides* was used to test and validate the ability of the NIR Specular Reflectance Flow Cell to measure biomass concentration. Figure 5-9 shows the spectra from heterotrophic and mixotrophic microalgae.

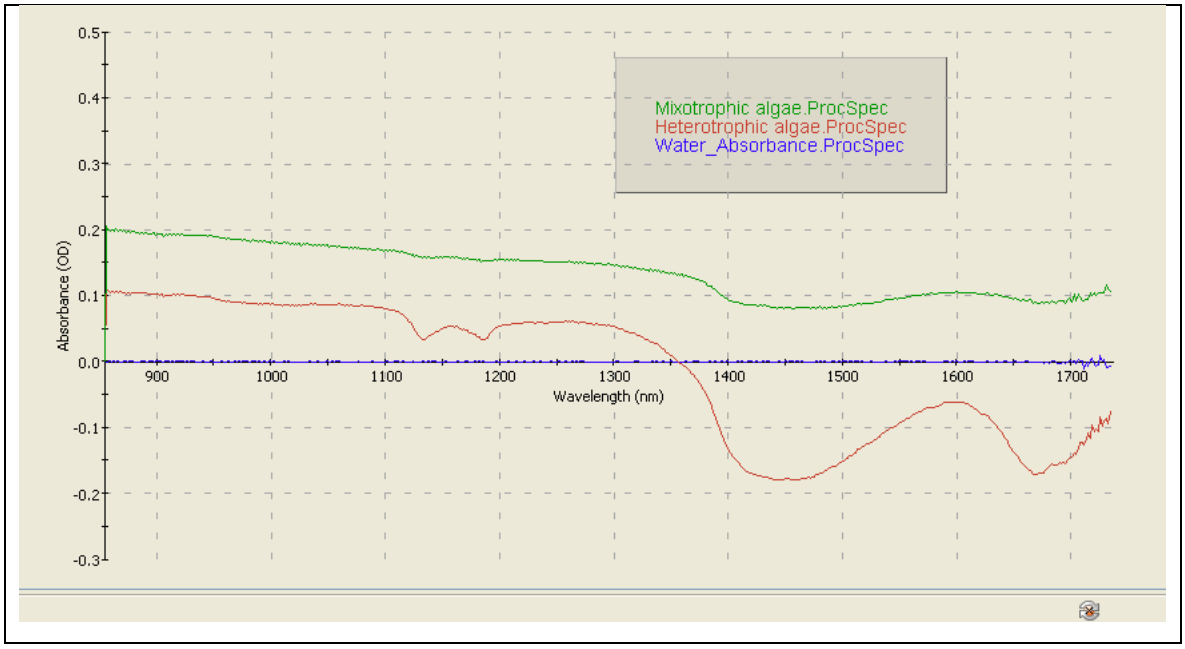

Figure 5-9 Spectra of water used as reference (blue line), heterotrophic (red line), and mixotrophic microalgae (green line) (Prototype I)

As reviewed in chapter 2 during the growth dynamics of microalgal cultures, microalgae export organic compounds into the culture broth. Figure 5-10 shows the spectrum of broth after cells were separated by centrifugation. Media was used as reference.

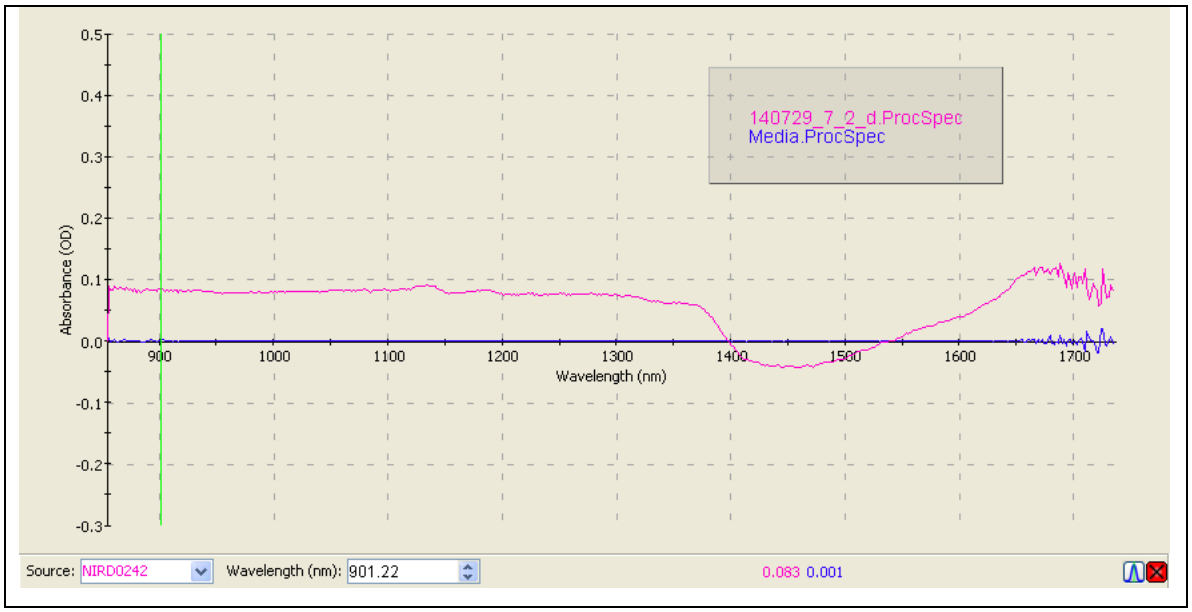

Figure 5-10 Spectrum of broth using media as reference

NIR specular reflectance of microalgal cultures with five different biomass densities (18 - 53 g/L) was determined in the flow cell. Water was used as reference. Duplicates were used for each sample. Six spectra were obtained for each sample (see Figure 5-11).

The required biomass densities were obtained using 2 600 mL of microalgal cultures in the stationary phase (~15 g/L). These cultures were first centrifuged, then supernatant was removed as needed, and samples were re-suspended.

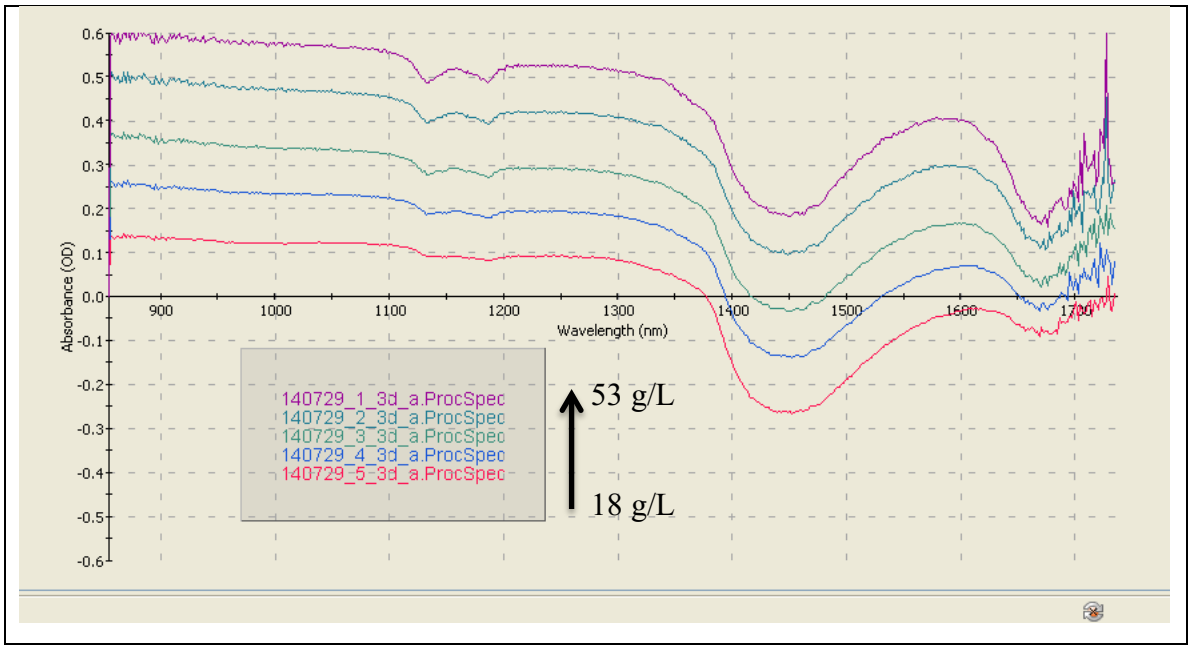

Figure 5-11 Microalgal cultures spectra (18 - 53 g/L)

Figures 5-12 and 5-13 show the linear relation between dry weight and absorbance at 1 225 and 1 449 nm respectively, in microalgal cultures. As a matter of fact, a linear relation is present practically along all the spectrum range up to 1 650 nm.

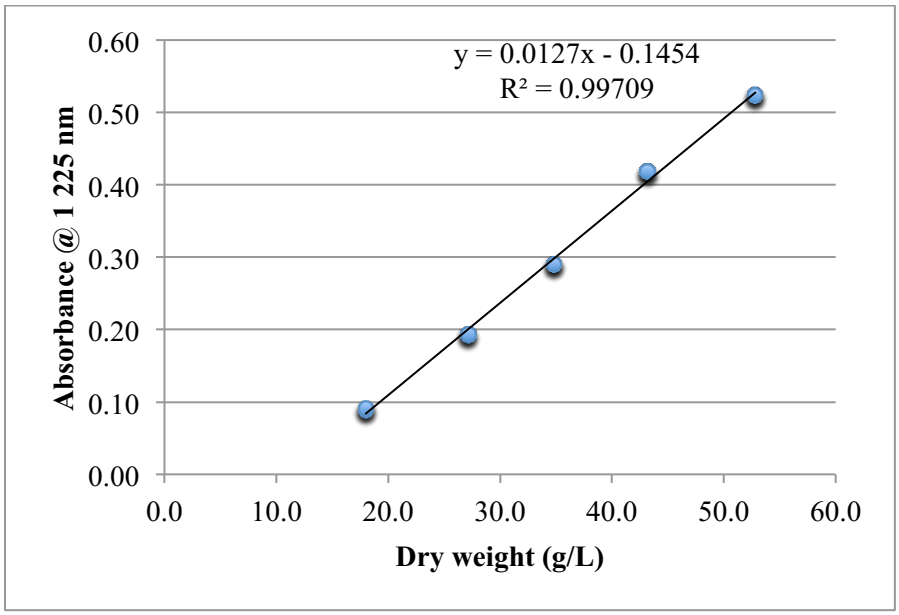

Figure 5-12 Dry weight of microalgal cultures & absorbance at 1 225 nm

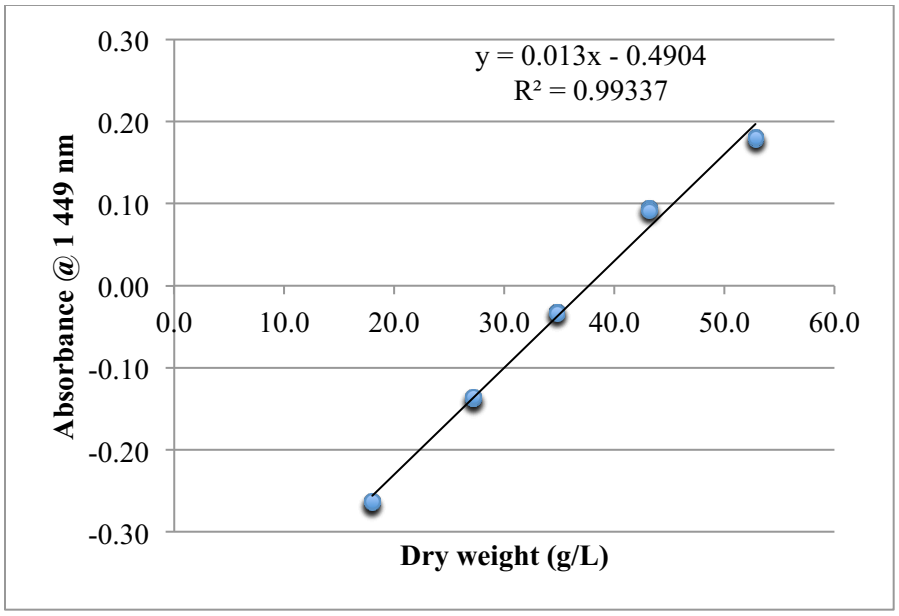

Figure 5-13 Dry weight of microalgal cultures & absorbance at 1 449 nm

The sensor has the potential to perform online measurements of dense microalgal cultures (~50 g/L) without needing dilution or any other sample preparation.

Sandnes *et al.* used transmittance in the NIR region of the spectrum (880 nm) for online estimation of dry cell mass in photoautotrophic cultures of *Nannochloropsis oceanica*, using an optical density sensor mounted externally on one of the horizontal tubes where microalgae was being cultivated *(47)* . The path length was 10 mm. The instrument sensitivity was suitable for a culture density range from 0.5 to 2 g/L, showing a maximum error of 8%. The data collected was used to maintain a constant culture density, by pumping a water/nutrient mix into the culture every 10 minutes while harvesting, in order to maintain an optimal population density (OPD) to maximize yields and reduce costs.

5.1.3 Simultaneous determination of glucose and biomass

Fix biomass and different glucose concentration

NIR specular reflectance of microalgal cultures (~9 g/L) with five different concentrations of glucose (20 - 100 g/L) was determined in the flow cell. Water was used as reference. Each sample was prepared in triplicate. Four spectra were obtained for each sample. Figure 5-14 shows the spectra obtained for the four consecutive readings of one microalgal sample. The coefficient of variation is 0.5 % at 1 449 nm wavelength.

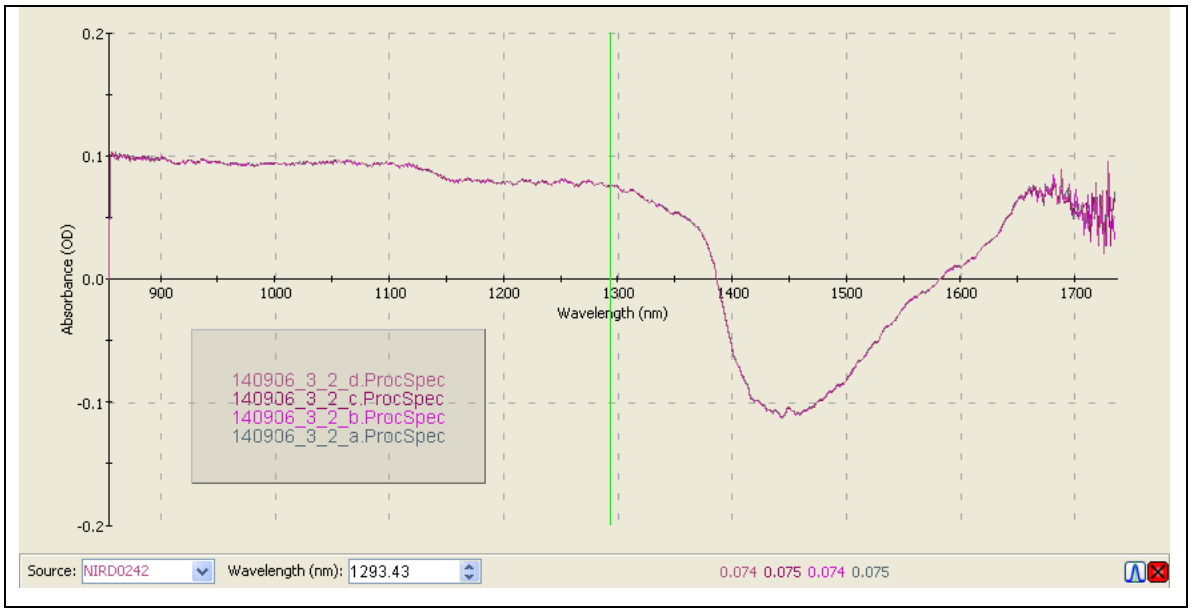

Figure 5-14 Four consecutive readings of one microalgal sample CV = 0.5 % (1 449 nm)

The required glucose concentrations were obtained using 1 500 mL of microalgal cultures in the stationary phase. These cultures were first centrifuged. Supernatant was removed, mixed with the corresponding amount of glucose, and returned to the samples before being re-suspended. Figure 5-15 shows the spectra obtained.

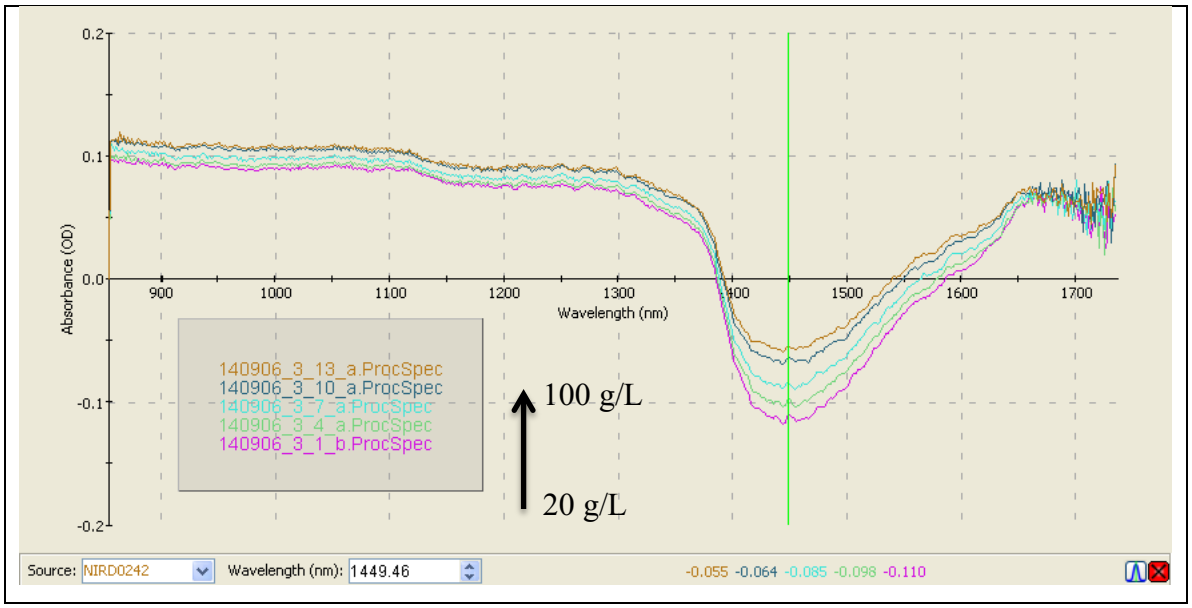

Figure 5-15 Microalgal cultures 9 g/L (20 - 100 g/L glucose concentration)

It is possible to observe the variation in the spectra as a result of different glucose concentrations. An increment in absorbance is detected along the entire spectrum, but especially around the region that corresponds to the O-H stretch first overtone.

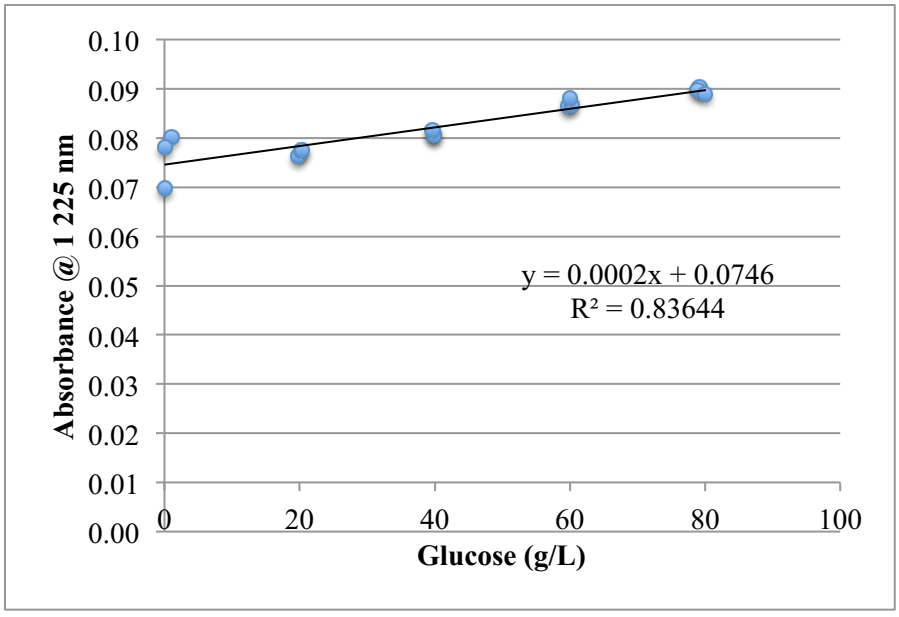

Figure 5-16 Glucose in microalgal cultures as determined by HPLC & absorbance at 1 225 nm

Figures 5-16 and 5-17 show the linear relation between glucose concentration increment in microalgal cultures and absorbance at 1 225 and 1 449 nm respectively, for the average of the three sets of samples.

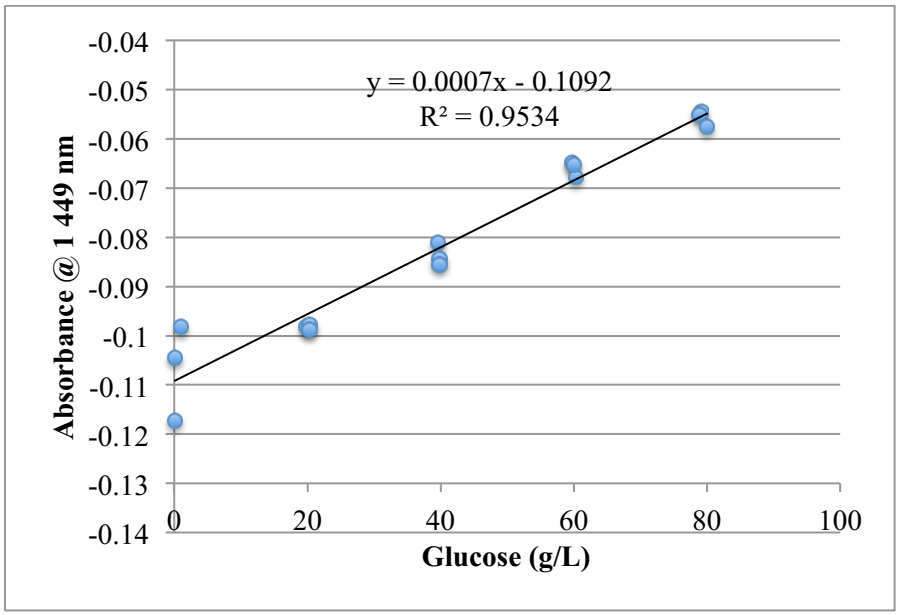

Figure 5-17 Glucose in microalgal cultures as determined by HPLC & absorbance at 1 449 nm

Different biomass and glucose concentrations

NIR specular reflectance of microalgal cultures with six different biomass densities (9 - 48 g/L) was determined in the flow cell. Each biomass density was evaluated using three different concentrations of glucose (1, 31, and 61 g/L). Water was used as reference. Four spectra were obtained for each sample.

The required biomass densities and glucose concentrations were obtained using 2 400 mL of microalgal cultures in the stationary phase (~20 g/L). These cultures were first centrifuged and supernatant was removed or added as needed. The corresponding amount of glucose was added as well (if required) and all the samples were re-suspended.

Figure 5-18 shows the spectra obtained for different biomass densities with glucose concentration of 1 g/L.

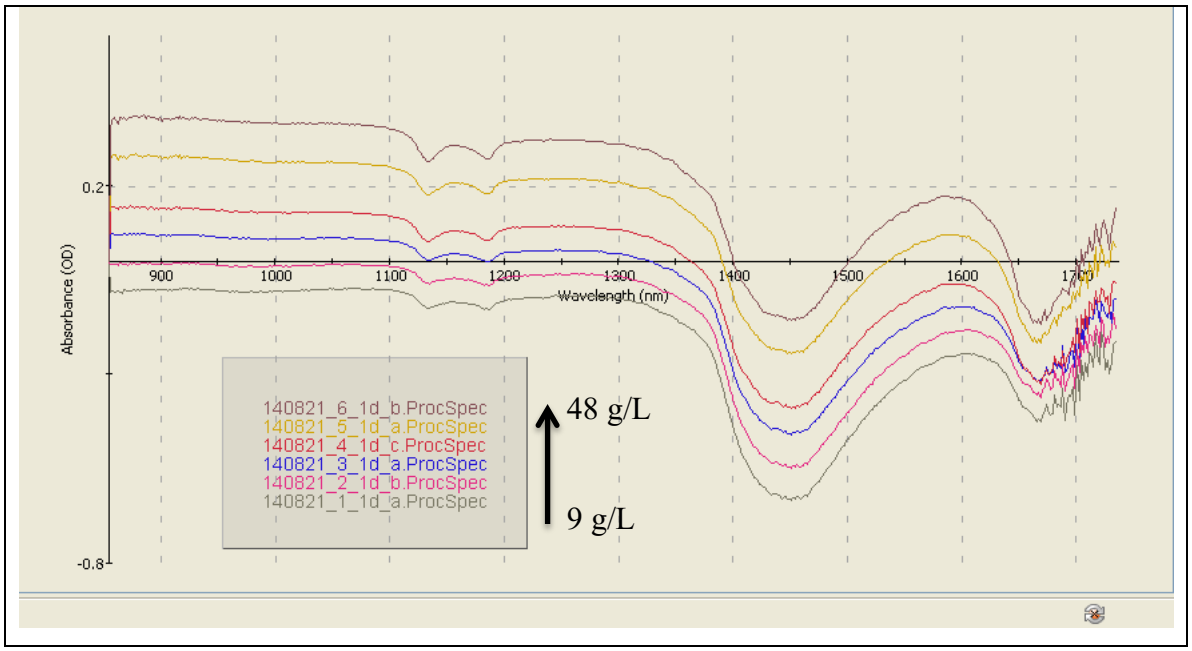

Figure 5-18 Microalgal cultures (9 - 48 g/L) with 1 g/L glucose concentration spectra

Figure 5-19 shows the spectra obtained for microalgal cultures with similar biomass density (18 g/L) and different glucose concentration (1, 31, and 61 g/L).

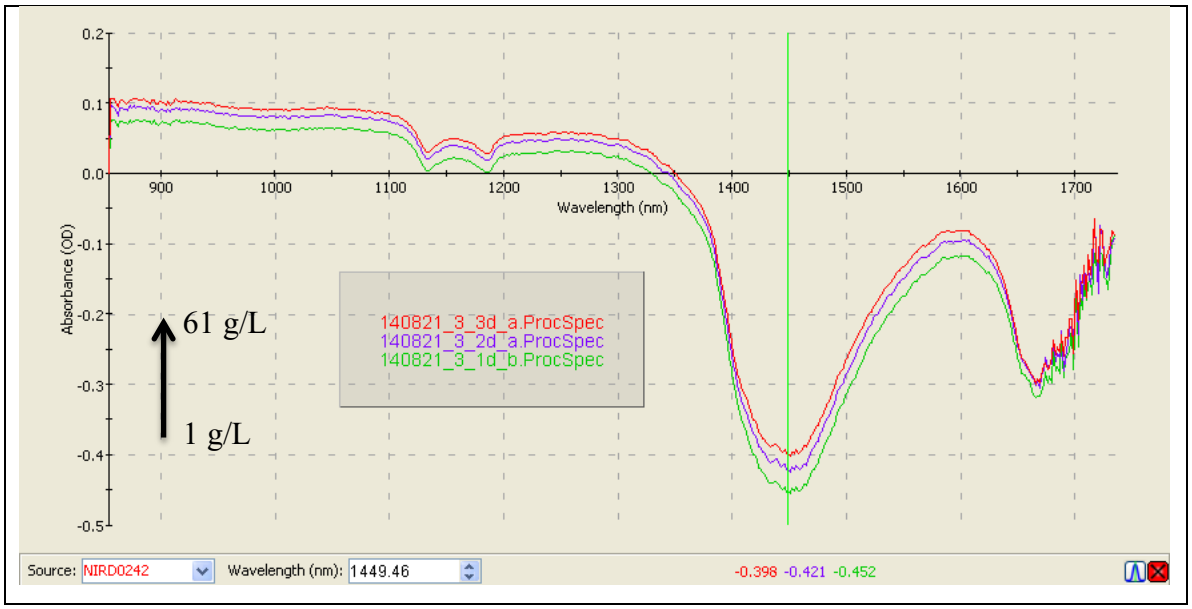

Figure 5-19 Microalgal cultures (18 g/L) with varying glucose concentrations (1, 31, and 61 g/L) spectra

Figures 5-20 and 5-21 show the relation between dry weight, glucose concentration, and absorbance at 1 225 and 1 449 nm in microalgal cultures.

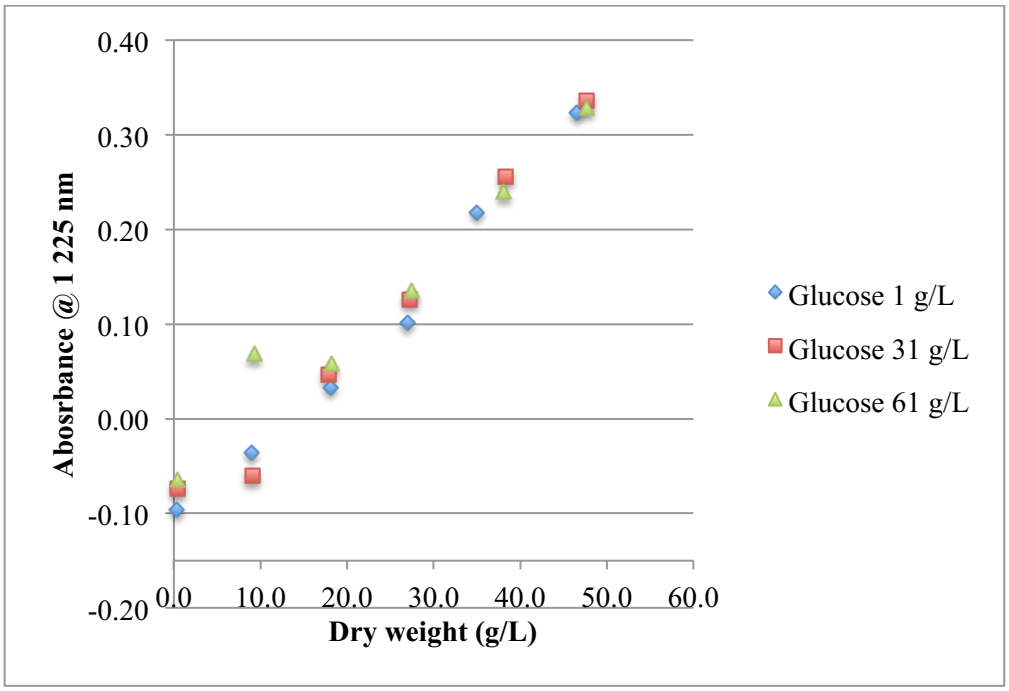

Figure 5-20 Microalgal cultures dry weight & absorbance at 1 225 nm

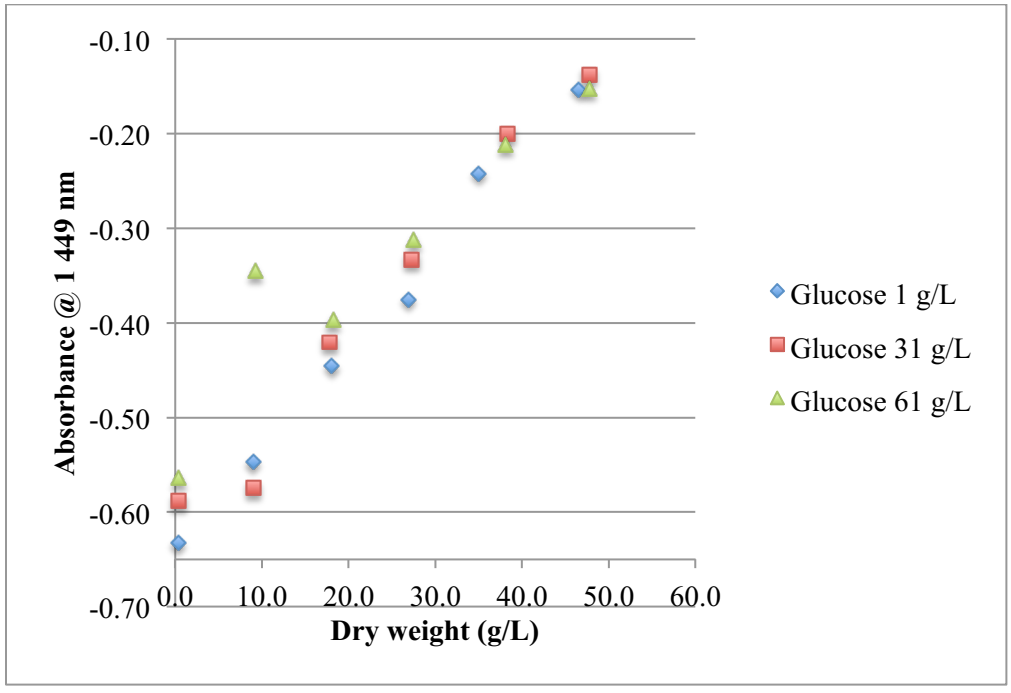

Figure 5-21 Microalgal cultures dry weight & absorbance at 1 449 nm

Data obtained for absorbance at 1 449 nm was evaluated to remove the apparent outlier present (9.3 g/L, -0.3455). Since the standardized residual for this point (-3.1) is out of ± 2 standard deviations, and that according to the residuals graph it is not consistent with its neighbors (see Figure 5-22), this point was confirmed as an outlier and removed from the data set.

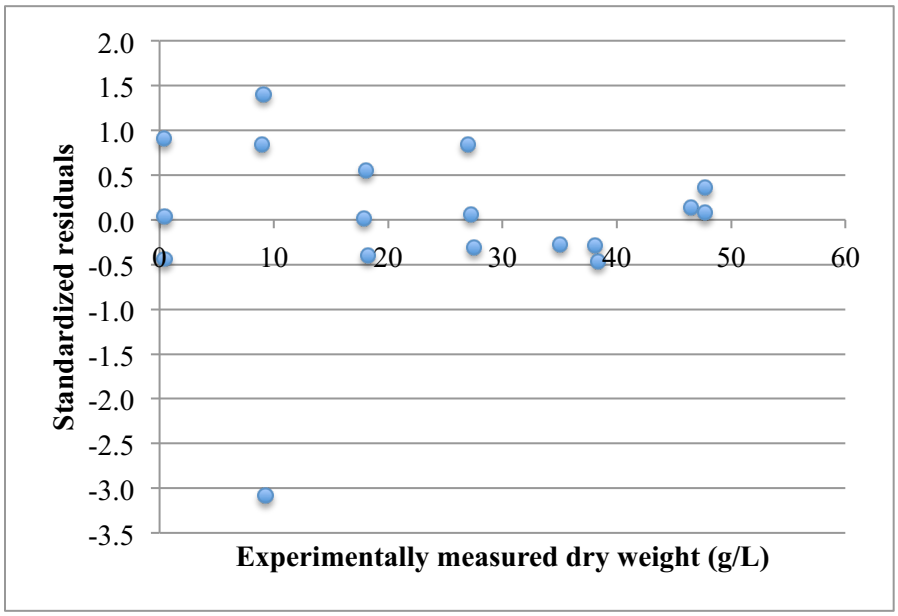

Figure 5-22 Residuals graph for data presented in Figure 5-21

Once the outlier was removed from the data set, the slopes of the three regression lines corresponding to a different glucose concentration were tested to evaluate if they were significantly different from the slope of the overall regression using an analysis of covariance (see Figure 5-23).

According to the analysis of covariance, there is not a significant difference between the slopes of the three regression lines corresponding to a different glucose concentration and the slope of the overall regression, which indicates that the sensibility of the sensor to changes in glucose concentration in microalgal cultures is limited.

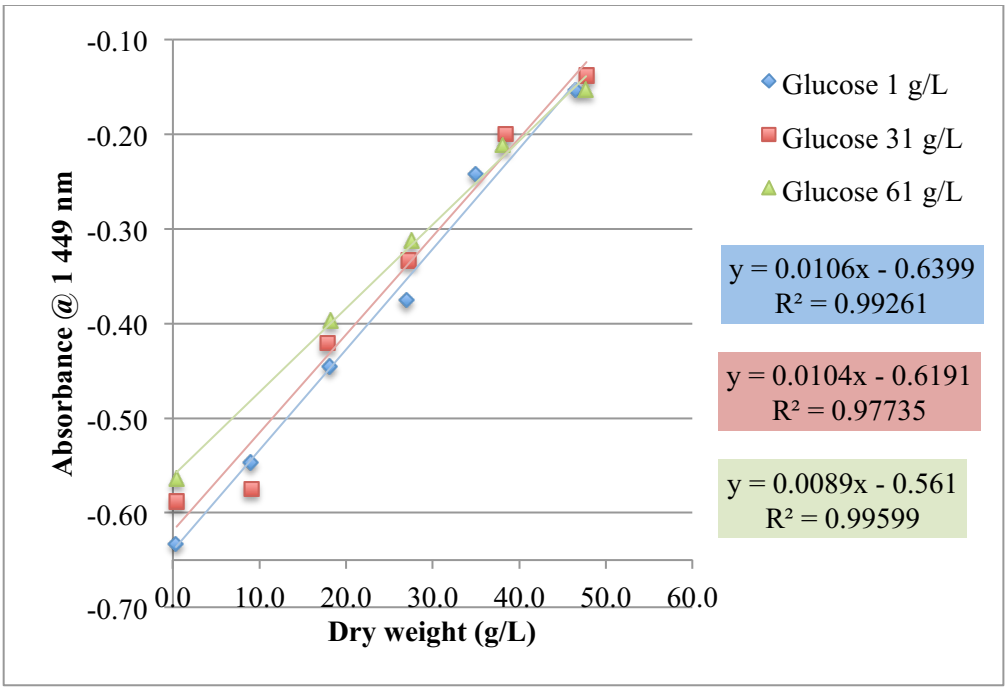

Figure 5-23 Slopes of each regression line with different glucose concentration

In order to verify that the variation obtained in the spectra of samples with similar biomass density and different glucose concentrations, was not the result of different size of the present cells, samples were observed under the microscopy, and evaluated using the size analyzer (see Figures 5-24 and 5-25).

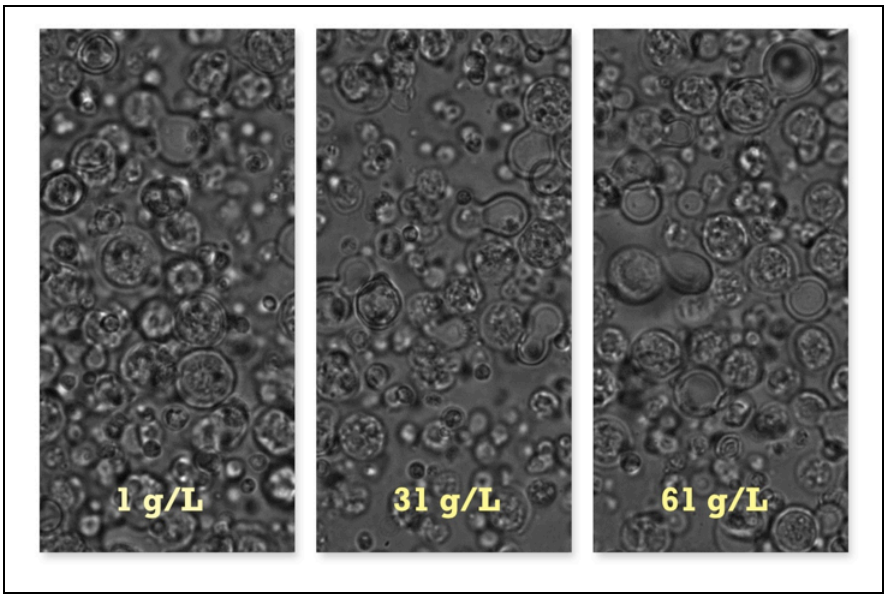

Figure 5-24 Microalgal cultures 18 g/L (1, 31, and 61 g/L glucose concentration)

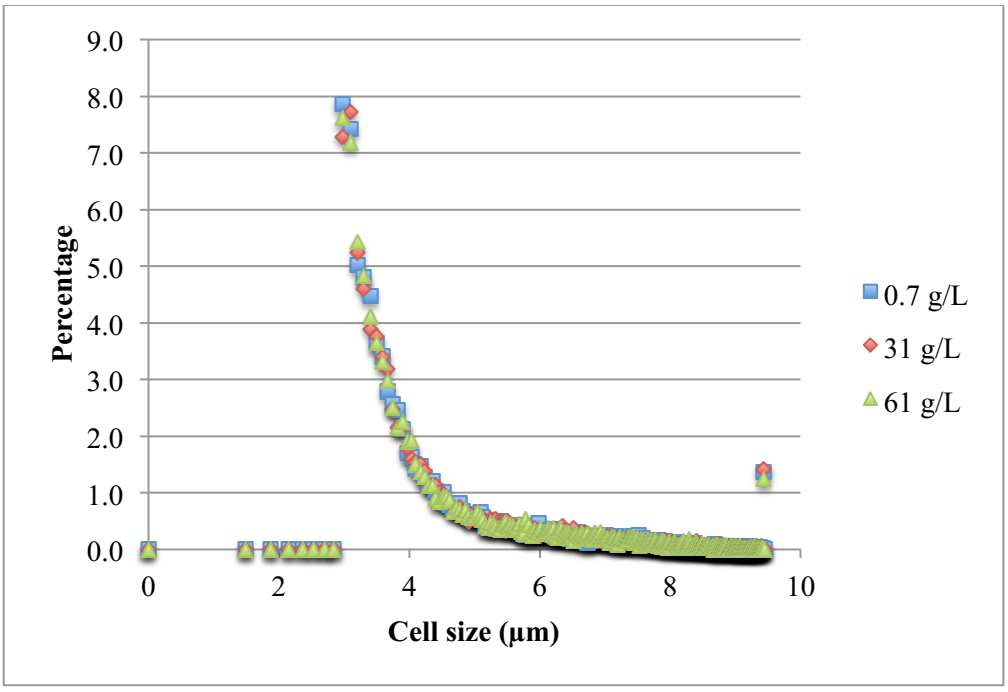

Figure 5-25 Size distribution of microalgal cultures (18 g/L)

Initial efforts to develop an optical glucose sensor were unsuccessful *(92)* . Eventually, NIR and MIR spectroscopy were used for glucose and fructose measurements in bioprocess media *(49)* . In that early work, one of the main drawbacks for the optical determination of glucose was the lack of sensitivity and/or specificity due to the influence of several factors in optical measurements. Therefore, adequate calibration of optical glucose measurements was essential for a correct determination *(92)* .

Noninvasive monitoring of blood glucose has been widely explored using NIR diffuse reflectance. The challenge faced during this kind of determination is the reduced concentration of the compound of interest compared to the vast and varying background. The main disadvantages encountered by Heise *et al*., who obtained spectra of mucous lip tissue, using Spectralon® reflectance standards, were the reproducibility of the tissue measurement as well as the positioning and contact pressure of the accessory used to collect the spectra *(121)* . Although Malin *et al*. used a fiber optic system and a support to take measurements from forearms, sample to sample variability remained, mainly due to variations in the skin surface roughness and hydration. Therefore, the need for a

comprehensive temperature control as well as compensation for variables intrinsic to the tissue sample was identified. Complexity of the NIR spectra made the identification of glucose absorbance very difficult. However, common sources of false correlation (*e.g.*, instrument drift and major blood analytes) were eliminated. An 80% Spectralon® reflectance standard was used during these determinations as well *(122)* .

In less complex systems, optical methods were successfully used to determine sugar content. Rambla *et al*. successfully determined total sugar, glucose, fructose, and sucrose content in fruit juices, employing partial least squares (PLS) treatment of first order derivative transmittance measurements. The wavelength ranges used were from 1 325 to 1 800 nm and from 2 020 to 2 390 nm. Samples were previously centrifuged and filtered before being evaluated utilizing a 1 mm path length *(123)* .

5.1.4 Oil determination

NIR specular reflectance of two microalgal cultures with different oil concentrations, and mixed in six different ratios was determined in the flow cell. Water was used as reference. Each sample was prepared in triplicate. Four spectra were obtained for each sample. Figure 5-26 shows the spectra obtained for one set of the six different mixtures.

There is a trend in the value of absorbance obtained. This value tends to decrease with increasing oil content at 1,449 nm as can be observed in Figure 5-27.

In contrast it was possible to obtain the same absorbance (-0.106) at 1 449 nm for triplicates of the same mixture (see Figure 5-28).

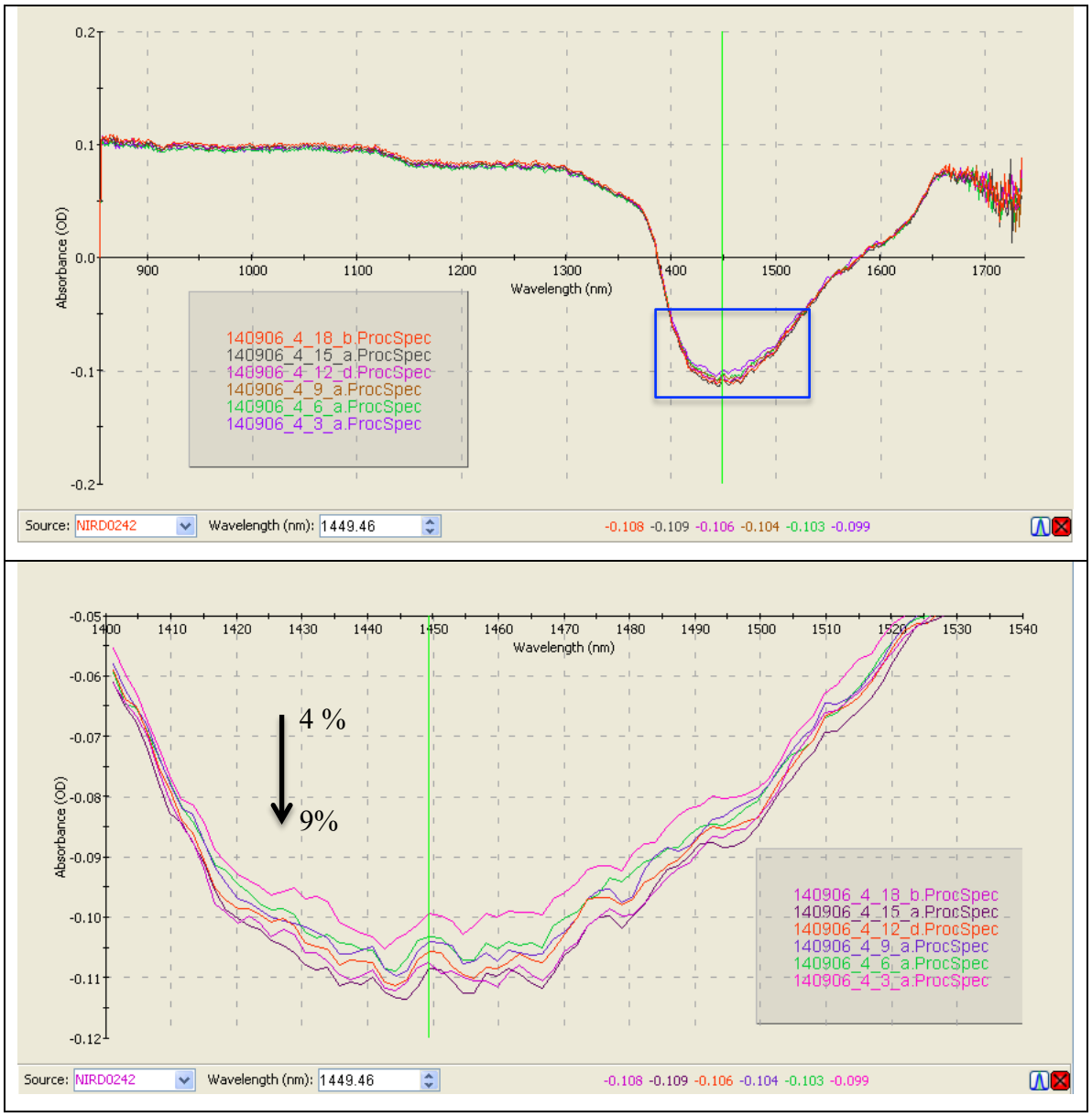

Figure 5-26 Microalgal cultures 9 - 10 g/L (4 - 9 % oil concentration) spectra

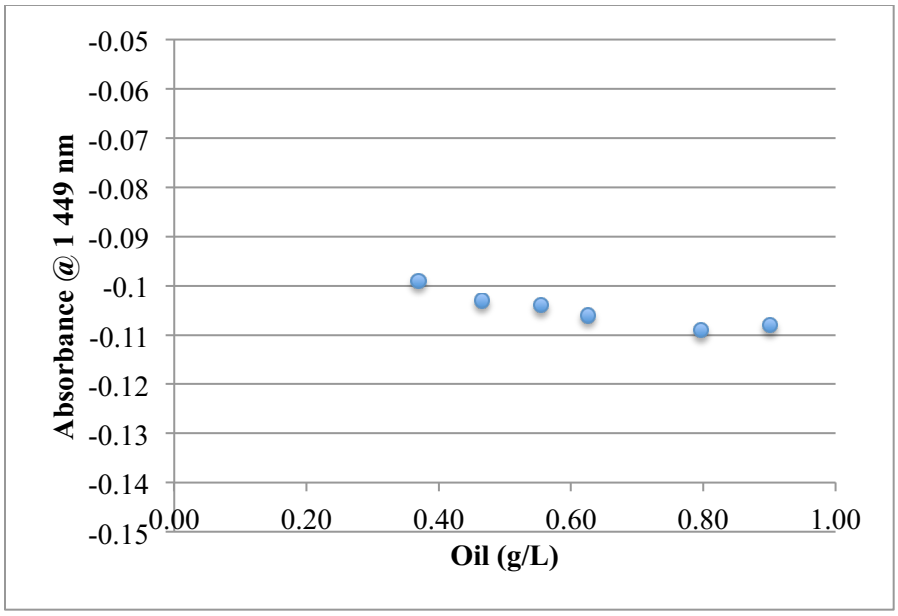

Figure 5-27 Oil in microalgal cultures as determined by fluorometric method & absorbance at 1 449 nm

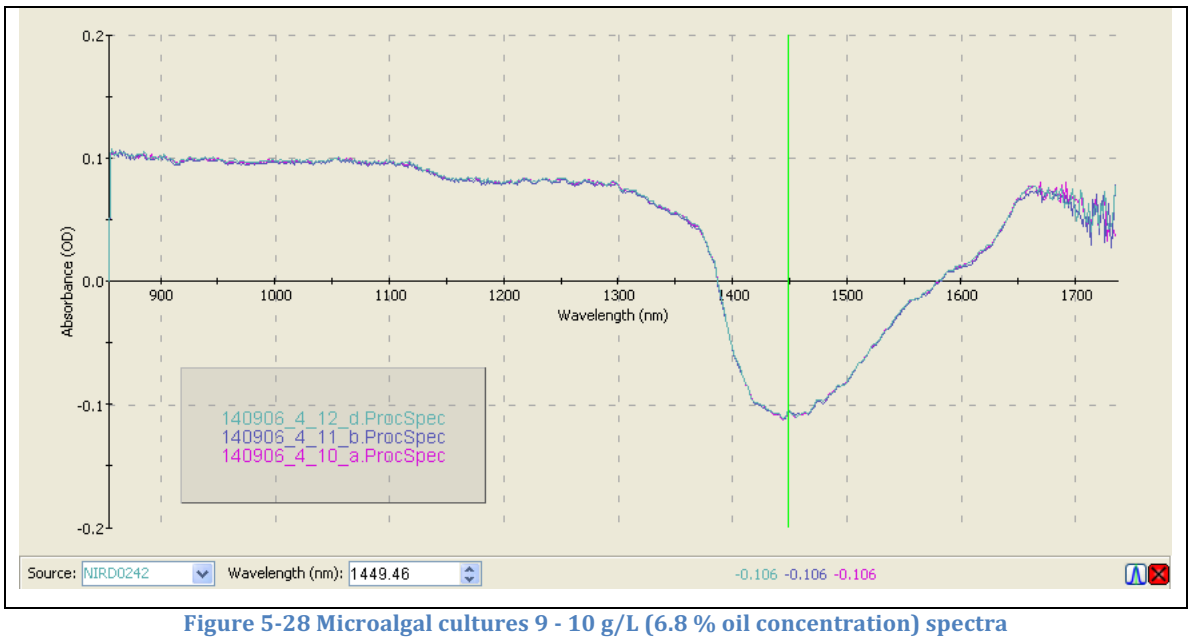

Figure 5-28 Microalgal cultures 9 - 10 g/L (6.8 % oil concentration) spectra

It is important to note that bands in the region between 1 380 – 1 500 nm contain contributions from the overtones of C-H vibrations and the first overtone of an O-H stretching mode, present in the monomeric specie of oleic acid, for example *(54)* . Table 5-1 presents the characteristic absorption bands of oils in the NIR range *(124)* .

Table 5-1 Characteristic absorption bands of oils in the NIR range

Bond vibration	Wavelength (nm)
First overtones of C-H stretching vibrations	(1 600 – 1 900 nm)
Second overtones of C-H stretching vibrations	(1 100 – 1 250 nm)
Combinations of C-H stretching vibrations	(1 350 – 1 500 nm)
	(2 000 – 2 200 nm)

Laurens *et al*. obtained accurate NIR reflectance models to predict exogenous lipid content and composition in microalgal biomass (previously lyophilized and ground in liquid nitrogen) of four phylogenetic species. Since one triglyceride and one phospholipid were used as references, it was demonstrated they have reasonably different NIR spectral fingerprints *(124)* . On the other hand, Brown *et al.* assessed NIR reflectance spectroscopy to determine potential fatty acid methyl esters (FAME) yield and biomass content of whole cells in a filter cake. The biomass was collected from microalgal cultures at late-logarithmic and stationary phases *(125)* . Samples were only filtered through 25 mm diameter glass fiber filters before being scanned, using as a reference a clean and dry glass fiber filter. Although very good predictability was obtained, spectra were dominated by strong absorption bands, which were related to the high moisture content.

5.2 Validation of the NIR Specular Reflectance Flow Cell

Actively growing cultures of *A. protothecoides* cultures were monitored to validate the usefulness of the NIR Specular Reflectance Flow Cell to monitor the dynamics of microalgal cultures.

5.2.1 Simultaneous monitoring of glucose and biomass

Variation between different batches, cultivated under apparently identical conditions, is an intrinsic characteristic of biological cultures *(28)* .

Ten microalgal batch cultures were conducted by sextuplicate (100 mL each). Each batch was inoculated every 48 hours. Media was refreshed for the first 5 batches after 300 hours. All batch cultures were stopped on the same day, and monitored in the NIR Specular Reflectance Flow Cell. Water was used as reference. Four spectra were used for each sample. Figure 5-29 shows the dry weight of the cultures. It was possible to reach up to 25 g/L.

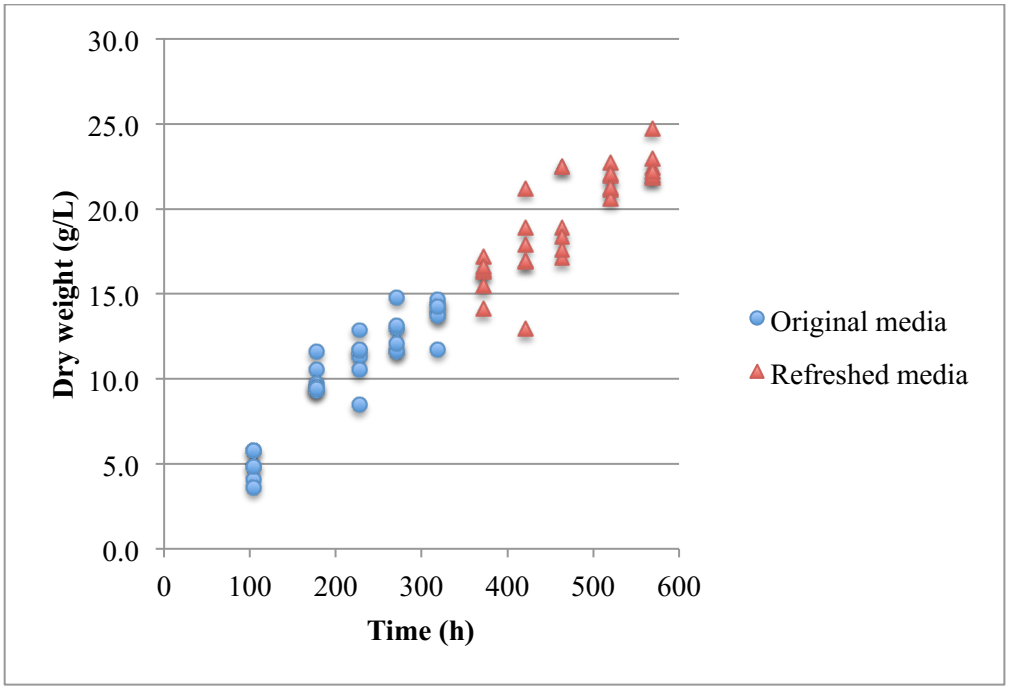

Figure 5-29 Dry weight of the microalgal batch cultures

Figure 5-30 shows the glucose concentration of the microalgal cultures.

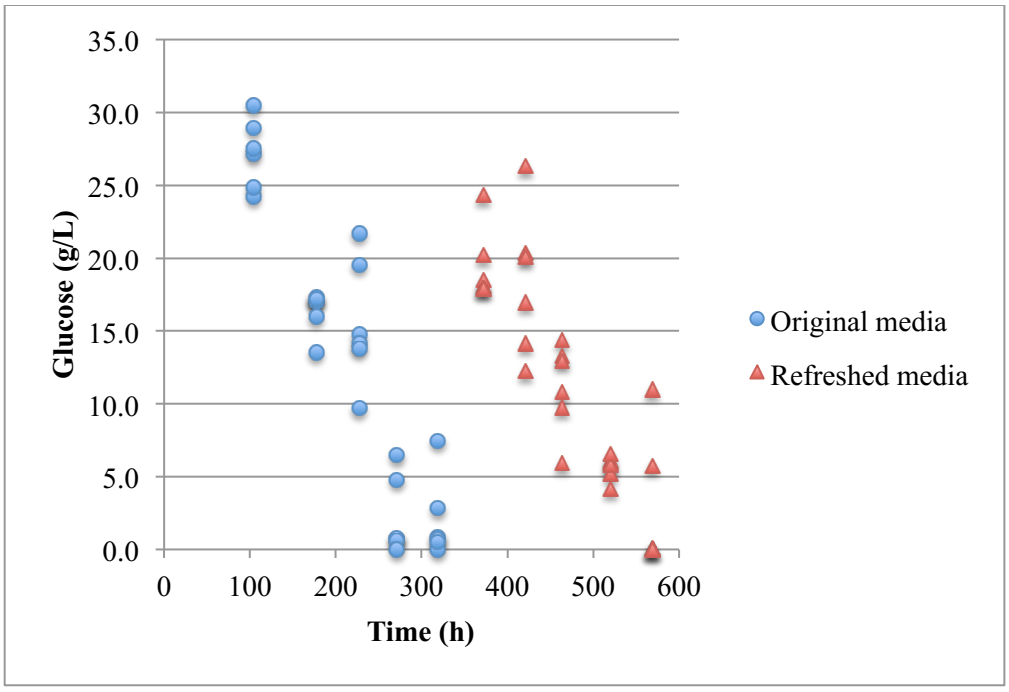

Figure 5-30 Glucose concentration of the microalgal batch cultures as determined by HPLC

Figure 5-31 shows the values of absorbance obtained for each sample at 1 225 and 1 449 nm.

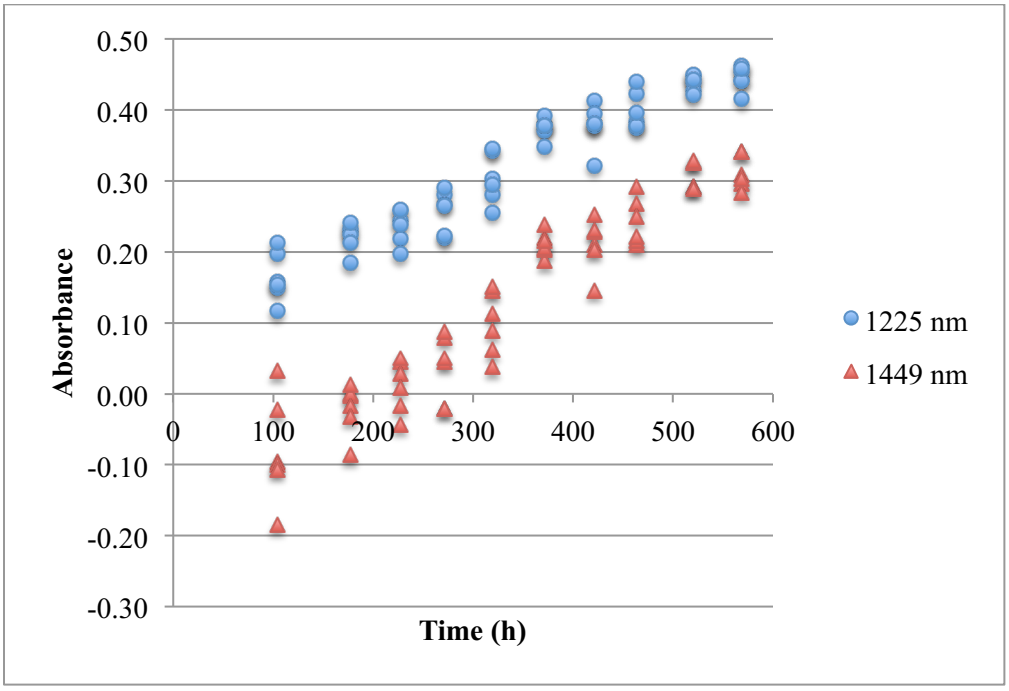

Figure 5-31 Absorbances of each sample at 1 225 and 1 449 nm

Figures 5-32 and 5-33 show the relation between dry weight and absorbance at 1 225 and 1 449 nm, respectively.

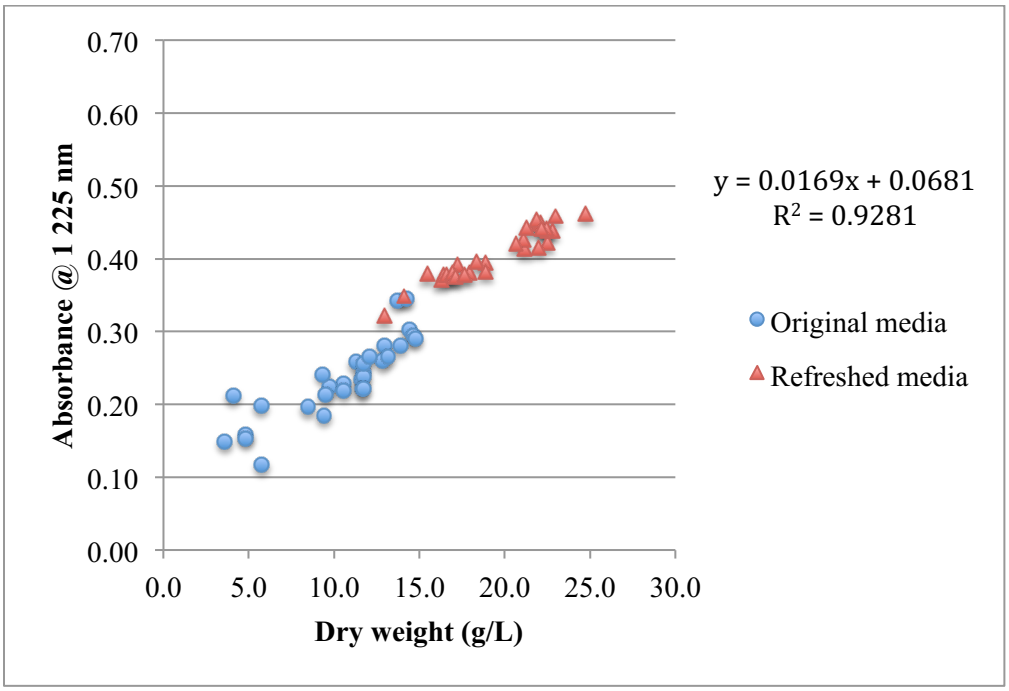

Figure 5-32 Dry weight of microalgal cultures & absorbance at 1 225 nm

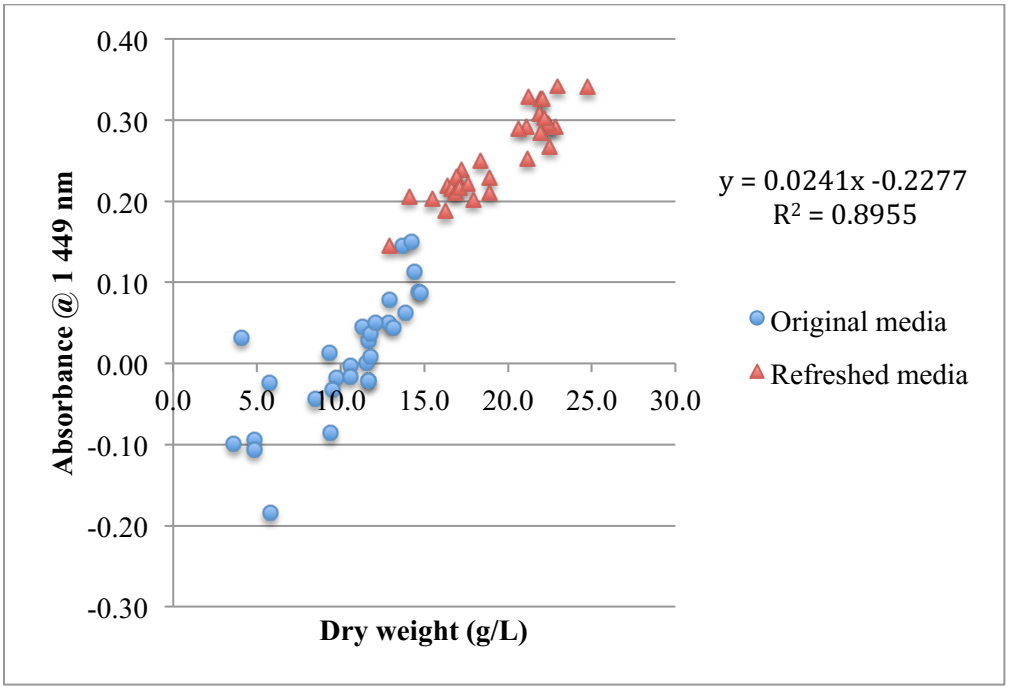

Figure 5-33 Dry weight of microalgal cultures & absorbance at 1 449 nm

Although, a relation can be observed between dry weight and absorbance at 1 225 nm, there is a high variation present when biomass concentration is below 10 g/L. This behavior is similar to that previously observed with Raman spectroscopy where high variance in biomass determination was observed during the first hours of a culture *(55)* . This error at low biomass concentration was attributed to interferences due to the significant number of changes in the culture media and in the microalgal cells during the lag phase.

In this work, a model was calibrated using the value of absorbance obtained at 1 225 nm for a training set of 30 of the 60 samples evaluated (odd samples from each of the 10 batches were arbitrarily chosen for the training set). The remaining samples (even samples) were used as a validation set to test the accuracy of the model. Figure 5-34 shows the measured versus predicted values of dry weight for the validation set. The root mean square error (RMSE) value was 1.3. The model will predict reliable, accurate, and reproducible values of dry weight for samples within the calibration range.

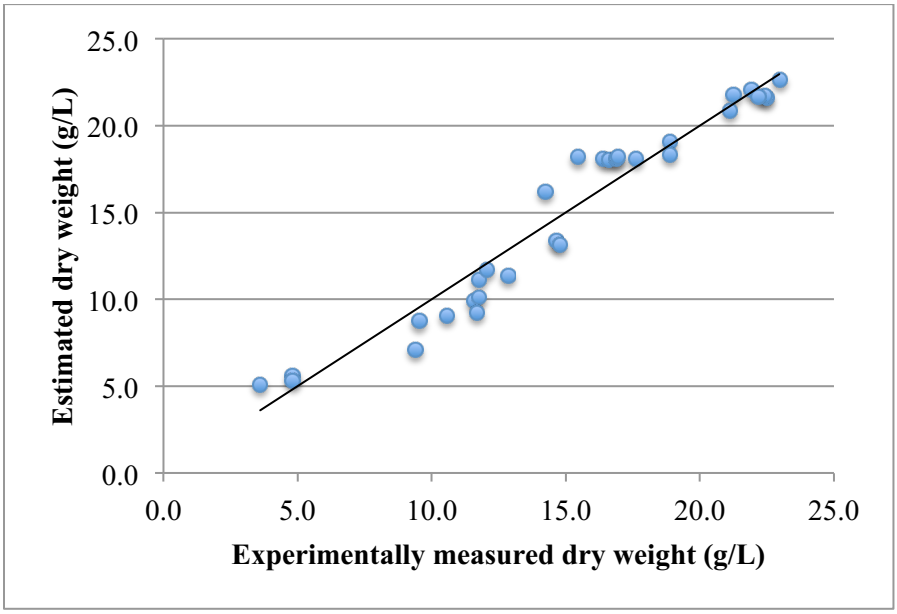

Figure 5-34 Measured versus predicted dry weight concentration and identity line

Since a nonzero bias is not observed, it can be concluded that there is no background interference or scattering whiting the range of the calibration line *(91)* .

Another model was calibrated using the two wavelengths utilized during this work (1 225 and 1 449 nm) to determine dry weight. However, the quality of the model calibrated using only one wavelength (1 225 nm) was better.

Figures 5-35 and 5-36 show the relation between glucose concentration and absorbance at 1 225 and 1 449 nm, respectively. Please note that graphs are conventionally presented.

In practice, glucose concentration decreases with time while biomass increases as can be observed in Figures 5-30 and 5-29, respectively.

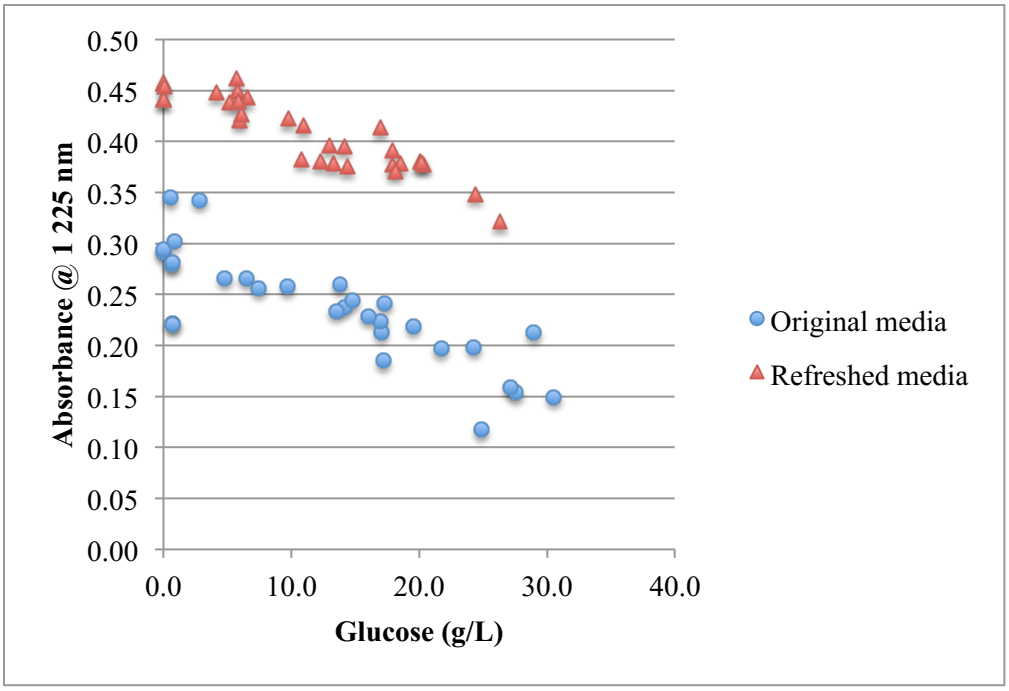

Figure 5-35 Glucose in microalgal cultures as determined by HPLC & absorbance at 1 225 nm

In both graphs, the strong effect that biomass concentration has on the spectra can be observed. Even when glucose concentration is decreasing, absorbance keeps increasing in accordance with increasing biomass density. In agreement with the results obtained at the beginning of chapter 5 when addressing glucose determination, absorbance values should decrease with decreasing glucose concentrations.

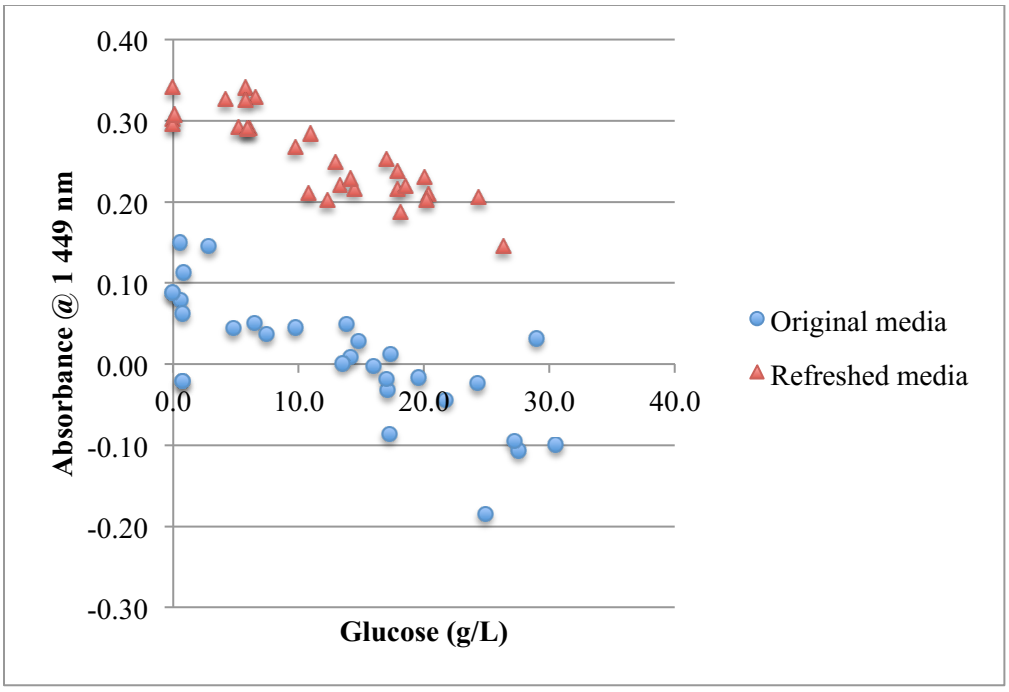

Figure 5-36 Glucose in microalgal cultures as determined by HPLC & absorbance at 1 449 nm

We now have an overall picture of the performance and potential of the NIR Specular Reflectance Flow Cell to monitor microalgal cultures. The sensor has the capacity to continuously determine glucose concentrations in aqueous solutions as well as in non-sterile and sterile media. In addition, fast and continuous determination of biomass density of microalgal cultures can be performed using the sensor. Simultaneous evaluation of biomass and glucose concentration in microalgal cultures is not possible with the existing configuration as a result of the large influence that biomass has on the spectra. Oil estimation was also evaluated, however, only a weak response was observed.

6

Conclusions and Recommendations

6.1 Conclusions

The ability to continuously monitor critical process parameters and quality attributes of microalgal cultures is necessary to understand the physiological effects that culture conditions have on the mechanisms that govern the natural cycles of microalgal productivity. In consequence, these observations are essential to optimize the performance of complex processes like microalgal cultures in order to achieve optimal productivity. To reach this goal, it is essential to develop quality instrumentation that enables the online acquisition of data during microalgal processes. Measurement devices for microalgal cultivation should ideally be: on-line, rapid, sterilizable, stable, and selective with minimal need of calibration *(58)* . Some of the most promising analytical procedures to develop robust, real time analytical tools are those based on NIR spectroscopy.

With this in mind, the general objective of this research work was the use of NIR Spectroscopy for online monitoring of microalgal cultures. The specific purpose was the evaluation of biomass, glucose, and lipid concentration.

In order to achieve this objective, a NIR Specular Reflectance Flow Cell was developed. It was proved that this device has the potential to provide fast and automatic determination of biomass density of microalgal cultures, without the need to remove cells from the sample. Unfortunately, determination of glucose concentration is not possible with the present configuration due the large impact that biomass has on the spectra obtained. In the case of oil determination, the response obtained is very weak, and in consequence oil determination is not possible with the present configuration as well.

This flow cell is an online monitoring dispositive that requires less than 40 mL of sample volume to fill the loop of the system. Since measurements are determined by specular reflection, suspended solids or other scattering material do not have an effect on the determination as in the case of diffusive reflectance measurements *(126)* . This characteristic is very important taking on account that, significant changes in cell size, shape, and color can occur during microalgal cultivation *(58)* . Once the sample is recirculating through the NIR Specular Reflectance Flow Cell, a spectrum is obtained every 3.6 seconds.

An efficient monitoring of microalgal processes in one of the key pieces to satisfactorily understand their complex growth dynamics. As a result, the effective optimization of different microalgal processes being developed around the world will be possible.

6.2 Recommendations

Since the NIR Specular Reflectance Flow Cell is a novel technique for online monitoring of microalgal cultures, there is plenty of room for improvement.

Evaluation of the determination of oil concentration using instrumentation with a complete range of NIR spectroscopy (0.8 - 2.5 mm) is advisable due to the presence of characteristic absorption bands of oils within the missing part of the range in the present instrumentation.

Preprocessing of the raw data such as the obtainment of first or second derivatives in order to deconvolute possible overlapped peaks is recommended. This procedure may be especially helpful to improve glucose determination. In addition, determination of glucose concentration in the culture broth once microalgal cells have been removed should be addressed. According to the results obtained during the length of this work, this procedure may be a possibility for a continuous quantification of glucose in microalgal cultures.

Further work will involve the inclusion of measures to ensure sterility inside the NIR Specular Reflectance Flow Cell, and to overcome different drawbacks derived from encapsulating the flow cell. Blowing of nitrogen gas could be one strategy to prevent water condensation inside the flow cell, which will definitely affect the performance of the reflectance probe.

Since monitoring of microalgal cultures will be a prolonged determination, it is advisable to monitor the light source and take the actions required to correct for any drift that may occur in order to achieve optimal results. Nevertheless, for tungsten lamps, the drift associated is often spectrally uniform.

It will also be important to evaluate the effect on the spectra of additional factors that could be potentially present during the length of the culture, such as turbidity caused by small bubbles trapped in the culture media.

Physicochemical surface properties of microalgae are relevant when it comes to biofouling of surfaces due to cell to substrate interactions. Evaluation of the effect of possible biofouling of the channel due to extended use should be addressed. For instance, according to Ozkan *et.al Chlorella vulgaris* (green alga, UTEX 2714) has a hydrophilic surface. Differences in surface properties of microalgae can be attributed to their cell wall structures, and the surface groups present on them. Hydrophilic species do not form flocs easily but rather form planktonic cultures. In contrast, species known to form colonies have markedly hydrophobic surfaces, where surface-surface interactions are stronger than surface-water interactions. This characteristic usually leads to biofouling, because hydrophobic alga attached at higher density and with higher strength of adhesion to surfaces, especially to the hydrophobic ones. Desorption experiments to quantify the adhesion strength were performed by varying flow rates in a parallel-plate flow chamber, which resulted in an increment in wall shear rates, where cells experienced lift and mainly drag forces *(127, 128)* . In a further study, after the evaluation of cell-substratum and cell-cell interactions, of 10 different microalgal species and 6 different substrates (including polycarbonate), the use of hydrophilic algae and hydrophilic surfaces was

suggested to minimize biofouling. In conclusion, since cell size is also an important factor in the mentioned interactions, to inhibit the adhesion of algal cells, both surface interaction energies and hydrodynamic effects should be taken into account to select algae and substrata pairs *(129)* . An *in situ* cleaning procedure or self- cleaning surface materials would be ideal for online optical sensors *(58)* .

Further work to ensure enough reliability and stability of the NIR Specular Reflectance Flow Cell, will guarantee its appropriate use as an on-line analyzer of microalgal cultures.

References

1. Workman, J., Jr.; Lavine, B.; Chrisman, R.; Koch, M. Process Analytical Chemistry. *Anal. Chem.* **2011**, *83*, 4557-4578.

2. Advance Biofuels Association Biofuels - Feedstock. *http://advancedbiofuelsassociation.com/page.php?sid=2&id=19* (accessed 10/10, 2014).

3. Kommers, N. Algae biomass organization applauds WV Sen. Manchin and RI Sen. Whitehouse for support of Carbon Utilization Technology. *http://www.biofuelsjournal.com/articles/Algae_Biomass_Organization_Applauds_WV_Sen__Manchin_and_RI_Sen__Whitehouse_For_Support_of_Carbon_Utilization_Technology-146728.html* (accessed 01/21, 2015).

4. Thurmond, W. Latina American feedstock trends. *http://www.emergingmarkets.com/biodiesel/pdf/BiofuelsInternational_FeedstockPriceTrends_LatinAmerica_Nov2007_WillThurmond_EmergingMarketsOnline.pdf* (accessed 01/21, 2015).

5. Thurmond, W. Algae investment trends & markets insight. *http://www.emergingmarkets.com/algae/Algae_Investment_Trends_Markets_Insight_EmergingMarketsOnline.pdf* (accessed 01/16, 2015).

6. Thurmond, W. Biofuels: a sea change. *http://www.emergingmarkets.com/algae/A%20Sea%20Change%20For%20Biofuels_Emerging%20Markets%20Online.pdf* (accessed 01/16, 2015).

7. Richmond, A. *Handbook of microalgal culture: biotechnology and applied phycology;* Oxford, OX, UK; Ames, Iowa, USA: Blackwell Science, 2004.

8. Thurmond, W. Algae's culture club: San Diego. *http://www.emergingmarkets.com/algae/Algae_2020_Study_Site_Tour_San_Diegos_Culture_Club.pdf* (accessed 01/15, 2015).

9. Emerging markets online Algae 2020 Vol 2 Summary and Contents. *http://www.emergingmarkets.com/algae/Algae2020StudyandCommercializationOutlook.pdf* (accessed 01/16, 2014).

10. Thurmond, W. Five key strategies for algae biofuels commercialization. *http://www.emergingmarkets.com/algae/Algae%2020205%20Strategies%20For%20*

Commercialization%20Emerging%20Markets%20Online.pdf (accessed 01/17, 2015).

11. Watson, E. Astaxanthin: Still red hot or cooling off? *http://www.nutraingredientsusa.com/Suppliers2/Astaxanthin-Still-red-hot-or-cooling-off-The-Dr-Oz-effect-two-years-on* (accessed 02/06, 2015).

12. Enzing, C.; Ploeg, M.; Barbosa, M.; Sijtsma, L. Microalgae-based products for the food and feed sector: an outlook for Europe. *JRC Scientific and Policy Reports* **2014**, *EUR 26255 EN*.

13. Algae Biomass Organization Algae Industry Project Book 2013. *http://www.algaebiomass.org/wp-content/uploads/2010/06/ABO_project_book_lo-res_July2013.pdf* (accessed 02/06, 2015).

14. Gorman, C. EPA Approves Algenol fuels for renewable fuel standard. *http://www.algenol.com/sites/default/files/press_releases/EPA%20Approves%20Algenol%20Fuels%20for%20RFS.pdf* (accessed 02/06, 2015).

15. Sapphire Energy Products. *http://www.sapphireenergy.com/products* (accessed 02/09, 2015).

16. Solazyme Microalgae. Macro Solutions. *http://solazyme.com/?lang=en* (accessed 02/09, 2015).

17. Thurmond, W. Algae-powered plane takes flight. *http://www.emergingmarkets.com/algae/Algae%20Biofuel%20Takes%20Off%20Emerging%20Markets%20Online.pdf* (accessed 01/19, 2015).

18. Catarina Guedes, A.; Amaro, H. M.; Xavier Malcata, F. Microalgae As Sources of High Added-Value Compounds-A Brief Review of Recent Work. *Biotechnol. Prog.* **2011**, *27*, 597-613.

19. Gouveia, L. *Microalgae as a feedstock for biofuels;* Springer: 2011; pp v, 69 p.

20. Chiaramonti, D.; Prussi, M.; Casini, D.; Tredici, M. R.; Rodolfi, L.; Bassi, N.; Zittelli, G. C.; Bondioli, P. Review of energy balance in raceway ponds for microalgae cultivation: Re-thinking a traditional system is possible. *Appl. Energy* **2013**, *102*, 101-111.

21. Rawat, I.; Ranjith Kumar, R.; Mutanda, T.; Bux, F. Biodiesel from microalgae: A critical evaluation from laboratory to large scale production. *Appl. Energy* **2013**, *103*, 444-467.

22. Thurmond, W. Future shock: new paradigm in algal biofuels. *http://www.emergingmarkets.com/algae/Algae%202020%20New%20Paradigm%20In%20Fuels%20Emerging%20Markets%20Online.pdf* (accessed 01/18, 2015).

23. Flynn, K. J.; Mitra, A.; Greenwell, H. C.; Sui, J. Monster potential meets potential monster: pros and cons of deploying genetically modified microalgae for biofuels production. *Interface Focus* **2013**, *3*.

24. Glass, D. Risk assessment and regulation of open-pond use of genetically modified algae. *https://dglassassociates.wordpress.com/2013/11/01/risk-assessment-and-regulation-of-open-pond-use-of-genetically-modified-algae/* (accessed 04/24, 2015).

25. Glass, D. J. Pathways to Obtain Regulatory Approvals for the Use of Genetically Modified Algae in Biofuel or Biobased Chemical Production. *Industrial Biotechnology* **2015**, *11*, 71.

26. Cai, T.; Park, S. Y.; Li, Y. Nutrient recovery from wastewater streams by microalgae: Status and prospects. *Renewable & Sustainable Energy Reviews* **2013**, *19*, 360-369.

27. Brennan, L.; Owende, P. Biofuels from microalgae—A review of technologies for production, processing, and extractions of biofuels and co-products. *Renewable and Sustainable Energy Reviews* **2010**, *14*, 557-577.

28. De la Hoz Siegler, Hector, Jr. Optimization of Biomass and Lipid Production in Heterotrophic Microalgal Cultures, University of Alberta, Canada, 2011.

29. Chen, C.; Yeh, K.; Aisyah, R.; Lee, D.; Chang, J. Cultivation, photobioreactor design and harvesting of microalgae for biodiesel production: A critical review. *Bioresour. Technol.* **2011**, *102*, 71-81.

30. Carvalho, A. P.; Meireles, L. A.; Malcata, F. X. Microalgal reactors: A review of enclosed system designs and performances. *Biotechnol. Prog.* **2006**, *22*, 1490-1506.

31. Becker, E. W. *Microalgae: biotechnology and microbiology;* Cambridge; New York: Cambridge University Press, 1994.

32. Garcia, M.; Miron, A.; Sevilla, J.; Grima, E.; Camacho, F. Mixotrophic growth of the microalga Phaeodactylum tricornutum - Influence of different nitrogen and organic carbon sources on productivity and biomass composition. *Process Biochemistry* **2005**, *40*, 297-305.

33. Algae Biomass Organization Algae Basics: Open Pond Systems. *http://allaboutalgae.com/open-pond/* (accessed 02/18, 2015).

34. Xu, L.; Weathers, P. J.; Xiong, X.; Liu, C. Microalgal bioreactors: Challenges and opportunities. *Engineering in Life Sciences* **2009**, *9*, 178-189.

35. Oilgae Cultivation of algae in closed ponds. http://www.oilgae.com/algae/cult/cp/cp.html (accessed 04/24, 2015).

36. Zhu, L. D.; Hiltunen, E.; Antila, E.; Zhong, J. J.; Yuan, Z. H.; Wang, Z. M. Microalgal biofuels: Flexible bioenergies for sustainable development. *Renewable and Sustainable Energy Reviews* **2014**, *30*, 1035-1046.

37. Andersen, R. A. *Algal Culturing Techniques;* Elsevier Academic Press: Burlington, MA, 2005.

38. Vasumathi, K. K.; Premalatha, M.; Subramanian, P. Parameters influencing the design of photobioreactor for the growth of microalgae. *Renewable & Sustainable Energy Reviews* **2012**, *16*, 5443-5450.

39. Sobczuk, T.; Camacho, F.; Grima, E.; Chisti, Y. Effects of agitation on the microalgae Phaeodactylum tricornutum and Porphyridium cruentum. *Bioprocess and Biosystems Engineering* **2006**, *28*, 243-250.

40. Alias, C.; Lopez, M.; Fernandez, F.; Sevilla, J.; Sanchez, J.; Grima, E. Influence of power supply in the feasibility of Phaeodactylum tricornutum cultures. *Biotechnol. Bioeng.* **2004**, *87*, 723-733.

41. Garcia Camacho, F.; Gallardo Rodriguez, J. J.; Sanchez Miron, A.; Ceron Garcia, M. C.; Belarbi, E. H.; Grima, E. M. Determination of shear stress thresholds in toxic dinoflagellates cultured in shaken flasks - Implications in bioprocess engineering. *Process Biochemistry* **2007**, *42*, 1506-1515.

42. Gallardo Rodriguez, J. J.; Sanchez Miron, A.; Garcia Camacho, F.; Ceron Garcia, M. C.; Belarbi, E. H.; Chisti, Y.; Molina Grima, E. Carboxymethyl cellulose and Pluronic F68 protect the dinoflagellate Protoceratium reticulatum against shear-associated damage. *Bioprocess. Biosyst. Eng.* **2011**, *34*, 3-12.

43. Leupold, M.; Hindersin, S.; Gust, G.; Kerner, M.; Hanelt, D. Influence of mixing and shear stress on Chlorella vulgaris, Scenedesmus obliquus, and Chlamydomonas reinhardtii. *J. Appl. Phycol.* **2013**, *25*, 485-495.

44. Siegler, H. D. l. H.; Ben-Zvi, A.; Burrell, R. E.; McCaffrey, W. C. The dynamics of heterotrophic algal cultures. *Bioresour. Technol.* **2011**, *102*, 5764-5774.

45. Adesanya, V. O.; Davey, M. P.; Scott, S. A.; Smith, A. G. Kinetic modelling of growth and storage molecule production in microalgae under mixotrophic and autotrophic conditions. *Bioresour. Technol.* **2014**, *157*, 293-304.

46. Angelis, S.; Novak, A. C.; Sydney, E. B.; Soccol, V. T.; Carvalho, J. C.; Pandey, A.; Noseda, M. D.; Tholozan, J. L.; Lorquin, J.; Soccol, C. R. Co-Culture of Microalgae, Cyanobacteria, and Macromycetes for Exopolysaccharides Production: Process

Preliminary Optimization and Partial Characterization. *Appl. Biochem. Biotechnol.* **2012**, *167*, 1092-1106.

47. Sandnes, J.; Ringstad, T.; Wenner, D.; Heyerdahl, P.; Kallqvist, I.; Gislerod, H. Real-time monitoring and automatic density control of large-scale microalgal cultures using near infrared (NIR) optical density sensors. *J. Biotechnol.* **2006**, *122*, 209-215.

48. Morweiser, M.; Kruse, O.; Hankamer, B.; Posten, C. Developments and perspectives of photobioreactors for biofuel production. *Appl. Microbiol. Biotechnol.* **2010**, *87*, 1291-1301.

49. Vojinovic, V.; Cabral, J.; Fonseca, L. P. Real-time bioprocess monitoring Part I: In situ sensors. *Sensors and Actuators B-chemical* **2006**, *114*, 1083-1091.

50. Mulbry, W.; Reeves, J.; Liu, Y.; Ruan, Z.; Liao, W. Near- and mid-infrared spectroscopic determination of algal composition. *J. Appl. Phycol.* **2012**, *24*, 1261-1267.

51. Laurens, L. M. L.; Dempster, T. A.; Jones, H. D. T.; Wolfrum, E. J.; Van Wychen, S.; McAllister, J. S. P.; Rencenberger, M.; Parchert, K. J.; Gloe, L. M. Algal Biomass Constituent Analysis: Method Uncertainties and Investigation of the Underlying Measuring Chemistries. *Analytical Chemistry* **2012**, 1879.

52. Laurens, L. M. L.; Van Wychen, S.; McAllister, J. P.; Arrowsmith, S.; Dempster, T. A.; McGowen, J.; Pienkos, P. T. Strain, biochemistry, and cultivation-dependent measurement variability of algal biomass composition. *Anal. Biochem.* **2014**, *452*, 86-95.

53. Thermo Scientific Process monitoring and analysis. Biofuels workflows. *http://www.dionex.com/en-us/webdocs/114157-Bro-IC-LC-GC-NIR-Biofuel-Workflow-BR70346_E.pdf* (accessed 06/09, 2015).

54. Siesler, H. W. *Near-infrared spectroscopy: principles, instruments, applications;* Weinheim: Wiley-VCH, c2002: 2002.

55. Nadadoor, V. R.; De la, H. S.; Shah, S. L.; McCaffrey, W. C.; Ben-Zvi, A. Online sensor for monitoring a microalgal bioreactor system using support vector regression. *Chemometrics Intellig. Lab. Syst.* **2012**, *110*, 38-48.

56. Han, Y.; Wen, Q.; Chen, Z.; Li, P. Review of Methods Used for Microalgal Lipid-Content Analysis. *Proceedings of International Conference on Smart Grid and Clean Energy Technologies (Icsgce 2011)* **2011**, *12*.

57. Laurens, L. M. L. *Summative mass analysis of algal biomass, integration of analytical procedures : laboratory analytical procedures (LAP), issue date December 2, 2013 / L.M.L. Laurens;* 2013.

58. Havlik, I.; Lindner, P.; Scheper, T.; Reardon, K. F. On-line monitoring of large cultivations of microalgae and cyanobacteria. *Trends Biotechnol.* **2013***, 31*, 406-414.

59. Fonseca,V.Vojinovic, J.M.S.Cabral, L.P. Ex Situ Bioprocess Monitoring Techniques. *Chemical Industry and Chemical Engineering Quarterly* **2007**, 103.

60. Burns, D. A.; Ciurczak, E. W. *Handbook of near-infrared analysis. [electronic resource];* Boca Raton, Fla.: CRC Press, 2008; 3rd ed: 2008.

61. Concas, A.; Lutzu, G. A.; Pisu, M.; Cao, G. Experimental analysis and novel modeling of semi-batch photobioreactors operated with Chlorella vulgaris and fed with 100% (v/v) CO2. *Chem. Eng. J.* **2012***, 213*, 203-213.

62. Gomes, J.; Chopda, V. R.; Rathore, A. S. Integrating systems analysis and control for implementing process analytical technology in bioprocess development. *Journal of Chemical Technology and Biotechnology* **2015***, 90*, 583-589.

63. Clementschitsch, F.; Bayer, K. Improvement of bioprocess monitoring: development of novel concepts. *Microbial Cell Factories* **2006***, 5*, 19.

64. Thurmond, W. Algae investments reach 233 million euros in 2008. *http://www.emergingmarkets.com/biodiesel/pdf/BiofuelsInternational_AlgaeInvestmentTrends_November2008_WillThurmond.pdf* (accessed 01/19, 2015).

65. Gründler, P. *Chemical sensors. [electronic resource]: an introduction for scientists and engineers;* Berlin; New York: Springer, c2007: 2007.

66. Carey, P. R. *Biochemical applications of Raman and resonance Raman spectroscopies;* New York: Academic Press, 1982.

67. Siesler, H. In *Basic Principles of Near-Infrared Spectroscopy;* CRC Press: 2007; pp 7-19.

68. Wiesner, K.; Fuchs, K.; Gigler, A. M.; Pastusiak, R. Trends in Near Infrared Spectroscopy and Multivariate Data Analysis From an Industrial Perspective. *Procedia Engineering* **2014***, 87*, 867-870.

69. Heise, H. M.; Fritzsche, J.; Tkatsch, H.; Waag, F.; Karch, K.; Henze, K.; Delbeck, S.; Budde, J. Recent advances in mid- and near-infrared spectroscopy with applications for research and teaching, focusing on petrochemistry and biotechnology relevant products. *European Journal of Physics* **2013***, 34*, S139-S159.

70. Stuart, B. *Infrared spectroscopy: fundamentals and applications;* Chichester, West Sussex, England; Hoboken, NJ: J. Wiley, c2004: 2004.

71. McCartney, C. Constraints on algal biofuel production, The University of Texas at Austin, **2011**.

72. Sharp, J. Near-infrared diffuse reflection analysis of fruit using the vivo direct illuminated reflection stage and NIRQuest265-2.5 extended range NIR spectrometer. *http://oceanopticsfaq.com/apps/consumer-products/near-infrared-diffuse-reflection-analysis-of-fruit-using-the-vivo-direct-illuminated-reflection-stage-and-nirquest256-2-5-extended-range-nir-spectrometer/* (accessed 10/15, 2014).

73. Shenk, J.; Westerhaus, M.; Workman, J. In *Application of NIR Spectroscopy to Agricultural Products;* CRC Press: 2007; pp 347-386.

74. Omar, A. F.; Atan, H.; MatJafri, M. Z. NIR Spectroscopic Properties of Aqueous Solutions. *Molecules* **2012***, 17*, 7440-7450.

75. Ocean optics Spectra Suite. Spectrometer Operating Software. Installation and Operation Manual. *, 000-20000-300-02-201110*.

76. Mattley, Y. Effect of sandblasting on the specular reflection from encoder wheels. *http://oceanoptics.com/application-note-the-secrets-of-encoder-wheels/* (accessed 01,12, 2015).

77. Specac Product Catalogue. **2014**, 17-18, 19, 41, 42, 43, 44.

78. Bremmer, R. H. Non-contact spectroscopy age determination of bloodstains, University of Amsterdam, Amsterdam, 2011.

79. Frankhuizen, R. In *NIR Analysis of Dairy Products;* CRC Press: 2007; pp 415-437.

80. Kington, L.; Jones, T. In *Application for NIR Analysis of Beverages;* CRC Press: 2007; pp 457-463.

81. Setnicka, V. FT-IR Reflection Tecniques. *http://old.vscht.cz/anl/vibspec/FTIR%20Reflection%20Techniques.pdf* (accessed 06/01, 2014).

82. Ocean optics Staff Metallurgical Analysis, Application Note, Reflection of Aluminum Alloys for Automotive Wheels. *http://oceanoptics.com/application/metallurgicalanalysis/* (accessed 01,12, 2015).

83. Ocean optics Agricultural measurements and monitoring. NIR Reflection, example set up. *http://oceanoptics.com/application/agricultural-measurements-monitoring/* (accessed 01,12, 2015).

84. PIKE Technologies Specular reflectance - Theory and applications. http://www.piketech.com/files/pdfs/SpecularReflectAN611.pdf (accessed 08/15, 2014).

85. Filmetrics Thin-film measurement. http://wcam.engr.wisc.edu/Public/Tools/Analysis/Filmetrics%20F20%20technical%20reference.pdf (accessed 05/21, 2014).

86. Wolfbeis, O. S. Fiber-optic chemical sensors and biosensors. *Anal. Chem.* **2006**, *78*, 3859-3873.

87. Yotter, R. A.; Lee, L. A.; Wilson, D. M. Sensor technologies for monitoring metabolic activity in single cells-part I: optical methods. *Sensors Journal, IEEE* **2004**, *4*, 395-411.

88. Pell, R. J.; Seasholtz, M. B.; Beebe, K. R.; Koch, M. V. Process analytical chemistry and chemometrics, Bruce Kowalski's legacy at The Dow Chemical Company. *J. Chemometrics* **2014**, *28*, 321-331.

89. Kessler, R. W. Perspectives in process analysis. *J. Chemometrics* **2013**, *27*, 369-378.

90. Martens, H.; Naes, T. *Multivariate calibration;* Chichester : John Wiley & Sons, 1991.

91. Workman, J. In *NIR Spectroscopy Calibration Basics;* CRC Press: 2007; pp 123-150.

92. McNichols, R. J.; Cote, G. L. Optical glucose sensing in biological fluids: an overview. *J. Biomed. Opt.* **2000**, *5*, 5-16.

93. Chaudhry, M. H. *Open-channel flow. [electronic resource];* New York, NY: Springer, 2008; 2nd ed: 2008.

94. Massey, B. S.; Ward-Smith, A. *Mechanics of fluids;* Abingdon, Oxon ; New York, NY: Spon Press, 2012; 9th ed: 2012.

95. Potter, M. C.; Wiggert, D. C. *Mechanics of fluids;* Prentice Hall: Englewood Cliffs, N.J., 1991; pp 692.

96. Inamdar, S. Open channel flow. http://udel.edu/~inamdar/EGTE215/Open_channel.pdf (accessed 05/20, 2014).

97. MIT Open Course Ware Introduction to Fluid Motions, Sediment Transport, and Current-Generated Sedimentary Structures Chapter 3. *http://ocw.mit.edu/courses/earth-atmospheric-and-planetary-sciences/12-090-special-topics-an-introduction-to-fluid-motions-sediment-transport-and-current-generated-sedimentary-structures-fall-2006/lecture-notes/* (accessed 07/27, 2015).

98. Smolentsev, S.; Miraghaie, R. Study of a free surface in open-channel water flows in the regime from "weak" to "strong" turbulence. *Int. J. Multiphase Flow* **2005***, 31*, 921-939.

99. Pang, X. *Water: Molecular Structure and Properties;* World Scientific Publishing Company: Hackensack, New Jersey, 2013; .

100. MIT Open Course Ware Introduction to Fluid Motions, Sediment Transport, and Current-Generated Sedimentary Structures Chapter 4. *http://ocw.mit.edu/courses/earth-atmospheric-and-planetary-sciences/12-090-introduction-to-fluid-motions-sediment-transport-and-current-generated-sedimentary-structures-fall-2006/course-textbook/ch4.pdf* (accessed 07/27, 2015).

101. Bormashenko, E. A. *Wetting of real surfaces. [electronic resource];* Berlin; New York: De Gruyter, 2013.

102. Schramm, L. L. *Emulsions, foams, suspensions, and aerosols: microscience and applications;* Weinheim, Germany: Wiley-VCH, 2014; Second edition: 2014.

103. Fleischer, S.; Roichman, Y. Surface Tension. *http://www.tau.ac.il/~phchlab/experiments_new/surface_tenstion/theory.html* (accessed 07/13, 2015).

104. Blossey, R. *Thin liquid films. [electronic resource]: dewetting and polymer flow;* Dordrecht; New York: Springer, c2012: 2012.

105. White, F. M. *Fluid mechanics;* New York, N.Y.: McGraw Hill, 2011; 7th ed: 2011.

106. Schneider, H.; Niegisch, N.; Mennig, M.; Schmidt, H. In *Hydrophilic Coating Materials;* Aegerter, M., Mennig, M., Eds.; Springer US: 2004; pp 187-194.

107. Snoeijer, J. H.; Andreotti, B. Moving Contact Lines: Scales, Regimes, and Dynamical Transitions. *Annual Review of Fluid Mechanics, Vol 45* **2013***, 45*, 269-292.

108. Moulinet, S.; Guthmann, C.; Rolley, E. Roughness and dynamics of a contact line of a viscous fluid on a disordered substrate. *European Physical Journal E* **2002***, 8*, 437-443.

109. Vanden-Broeck, J. *Gravity-capillary free-surface flows;* New York: Cambridge University Press, 2010.

110. Furrer, M.; Saraceno, L.; Mariani, A.; Celata, G. P. Capillary pressure influence on open channels pressure drop. *International Journal of Thermal Sciences* **2013***, 70*, 102-113.

111. Scholle, M.; Aksel, N. An exact solution of visco-capillary flow in an inclined channel. *Zeitschrift für angewandte Mathematik und Physik ZAMP* **2001***, 52*, 749-769.

112. Zheng, W.; Wang, L.; Or, D.; Lazouskaya, V.; Jin, Y. Role of Mixed Boundaries on Flow in Open Capillary Channels with Curved Air-Water Interfaces. *Langmuir* **2012***, 28*, 12753-12761.

113. Ocean optics NIR Near Infrared. Fiber Optic Spectrometers. Installation and Operation Manual*., 197-00000-512-02-0707*.

114. Ocean optics LS-1 Series Tungsten Halogen Light Sources. Installation and Operation Instructions*., 009-0000-STD-01-201010*.

115. Ocean optics Fibers and Probes. http://oceanoptics.com/wpcontent/uploads/Ocean_Optics_Fibers_Probes.pdf

116. Sharp, J. Coated printed circuit board reflectance with the R400-7-VIS-NIR reflection probe. *http://oceanopticsfaq.com/apps/reflectance-2/coated-printed-circuit-board-reflectance-with-the-r400-7-vis-nir-reflection-probe/* (accessed 10/14, 2014).

117. Wang, X.; Hsiao, K. Sugar Degradation during Autoclaving - Effects of Duration and Solution Volume on Breakdown of Glucose. *Physiol. Plantarum* **1995***, 94*, 415-418.

118. Diversified Enterprises Critical Surface Tension and Contact Angle with Water for Various Polymers. *http://www.accudynetest.com/polytable_03.html?sortby=contact_angle* (accessed 04/30, 2014).

119. Giangiacomo, R. Study of water–sugar interactions at increasing sugar concentration by NIR spectroscopy. *Food Chem.* **2006***, 96*, 371-379.

120. Hsiao, K. C.; Bornman, C. H. Further-Studies on Autoclaved-Induced Toxicity in Tissue-Culture Media - Gauging Sugar Breakdown by Spectrophotometry. *Physiol. Plantarum* **1991***, 82*, 261-265.

121. Heise, H. M.; Marbach, R.; Koschinsky, T.; Gries, F. A. Noninvasive Blood-Glucose Sensors Based on Near-Infrared Spectroscopy. *Artif. Organs* **1994***, 18*, 439-447.

122. Malin, S. F.; Ruchti, T. L.; Blank, T. B.; Thennadil, S. N.; Monfre, S. L. Noninvasive prediction of glucose by near-infrared diffuse reflectance spectroscopy. *Clin. Chem.* **1999**, 1651.

123. Rambla, F. J.; Garrigues, S.; de la Guardia, M. PLS-NIR determination of total sugar, glucose, fructose and sucrose in aqueous solutions of fruit juices. *Anal. Chim. Acta* **1997***, 344*, 41-53.

124. Laurens, L. M. L.; Wolfrum, E. J. Feasibility of Spectroscopic Characterization of Algal Lipids: Chemometric Correlation of NIR and FTIR Spectra with Exogenous Lipids in Algal Biomass. *Bioenergy Research* **2011***, 4*, 22-35.

125. Brown, M. R.; Frampton, D. M. F.; Dunstan, G. A.; Blackburn, S. I. Assessing near-infrared reflectance spectroscopy for the rapid detection of lipid and biomass in microalgae cultures. *J. Appl. Phycol.* **2014***, 26*, 191-198.

126. Kemeny, G. In *Process Analysis;* CRC Press: 2007; pp 717-759.

127. Ozkan, A.; Berberoglu, H. Physico-chemical surface properties of microalgae. *Colloid Surf. B-Biointerfaces* **2013***, 112*, 287-293.

128. Ozkan, A.; Berberoglu, H. Adhesion of algal cells to surfaces. *Biofouling* **2013***, 29*, 469-482.

129. Ozkan, A.; Berberoglu, H. Cell to substratum and cell to cell interactions of microalgae. *Colloids and Surfaces B-Biointerfaces* **2013***, 112*, 302-309.